Development of activated carbon-supported bimetallic catalysts and microreactors for the production of lactic acid, 2,5-furandicarboxylic acid, and 5-hydroxymethylfurfural

A Thesis

Submitted in Partial Fulfillment of the Requirements for the Degree of

DOCTOR OF PHILOSOPHY

By

Hanumanth Reddy Pemmana

Department of Chemical Engineering

Indian Institute of Technology Guwahati

Guwahati, India

August 2024

TH-3456_166107017

TH-3456_166107017

Dedicated

To

My Parents & Teachers

TH-3456_166107017

Indian Institute of Technology Guwahati

Department of Chemical Engineering

Statement

I, hereby declare that the work presented in this thesis titled "**Development of activated carbon-supported bimetallic catalysts and microreactors for the production of lactic acid, 2,5-furandicarboxylic acid, and 5-hydroxymethylfurfural**" is entirely original and conducted by me at the Department of Chemical Engineering, Indian Institute of Technology Guwahati, Guwahati, India. This research was carried out under the supervision of **Prof. Nageswara Rao Peela** and **Prof. Ramagopal V. S. Uppaluri**. The content of this thesis has not been submitted to any other institute for any degree or diploma. I affirm that I have adhered to the guidelines provided by the Institute in preparing this thesis and have complied with the ethical code of conduct. Whenever external materials such as data, theoretical analysis, figures, and other sources were used, proper credit was given by citing them in the thesis text and providing detailed references. Additionally, I obtained necessary permissions from the copyright owners of these sources, where applicable.

Guwahati,

August, 2024

Hanumanth Reddy Pemmana

166107017

TH-3456_166107017

Indian Institute of Technology Guwahati

Department of Chemical Engineering

Certificate

It is certified that the work described in this thesis entitled "**Development of activated carbon-supported bimetallic catalysts and microreactors for the production of lactic acid, 2,5-furandicarboxylic acid, and 5-hydroxymethylfurfural**" by Mr. Hanumanth Reddy Pemmana for the award of degree of Doctor of Philosophy is an authentic record of the results obtained from the research work carried out under our supervision at the Department of Chemical Engineering, Indian Institute of Technology Guwahati, Guwahati, India. This work has not been submitted elsewhere for a degree.

Prof. Ramagopal V. S. Uppaluri

Thesis Co-Supervisor

Professor

Department of Chemical Engineering

IIT Guwahati, Guwahati – 781039

Assam, India

Prof. Nageswara Rao Peela

Thesis Supervisor

Professor

Department of Chemical Engineering

IIT Guwahati, Guwahati – 781039

Assam, India

TH-3456_166107017

TH-3456_166107017

Acknowledgement

This doctoral thesis would not have been completed without several people's help and extended hands. I take this opportunity to express my sincere thankfulness to all of them. Firstly, I express my sincere gratitude and most profound respect to my thesis supervisors, **Prof. Nageswara Rao Peela & Prof. Ramagopal V. S. Uppaluuri,** Department of Chemical Engineering, for their continuous guidance, support, and encouragement throughout my thesis work. His valuable insights, feedback, timely assistance, and criticisms helped me gain knowledge and interest in improving the work. I thank him for accepting the collaboration and allowing the interns to widen the research area. I am honored to work under him. Thank you very much to my supervisors for their unforgettable help and support.

I would also like to thank my doctoral committee members, Prof. Tapas Kumar Mandal, Prof. Animes Kumar Golder, Prof. Akshai Kumar Alape Seetharam, and Dr. Anki Reddy Katha, for their valuable suggestions and constructive criticism during all assessments of the Ph.D. program.

I also thank **Prof. Kaustubha Mohanty,** Head of the Department of Chemical Engineering, for his administrative support. Furthermore, I would like to thank other faculty members, research scholars, and non-teaching staff of the Department of Chemical Engineering, IIT Guwahati, for their kind cooperation. I also thank the technical staff of Central Instruments Facilities (CIF) for their support during the analysis.

I acknowledge the Ministry of Human Resource Development **(MHRD)** and our institute for providing fellowship throughout the PhD program. Science and Engineering Research Board **(SERB, File Number: CRG/2022/005144),** New Delhi, India, is gratefully acknowledged for the financial support to carry out the research.

TH-3456_166107017

The analytical facilities from Central Instruments Facilities **(CIF),** as well as the analytical lab of the Department of Chemical Engineering of Indian Institute of Technology Guwahati, were also acknowledged.

I am grateful to my lab mates and friends; Dr. Santosh Kumar Yedla, Dr. Devipriya Gogoi, Dr. Bharath Velaga, Dr. Rambabu Ponnala, Dr. Anirban Chowdhury, Dr. Laxmi Prasad Pala, Mr. Ameer Suhail, Dr. Rammohan D, Ms. Sarmistha Baruah, Mr. Masresha Adasho Achomo, Dr. Mallikarjuna Mallela, Dr. Ramesh T, Dr. Venkatesh Chejarla, Mr. Vishnu Raja Reddy, Mr. Mukesh, Dr. Viswanth and Mr. Kranthi Kumar for their cooperative assistance and suggestions for performing experiments and collaborating on the work.

I am deeply grateful to convey my sincere gratitude to my parents and family members for their sustained help and encouragement in all my personal and academic ventures. I feel proud and blessed to have such parents: my mother, Mrs. Sakunthala Pemmana Garu, and my father, **Mr. Lakshmi Narayana Reddy** Garu. Special thanks to my sister, Mrs. Prasanthi Pannuru, and brother-in-law, Mr. Ramakrishna Reddy Pannuru, who always strengthened me by standing by me in all situations.

I want to express my gratitude to numerous individuals whose names may not be specifically mentioned here, but their support has been invaluable. This acknowledgment in no way diminishes the significance of their contributions. Most importantly, I extend my heartfelt thanks to God Almighty for blessing me with a beautiful and healthy life.

Hanumanth Reddy Pemmana

TH-3456_166107017

ABSTRACT

With the depletion of fossil resources and the catastrophic environmental pollution caused by their exploitation, biomass resources to produce fuels and chemicals are becoming increasingly popular. Among various biomass-derived building blocks/platform chemicals, lactic acid, 5-hydroxymethylfurfural (HMF), and 2,5-furan-dicarboxylic acid (FDCA) play an essential role due to their potential applications in polymer and fine chemical industries. Lactic acid can be obtained through the catalytic transformation of glycerol derived from the biodiesel plants through transfer esterification of fatty acid methyl esters (FAME). The FDCA can be obtained from the catalytic oxidation of HMF, and it can be directly synthesized from monosaccharides such as fructose, glucose, and cellulose through chemical transformations. Moreover, HMF can also be used to produce other value-added chemicals such as levulinic acid, 2,5-diformylfuran (DFF), maleic acid (MA), maleic anhydride (MAn) 2,5-dimethylfuran (DMF) and 1,6-hexanediol. The present study focuses on the catalytic transformation of glycerol to lactic acid and HMF to FDCA. The activated carbon-supported bimetallic catalytic systems were developed and employed for these transformations. In addition, the HMF production from fructose dehydration was carried out in helical coil microreactors (HCMR) using homogeneous catalysts (H_2SO_4 and maleic acid).

The conventional use of batch processing for biomass conversion to value-added chemicals and fuels faces limitations in reaction time and economic viability, hindering efficient biorefineries. The HCMRs present a promising solution, enabling process intensification and miniaturization. Our study demonstrated the catalytic dehydration of fructose to HMF in HCMR, using sulfuric acid and maleic acid as catalysts. Optimization of parameters resulted in improved reactor throughput, achieving a notable HMF space-time yield

TH-3456_166107017

of 380 gHMF/gCat/h. Moreover, maleic acid exhibited superior selectivity (83%) towards HMF compared to sulfuric acid (80%), with reduced HMF degradation and humins formation.

2,5-Furandicarboxylic acid (FDCA) is a crucial monomer, given its structural resemblance to terephthalic acid (TPA) in the polymer industry. The synthesis of FDCA involves the oxidation of hydroxyl and aldehyde groups of HMF. In this study, activated carbon-supported Ru-V and Ru-Ni catalysts were synthesized and applied for the oxidation of HMF to FDCA under base-free and aqueous conditions in a batch reactor system. The investigation delved into the impact of temperature, pressure, time, solvent type, and metal weight percentage. A two-step temperature approach was also explored for HMF oxidation using the Ru-V/AC bimetallic catalyst. Under optimized conditions, the Ru-V/AC bimetallic catalyst achieved a remarkable 74.4% yield of FDCA with complete conversion of HMF at 100 °C (2 h) and 130 °C (2 h). In contrast, a molar yield of 65.3% was attained with the 1.5%Ru-0.5%Ni/AC bimetallic catalyst (130 °C, 12 h, 1.0 MPa O_2). A simple acetone wash effectively regenerated the catalyst, restoring its activity completely. This wash removed humins deposited on the catalyst surface, exposing the active sites.

The physicochemical properties of the prepared bimetallic catalysts were comprehensively explored. Advanced characterization techniques, such as powder X-ray diffraction (p-XRD) analysis, N2-sorption studies utilizing a BET surface area analyzer, Field Emission Transmission Electron Microscopy (FETEM), High-Resolution Transmission Electron Microscopy (HRTEM), Energy-Dispersive X-ray (EDX) analysis, and X-ray Photoelectron Spectroscopy (XPS), were employed for a detailed understanding of the catalysts. This thorough examination aimed to provide insights into the structural and chemical aspects of the catalysts, ensuring a comprehensive understanding of their performance and longevity in the catalytic processes.

TH-3456_166107017

A valuable and alternative method for producing lactic acid involves the selective oxidation of glycerol. In this study, activated carbon-supported monometallic Pt, Ru, V, and bimetallic Pt-V and Ru-V catalysts were prepared using a simple wet-impregnation method. These catalysts were assessed for their efficacy in the aerobic oxidation of glycerol to lactic acid, demonstrating excellent performance and stability. Under optimized conditions, a remarkable 79.62% and 75.53% yield of lactic acid was achieved with 100% glycerol conversion using Pt-V/AC and Ru-V/AC in 12 h and 3 h, respectively, at 200 °C.

Keywords: 5-Hydroxymethylfurfural; Fructose; Helical coil microreactor; Bronsted acid; 2,5-furandicarboxilic acid (FDCA); Base-free oxidation, Ru-V bimetallic catalysts; Glycerol, Lactic acid, Selective Oxidation, Activated carbon catalyst support, Pt-V bimetallic catalysts.

TH-3456_166107017

ABBREVATIONS

AA	Acetic acid
AC	Activated carbon
Al_2O_3	Alumina oxide
APD	Average pore diameter
BET	Brunauer, Emmett and Teller
BHMF	2,5-Bis(hydroxymethyl)furan
BHMTHF	2,5-Bis(hydroxymethyl)tetrahydrofuran
BJH	Barrett, Joyner and Halenda
CNT	Carbon nanotubes
CTF	Covalent triazine frameworks
CeO_2	Cerium oxide
DFF	2,5-Diformylfuran
DMSO	Dimethyl sulfoxide
DMF	2,5-dimethylfuran
EG	Ethylene glycol
FA	Formic acid
FAME	Fatty acid methyl esters
FDCA	2,5-Furandicarboxylic acid
FESEM	Field emission scanning electron microscopy
FFCA	5-Formyl-2-furan carboxylic acid
FETEM	Field emission transmission electron microscopy

TH-3456_166107017

FF	Furfural
GL	Glycerol
GLA	Glycolic acid
GNP	Graphene nanoplatelets
H	Hours
HAPP	Hydroxyapatite
HCN	Hydrogen cyanide
H2SO4	Sulfuric acid
HCl	Hydrochloric acid
H_3PO_4	Phosphoric acid
HMF	5-Hydroxymethylfurfural
HMFCA	5-Hydroxymethyl-2-furancarboxylic acid
HPLC	High-performance liquid chromatography
HT	Hydrotalcite
HRTEM	High-resolution transmission electron microscopy
KOH	Potassium hydroxide
LA	Lactic acid
LuA	Levulinic acid
MA	Maleic acid
Man	Maleic anhydride
MgO	Magnesium oxide
MTHF	2-methyltetrahydrofuran
MIBK	Methyl isobutyl ketone
MilliQ	Deionized water
mL	Millilitre

TH-3456_166107017

Mmol	Millimole
NaOH	Sodium hydroxide
$NaHCO_3$	Sodium bicarbonate
PDA	Photodiode array
1,2-PDO	1,2-Propanediol
PEF	Polyethylene furanoate
PET	Polyethylene terephthalate
Ppm	Parts per million
PSD	Pore size distribution
RID	Refractive index detector
SAED	Selected area electron diffraction
SA	Specific surface area
SS	Stainless steel
STY	Space-time yield
TOF	Turnover frequency
TON	Turnover number
TPA	Terephthalic acid
V_2O_5	Vanadium pentoxide
XEDS	Energy dispersive X-ray spectroscopy
XPS	X-ray Photoelectron Spectroscopy
XRD	X-ray diffraction
ZrO_2	Zirconium oxide

TH-3456_166107017

Contents

TH-3456_166107017

TH-3456_166107017

TH-3456_166107017

TH-3456_166107017

TH-3456_166107017

List of Figures

TH-3456_166107017

TH-3456_166107017

TH-3456_166107017

TH-3456_166107017

TH-3456_166107017

TH-3456_166107017

TH-3456_166107017

TH-3456_166107017

List of Tables

TH-3456_166107017

Chapter 1

Background of the Work and Research Objectives

1.1 Introduction

Significant attention has been brought to the issue of fossil fuel depletion and increasing concern about the impact of greenhouse gas emissions on climate change. This has prompted research efforts to explore the production of fuels and chemicals from biomass as a sustainable alternative. Biomass, a renewable and abundantly accessible carbon source for producing value-added chemicals and fuels, is a promising alternative to fossil fuels. The intense demand for alternative resources to obtain fuels and chemicals from fossil feedstock attracted researchers to work on renewable resources.[1,2] Biomass has been demonstrated as a promising renewable feedstock for producing high-value-added chemicals and fuels. For example, biomass can be converted to bulk products, such as liquid fuels (biodiesel) or high value-added chemicals, including glucose, fructose, 5-hydroxymethylfurfural (HMF), furfural, levulinic acid, and glycerol through bio-refinery processes. Among the various biomass-derived platform molecules, lactic acid and FDCA were promising for biodegradable and bioplastic production. In addition, HMF, obtained from sugars (glucose or fructose) through catalytic dehydration, is a critical precursor for bio-renewable chemicals and materials production.

1.1.1 5-Hydroxymethylfurfural

5-Hydroxymethylfurfural, a compound of considerable significance across diverse industries, is obtained from carbohydrates and has attracted notable interest due to its wide-ranging applications. Originating from biomass and food sources, this organic compound plays a

TH-3456_166107017

pivotal role in scientific research and industrial processes, finding utility in synthesizing polymers and pharmaceuticals. The biomass conversion to valuable building/platform chemicals has grown due[3] to their versatility and ability to be converted to numerous valuable chemicals[4–7]. The 5-hydroxymethylfurfural (HMF) is such a renewable building block,[8–12] that is crucial for producing various chemicals such as 1,6-hexanediol[13,14], 2,5-dimethylfuran (DMF)[15], maleic anhydride (MA)[16,17], 2,5-diformylfuran (DMF)[17], and 2,5-furandicarboxylic acid (FDCA)[17,18]. In particular, 2,5-furandicarboxylic acid (FDCA)[2,19,20], produced from HMF, is a crucial building block to produce polyethylene furanoate (PEF), which has the potential to be a viable alternative to petroleum-based polyethylene terephthalate (PET)[2,21–24]. FDCA can be converted to polyethylene furanoate (PEF), a replacement for polyethylene terephthalate (PET).[25,26] Various HMF derivatives were presented in Fig. 1.1.

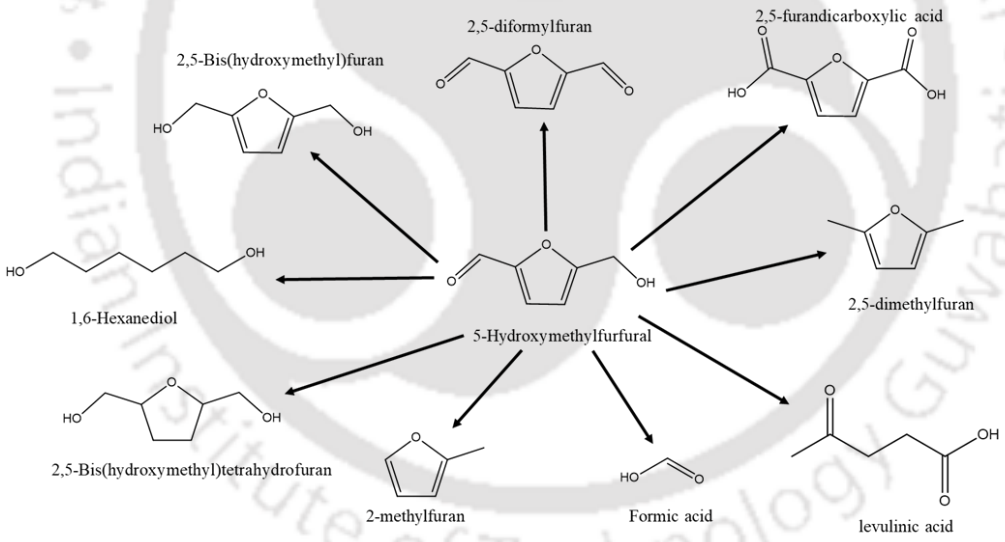

Figure 1.1: 5-Hydroxymethylfurfural derivatives.[2]

1.1.2 2,5-Furandicarboxylic acid

2,5-Furandicarboxylic acid (FDCA) is a key chemical compound relevant to various industries. It is derived from renewable resources such as biomass and is recognized for its potential to replace traditional petrochemical-based materials. FDCA serves as a building block for the production of bioplastics, offering a sustainable alternative to conventional plastics. Its unique

TH-3456_166107017

molecular structure and properties make it valuable in developing environmentally friendly materials and various applications, including packaging, textiles, and automotive products. This compound represents a promising avenue for reducing dependence on fossil fuels and promoting more sustainable practices in materials science. Substituting terephthalic acid (TPA) with FDCA is crucial for sustainability and its market[2,27,28]. The PEF is a bio-based polymer with better properties than PET[18,27,29]. The FDCA is also a valuable building block for other polymer-based materials[2,18,27,28]. Various FDCA derivatives are presented in Fig. 1.2.

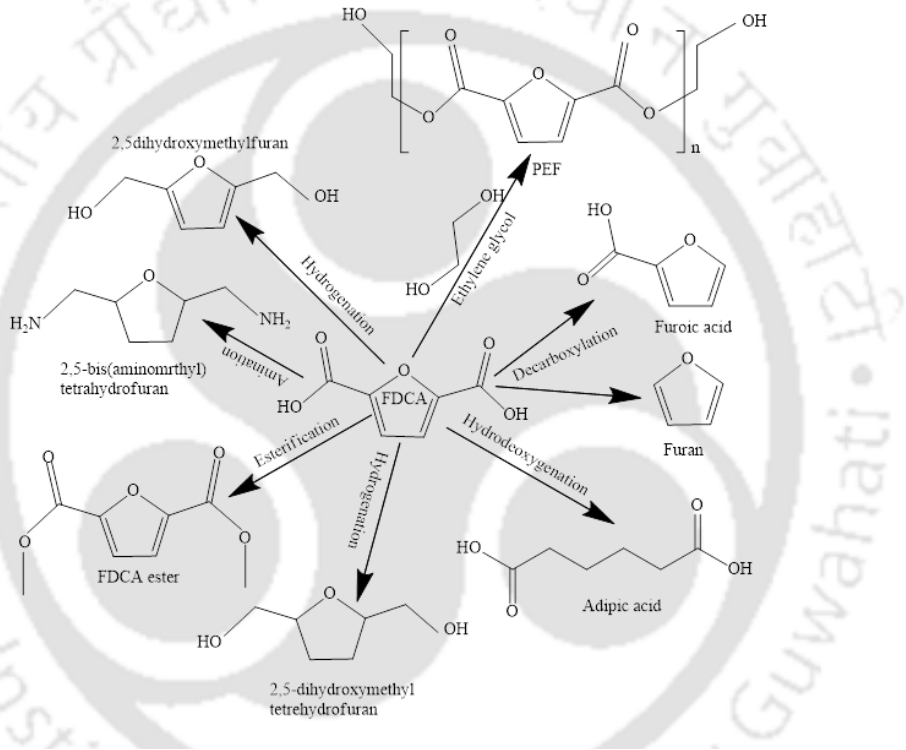

Figure 1.2: 2,5-Furandicarbboxylic acid derivatives.[17]

1.1.3 Lactic acid

The production of fatty acid methyl esters (FAME) by transesterification of triglycerides has increased severalfold in the last two decades. The FAME partially substitutes fossil fuel-derived diesel, reducing its impact on climate change[30]. However, the transesterification process generates 10-14 wt% of glycerol as a byproduct. Therefore, a quicker technological solution to utilize glycerol is needed on a short-term basis. The conversion of glycerol to other value-added chemicals is highly warranted[1,30]. The glycerol can be converted to high-value

TH-3456_166107017

chemicals such as 1,2-propanediol[31,32], 1,3-propanediol[31,33], 1-propanol[31], acrolein[34], and glyceric acid.[35–37]

Recently, lactic acid has emerged as another valuable product from glycerol[37–42]. Lactic acid (LA) or 2-hydroxy propionic acid is an essential value-added chemical widely used in food, pharmaceutical, cosmetics, textile, leather, and other industries.[39,40,43] It is also used to produce biodegradable polymers (polylactic acid). Lactic acid can be produced from various feedstocks via chemical and biological (fermentation) processes. Lactic acid, a compound with broad applications and biological importance, is pivotal in multiple domains. This organic acid is produced through fermentation from dairy products or chemical routes using HCN and acetaldehyde as feedstock and plays a vital role in the food and pharmaceutical industries. Beyond its functions in food preservation and flavor enhancement, lactic acid has diversified applications in skincare formulations, creating biodegradable polymers and exploring as a potential energy source.

1.2 Literature Review

1.2.1 5-Hydroxymethylfurfural synthesis

There is currently a high priority on converting abundant lignocellulosic biomass into 5-hydroxymethylfurfural (HMF), as it is a versatile and precious platform chemical that can be used to produce a variety of essential derivatives, including biofuels, chemicals, and bio-based polymers[2,7,44,45]. The selective hydrogenation of HMF results in the production of 2,5-Bis(hydroxymethyl)furan (BHMF) and 2,5-Bis(hydroxymethyl)tetrahydrofuran (BHMTHF). The synthesis of BHMF is challenging but of interest for the creation of thermosets and self-healing polymers due to the presence of conjugated bonds[46]. The BHMTHF, due to its ring-opened structure, has gained attention as a prospective bio-renewable source for producing 1,6-

TH-3456_166107017

hexanediol, which has the potential for large-scale polymer production[47,48]. Furthermore, hydrogenation of HMF also yields dimethylfuran (DMF) and 2-methyl furan[49], which could be used as potential additives for liquid transportation fuels[50]. The HMF can be rehydrated to produce levulinic acid[51], a viable platform chemical for synthesizing chemicals such as γ-valerolactone[52,53] and ethyl levulinate.[54,55]

The HMF is typically obtained through acid-catalyzed dehydration of lignocellulose-based hexoses such as fructose and glucose[56–60]. The yield of HMF highly depends on the hexose used. For example, the yield of HMF is significantly higher from fructose than from glucose as feedstock. As a result, several studies have reported on the catalytic dehydration of fructose to synthesize HMF. Additionally, higher humins formation is observed with glucose at higher temperatures. This is attributed to the difference in stability between the two cyclical sugar structures, with six atoms in glucose (pyranose form) and five in fructose (furanose form), as reported by Kuster[61] and Zakrzewska et al. [62]. The five-membered ring in fructose appears to aid the enolizations that lead to the formation of HMF. Therefore, fructose is more favorable than glucose in terms of yield and selectivity to HMF. The HMF can be produced through the dehydration of fructose using various heterogeneous and homogeneous catalytic systems. The heterogeneous catalysts, such as H-BEA[63,64], Sn-BEA[29,65,66], other functionalized Zeolites[58–60], TiO_2[67–69], ZrO_2[68–70], and Amberlyst-15[71–74], have been investigated for HMF production. The homogeneous Brønsted acid catalysts, such as sulfuric acid (H_2SO_4), hydrochloric acid (HCl), and phosphoric acid (H_3PO_4), have also been used for HMF production in batch reactor systems. However, these systems have limitations, such as lower heat and mass transfer rates due to low interfacial areas.

Microreactors have several advantages over batch reactors for synthesizing HMF[75,76] fructose, including higher heat and mass transfer rates, resulting in better space-time yields.

TH-3456_166107017

Tuercke et al.[77] investigated the synthesis of HMF in an aqueous phase using HCl as the catalyst. The experimental conditions involved a temperature of 185 °C and a pressure of 17 bar, with a constant residence time of 1 minute. They achieved a yield of 54% at 71% fructose conversion, a substantial improvement compared to traditional batch reactors [78], which yielded only 25.5% HMF at a fructose conversion of 50%. Further, the study was extended by adding an organic solvent as a co-solvent and an extracting agent, which increased the HMF yield to 82% at a fructose conversion of 100%. This shows that using a co-solvent as an extracting agent significantly improves the yield of HMF. Desir et al.[76] reported the fructose dehydration to HMF in a single-phase aqueous system using HCl as a catalyst in microreactors with a yield of 54% at 200 ^{o}C and 4 s of residence time. In the aqueous phase, the selectivity to HMF is reduced due to the formation of by-products such as levulinic acid and formic acid through HMF rehydration. In the presence of water as a solvent, the insoluble polymers, known as humins, also form due to the condensation and cross-polymerization of fructose and HMF, further reducing the selectivity. This highlights the challenges in achieving high selectivity to HMF in the aqueous phase using microreactors. This research is an active study area as researchers look for ways to improve the yield and selectivity of HMF. To suppress the formation of humins and enhance the yield of HMF, researchers have investigated the fructose dehydration reaction in biphasic systems (aqueous-organic).

Recently, Guo et al.[79] investigated the continuous production of HMF using slug-flow microreactors with H_2SO_4 as a catalyst in the presence of a water-MIBK system from the fructose-glucose mixture (0.1 M Fructose + 0.1 M Glucose). The study outcomes demonstrated a notable HMF yield of 81%, coupled with conversions of 96% for fructose and 5% for glucose, at a temperature of 155 °C using 0.05 M H_2SO_4 as the catalyst. This observation indicates that utilizing a biphasic system is highly effective in inhibiting the formation of humins while simultaneously enhancing the yield of HMF in the synthesis process. Recently, Desir et al.[75]

TH-3456_166107017

conducted a study on the effect of residence time, temperature, and fructose concentration on the synthesis of HMF using methyl butyl iso-ketone (MIBK) and 2-pentanol as extracting solvents. They found that the best conditions for synthesizing HMF were temperature 200 ℃, residence time 2 s, and fructose concentration 5 wt%. The yield of HMF was 93% and 87% in MIBK and 2-pentanol solvents, respectively.

TH-3456_166107017

Table 1.1: Typical reports for continuous production of 5-hydroxymethylfurfural.

Substrate	**Catalyst**	**Type of system (Single or Biphasic)**	**Reaction Conditions T (°C); residence time (min)**	**Conversion (%)**	**5-HMF Yield (%)**	**References**
Fructose	HCl	Single (water)	185; 1	71	54	[77]
Fructose	HCl	Single (water)	200; 0.067	100	54	[76]
Fructose-Glucose	H_2SO_4	Biphasic (water-MIBK)	155; 16	96	81	[79]
Fructose	HCl	Biphasic (water-MIBK)	200; 0.033	100	93	[75]
Fructose	HCl	Biphasic (water-2-pentanol)	200; 0.033	100	87	[75]
Fructose	HCl	Biphasic (water-MIBK)	180	97.1	88.5	[80]
Glucose	$AlCl_3$ + HCl	Biphasic (water-MIBK)	160; 16	83.2	66.2	[81]

TH-3456_166107017

1.2.2 2,5-Furandicarbboxylic acid synthesis from 5-hydroxymethylfurfural

The production of FDCA through the oxidation of HMF has been an area of interest. Noble metal-based catalysts, such as Au[23,82–84], Pt[83,85], Pd[83], and Ru[19,86], have been investigated for the oxidation of HMF to FDCA using molecular oxygen or air. Most studies used Au or Pt catalysts supported on hydrotalcite (HT)[84], TiO_2[82], and CeO_2[23]. Recent studies have shown that Pd supported on basicity-tuned hydrotalcite catalyst[87] and Pt nanoparticles deposited on low surface ZrO_2 catalysts[88] can efficiently produce FDCA under base-free and aqueous phase conditions with yields of >99.9% and 97.3%, respectively. The Pt supported on carbon nanotubes, hydrotalcite, and graphene oxide showed excellent performance with complete conversion of HMF and FDCA yields of 98%, 97%, and 95%, respectively [89]. A recent study also reported that Pt supported on a C-O-Mg catalyst produced FDCA with a yield of 97% at 100% HMF conversion[90].

Several studies have also used noble bimetallic catalysts to oxidize HMF to FDCA. Wan et al.[91] used functionalized carbon nanotube-supported Au-Pd bimetallic catalysts and achieved 94-96% FDCA yields in the presence of oxygen or air. The best performance was observed with 30% H_2O_2 pre-treated CNTs. The primary supports, MgO and HT, exhibited the maximum FDCA yield of 99% and 91%, respectively. Gao et al.[92] found that Au-Pd bimetallic catalysts supported on La-doped layer double hydroxides performed better than monometallic Au and Pd, with ≥99% FDCA yield. Danilo et al.[93] used Au-Pd monometallic and bimetallic catalysts supported on nanosized NiO and achieved 95% HMF conversion and 70% FDCA yield. Shen et al.[94] used 0.4 wt% Pt-loaded Ni catalysts supported on carbon and achieved 97.5% FDCA yield with 100% HMF conversion. Different Ru(OH)x catalyst supports have been evaluated with $MgO.La_2O_3$, MgO, and HT showed exceptional FDCA yields of >99, 92, and 90%, respectively [95]. However, the basicity of the supports, such as MgO and HT, decreases with reaction time due to leaching, and the activity

TH-3456_166107017

decreases. Moreover, noble metal catalysts are costly and rapidly depleted. Therefore, alternatives for supports and noble metals should be investigated to make the process more economical.

Using relatively inexpensive ruthenium and vanadium-based catalysts is advantageous in oxidizing HMF to produce DFF or FDCA. Using a commercial Ru/C catalyst, an 88% yield of FDCA was reported[19]. Ru-supported covalent triazine frameworks produced FDCA with a 77.6% yield[96]. Hydroxyapatite-supported Ru nanoparticles produced >99% FDCA yield[97]. $MnCo_2O_4$ spinel-supported ruthenium catalyst produced a 99.1% FDCA yield[98]. High surface area zirconia-supported Ru catalysts produced 97% FDCA yield[99]. Vanadium phosphate oxide catalysts produced 83.6% DFF yield and 9.2% FDCA yield[100]. Fe_3O_4 nanoparticles-supported vanadium-based catalysts produced 79.2% DFF yield, 9.2% FDCA yield, and 95.5% conversion[101]. Ruthenium-based bimetallic catalysts have also been studied to oxidize HMF to FDCA. Gao et al.[102] used Ru-Co composite catalysts, which gave a 99.9% FDCA yield and were stable for up to seven cycles. Alina et al.[103] evaluated a Ru-Fe_3O_4@SiO_2 catalyst for the base-free oxidation of HMF and obtained 80.6% FDCA selectivity at 92% HMF conversion.

1.2.3 Catalytic oxidation of glycerol to lactic acid

The currently used industrial chemical process is not environmentally friendly; it uses a mixture of HCN and acetaldehyde as feedstock. The hydrolysis of this mixture with HCl and ammonium chloride produces lactic acid, which results in byproduct formation.[43,104] The current commercial biological process involves the fermentation of various carbohydrate feedstocks, such as cellulose and sucrose[39,105]. However, the production cost of this process is very high due to low space-time yield and high energy requirements in the recovery of lactic acid.[43,105] Therefore, developing alternative catalytic routes to produce lactic acid is essential.

TH-3456_166107017

The conversion of glycerol to lactic acid by catalytic route has shown promise as a cost-effective and sustainable route to produce lactic acid. Previous studies have shown that the conversion of glycerol to lactic acid occurs through various catalytic processes, including hydrothermal conversion[106–110], hydrogenolysis[111–113], and selective oxidation[114–117]. For example, Shen et al.[108] reported the hydrothermal conversion of glycerol to lactic acid using alkali (KOH, NaOH, and LiOH) and alkaline earth metal hydroxides ($Ba(OH)_2$, $Sr(OH)_2$, $Ca(OH)_2$, and $Mg(OH)_2$). The results showed that 90% of lactic acid yield was achieved at 300 °C with NaOH or KOH as a catalyst. KOH and Ba(OH)2 performed best among these catalysts. Kishida et al.[107] reported the hydrothermal conversion of GL to LA with up to 90% LA yield at elevated temperatures and robust alkali conditions. Furthermore, using NaOH as a base material, Lopez *et al*.[106] reported 84% lactic acid yield with higher glycerol concentrations (2.5-3.5 M). In addition, the hydrogenolysis of glycerol was carried out using carbon-supported monometallic (Pt and Ru) and bimetallic (Au-Ru and Pt-Ru) catalysts under basic aqueous solutions at 200 °C and 4.0 MPa H_2. The authors reported 62% and 60% selectivity to lactic acid at glycerol conversion of 21% and 20% over Pt/C and AuRu/C, respectively[111,113]. Furthermore, Dam et al.[112] demonstrated the conversion of glycerol to lactic acid via the hydrogenolysis process using a $Pt/CaCO_3$ catalyst with 55% selectivity and 46% conversion.

Converting glycerol into lactic acid involves an initial step of oxidative dehydrogenation of glycerol to glyceraldehyde, which, in basic conditions, can be converted to dihydroxyacetone via an equilibrium reaction[118]. The glyceraldehyde and dihydroxyacetone can undergo rearrangement into lactic acid under alkaline conditions, which involves a base-catalyzed dehydration-rearrangement-rehydration mechanism with pyruvaldehyde (methylglyoxal) as an intermediate[117]. Glyceraldehyde has been proposed as the intermediate in the hydrothermal

TH-3456_166107017

conversion of glycerol into lactic acid by Kishida et al.[107] However, an undesired parallel pathway involves the catalytic oxidation of glyceraldehyde/dihydroxyacetone to glyceric acid and other oxidation products like glycolic acid, oxalic acid, acetic acid, and formic acid. Therefore, an optimal catalyst for converting glycerol into lactic acid should possess oxidative dehydrogenation capacity under mild conditions and be a highly inefficient oxidation catalyst for converting glyceraldehyde into glyceric acid and subsequent oxidation products.

Yan et al.[119] conducted a synergistic study on the performance of Ru-Pt/MCM-41 Nanocatalysts in base-free glycerol oxidation. The Ru promotes glyceric acid formation and catalytic kinetics when combined with Pt. The optimal Ru: Pt ratio of 1:1 resulted in a glycerol conversion of 78.2% and a high glyceric acid selectivity of 80.1% with a turnover frequency (TOF) of 823.9 h^{-1} under optimized conditions of 80 °C, 1 MPa O_2, and a reaction time of 12 h. Furthermore, Yan et al.[120] previously studied a PO_4^{3-} coordinated Pt single-atom catalyst supported on hydroxyapatite (HAP) for the selective oxidation of polyols using a hydrothermal strategy. The catalyst demonstrated the ability to selectively oxidize polyols to C_2-C_4 hydroxycarboxylic acids by activating the C-H bond of key oxygen-containing intermediates while suppressing the C-C bond cleavage in an aqueous NaOH medium. Jin et al.[121] studied catalysts based on Ru-MACHO for the one-pot synthesis of lactic acid and formic acid via glycerol dehydrogenation. The study demonstrated that a yield of 40% and 45% of formic acid and lactic acid was achieved under the reaction conditions of 200 °C and 48 h reaction time with 3 mg of the catalyst.

The selective catalytic oxidation over bimetallic catalysts converts glycerol to LA at milder reaction conditions than hydrothermal and hydrogenolysis processes. The inclusion of a second metal, based on the synergy of the two active phases, modifies the active sites to increase selectivity to specific products while promoting system stability. Several catalytic systems have

TH-3456_166107017

been discovered effective in the selective oxidation of glycerol to lactic acid [114–117]. Shen et al.[116] described the conversion of glycerol to lactic acid over Au-Pt, Au, Pt, and Pd catalysts supported on TiO_2. The Au-Pt/TiO_2 (1:1 atomic ratio) bimetallic catalyst showed higher activity (517.1 h^{-1}) with 86% selectivity towards lactic acid. In another study by the same research group[122] on Cu-Pd bimetallic nanoparticle catalysts for converting glycerol to lactic acid, the authors reported that the 1:2 atomic ratio of Cu: Pd gives higher selectivity (95.3%) towards lactic acid. Purushothaman et al.[117] studied the one-pot catalytic conversion of glycerol to lactic acid over Au-Pt/CeO_2 and reported a selectivity to lactic acid of 80% with 99% glycerol conversion. Zhang et al.[123,124] investigated the CeOx-supported Pt-Co bimetallic catalysts for converting glycerol to lactic acid and reported a selectivity of 87.7% lactic acid at a glycerol conversion of 85.3%. The enhanced activity and stability of the bimetallic catalysts are claimed to be due to Pt-Co and metal-CeO_x interactions. Zhang et al.[125] studied the Cu-promoted Pt bimetallic catalysts supported on activated carbon to convert glycerol to lactic acid. The 0.5%Cu-1.0%Pt/AC bimetallic catalyst performs better (80% glycerol conversion and 69.3% lactic acid selectivity) than its monometallic Cu/AC and Pt/AC counterparts.

Mimura et al.[126] investigated the continuous production of lactic acid and glyceric acid through the catalytic oxidation of glycerol over Au-Pt/Al_2O_3 bimetallic catalysts. The authors found that at 85°C and over a reaction time of 1000 min, the conversion of glycerol was 90%, with yields of lactic acid and glyceric acid at 40% and 20-25%, respectively. Xiao et al.[127] examined the impact of base on converting glycerol to lactic acid and glycolic acid over Cu/Al_2O_3. They found that the selectivity to lactic acid is favored in NaOH, while the selectivity to glycolic acid is higher in $NaHCO_3$. Xu et al.[128] investigated the conversion of glycerol to glycolic acid using Copper-Magnesium-based catalysts with different copper-to-magnesium ratios. The results

TH-3456_166107017

showed that the Cu_1Mg_4 catalyst is the most effective, yielding 71.8% glycolic acid. Chu et al.[129] examined the oxidation of glycerol to lactic acid using CrO_x-decorated Fe/TiO_2 catalysts with varying compositions of Cr and Fe. They found that a 5%Fe-10%Cr catalyst was optimal for lactic acid production, with a selectivity of 60.2% at 55.1% glycerol conversion. The researchers also investigated the impact of catalyst reduction temperature on glycerol oxidation. They found that $Fe\text{-}Cr/TiO_2$ reduced at 600°C resulted in the highest selectivity to lactic acid, with an improved conversion of glycerol. Liao et al.[130] reported glycerol oxidation to glycolic acid using Cu-based catalysts with various support systems such as Alumina (Al_2O_3), Ceria (CeO_2), Zirconia (ZrO_2), Hydrotalcite (HT), Activate carbon (AC) (derived from biochar), Carbon nanotubes (CNT), and Graphene nanoplatelets (GNP), in the presence and absence of base. The Cu/AC was the most efficient in glycerol conversion, with the highest selectivity to glycolic acid.

Yin et al.[131] investigated the lactic acid synthesis from biomass-derived glycerol using Ni nanoparticles supported on graphitic carbon under hydrothermal conditions at 230 ^oC and in NaOH. The study examined the effect of Ni percentage on glycerol conversion and lactic acid selectivity. 92.2% selectivity to lactic acid at 97.6% glycerol conversion is achieved with the following reaction conditions: glycerol and NaOH concentrations of 1.0 and 1.1 mol L^{-1} at 230℃ for 3 h over $Ni_{0.3}$/ graphite catalyst. Zhang et al.[132] described the process for glycerol dehydrogenation using encapsulated Cu-based catalysts by utilizing nitrogen-doped carbon. The $Cu\text{-}Cu_2O$@NC-400 catalyst achieved 100% glycerol conversion and 84.8% of lactic acid selectivity at 220 ℃ in 90 min. Shen et al.[133] reported the conversion of glycerol to acrylic acid via an oxy-dehydration reaction using Mo/V and W/V oxide catalysts. Acidic sites on the oxide catalysts facilitate the synthesis of acrolein and acetaldehyde. The acrylic acid yield increases by adding vanadium to MoO_3 ($Mo_1V_{0.25}$) and WO_3 (W_1 $V_{0.25}$). The higher vanadium concentrations

TH-3456_166107017

in the catalysts (Mo_1V_1 & W_1V_1) decrease the formation of acrylic acid. The increased vanadium content in the catalyst results in more V_2O_5, which possesses high oxidation activity and leads to increased oxidation of acrylic acid to CO and CO_2. The vanadium-promoted catalysts (Pt-V/Ce-Zr and V-Pt/Al_2O_3) were used to oxidize diesel exhaust (HC, CO, and NO)[134] and propane[135]. Recently, a few studies reported that the vanadium-promoted catalysts had been used for the glycerol valorization to acrolein[136] and methanol[137]. However, the studies reported so far in the literature used a higher base/glycerol molar ratio and a lower glycerol/metal molar ratio, which are not economical. A detailed literature review is given in Table 1.2 on bimetallic catalysts for converting GL to LA. Most bimetallic catalysts reported for the liquid phase oxidation of glycerol to lactic acid use gold as the primary metal and Pt, Pd, or Ru as the secondary metal. A few studies reported Pt as a primary metal and Ru, Co, and Cu as a second metal.

TH-3456_166107017

Table 1.2: Literature reports bimetallic catalysts for the oxidation of glycerol to lactic acid process.

Catalysts	T (°C)	P (bar)	Gas Medium	time (hr)	base	base/gly (mol/mol)	gly/ metal (mol/mol)	conversion (%)	L.A. selectivity (%)	References
1.9Pt-4.7Ru/C	200	40	H_2	5	NaOH	0.8	700	100	37	[111]
1Au-1Pd/TiO_2	160	10	O_2	2	BF	-	2500	29.7	58.5	[114]
1.5Pt/Sn-MFI	100	6.2	O_2	24	BF	-	350	89.8	80.5	[115]
1Au-1Pt/TiO_2	90	1	O_2	1	NaOH	4	8000	30	86	[116]
0.4Au-0.3Pt/CeO_2	100	5	O_2	0.5	NaOH	4	680	99	80	[117]
1Pt-1Co/CeO_2	200	10	N_2	4	NaOH	1	720	85	87.7	[123]
0.5Au-0.5Pt/Al_2O_3	85	6 (mlpm)	O_2	-	NaOH	4	-	>90	40	[126]
0.5%Cu-1.0%Pt/AC	90	100 (mlpm)	O_2	4	LiOH	1.5	-	80	69.3	[125]
10%Ni-1Co/CeO_2	160	20	N_2	6.5	NaOH	1.5	58.82	97	95.88	[138]
1.39Pt-0.5Co/CeO_2	200	10	N_2	4	NaOH	1	-	98	54	[124]
1Au-0.5Ru/CZ	50	3	O_2	0.25	NaOH	1	1000	28	22	[139]

TH-3456_166107017

1.3 Hypothesis and objectives of the work

Over the past two decades, significant attention has been directed towards designing and developing efficient catalytic systems and microreactor technology for the bio-based chemical industries. Exploring an innovative and efficient catalyst system for converting biomass and its derivatives into lactic acid and 2,5-furandicarboxylic acid (FDCA) under base and base-free conditions represents a developing research area. As far as our understanding goes, there is a scarcity of published reports in the open literature discussing Pt-V and Ru-V bimetallic catalysts supported on activated carbon for producing lactic acid from glycerol. Furthermore, there is a notable absence of literature reporting inexpensive bimetallic catalysts, combining noble and non-noble metals, for the base-free oxidation of 5-HMF to FDCA under aqueous conditions. Reasons for selecting Ru-V and Pt-V bimetallic catalysts.

Synergistic Effects**:** Bimetallic catalysts (such as Ru-V and Pt-V) exhibit synergistic effects where the combination of ruthenium or platinum with vanadium enhances catalytic activity and selectivity compared to catalysts containing only one metal (monometallic catalysts)[117,135,140,141].

Interaction and Active Sites: The interaction between vanadium, ruthenium, or platinum leads to unique active sites on the catalyst surface. These active sites are crucial for catalysing specific reaction pathways.

Electronic Modification: Vanadium modifies the catalyst's electronic properties of ruthenium or platinum. This modification optimizes the adsorption energies of reactants and intermediates on the catalyst surface, which is essential for efficient catalysis. Overall, the synergy between ruthenium or platinum and vanadium in bimetallic catalysts enhances their catalytic

TH-3456_166107017

performance by creating tailored active sites with optimized electronic properties, promoting specific reaction pathways effectively.

The synthesis of 5-HMF from fructose using a micro helical coiled reactor and employing homogeneous catalysts (such as maleic acid) has not been reported in the literature, indicating a gap in research on this specific process and reactor design. The rationale behind employing a tubular helical reactor with a homogeneous catalyst is its potential advantages over a packed-bed reactor with a heterogeneous catalyst for producing HMF from sugar. The advantages include:

Enhanced mass transfer: The helical reactor promotes better mixing and mass transfer, potentially leading to improved reaction kinetics and higher yields of the desired products.

Heat transfer efficiency: The helical configuration allows for efficient heat transfer, which can be crucial in exothermic reactions like those involved in HMF production. This can help control reaction temperature and minimize undesired side reactions.

Homogeneous catalyst activity: Homogeneous catalysts, uniformly distributed in the reaction mixture, can offer high selectivity and activity, leading to efficient sugar conversion into HMF.

Process intensification**:** Tubular helical reactors can facilitate process intensification by enabling higher throughput and reduced residence times compared to packed-bed reactors, potentially increasing productivity and lowering costs.

In contrast, a packed-bed reactor with a heterogeneous catalyst might offer higher stability and easier catalyst separation. Still, it may suffer from mass and heat transfer limitations and potential issues with catalyst deactivation. Moreover, the solid humins formed during the reaction may deposit on the heterogeneous catalyst packing and chock the catalyst bed, leading

TH-3456_166107017

to the reactor's colossal pressure drop and blockage. The choice between the two reactor types depends on reaction kinetics, selectivity, scalability, and operational considerations specific to the HMF production process. Combining a tubular helical reactor and a homogeneous catalyst offers advantages in mass and heat transfer, reaction selectivity, process intensification, and ease of catalyst handling, collectively contributing to improved efficiency and productivity in HMF production from sugar.

The monometallic Pt/AC, Ru/AC, V/AC, and bimetallic Pt-V/AC, Ru-V/AC, and Ru-Ni/AC catalysts were synthesized using the wet-impregnation method. These catalysts were systematically assessed for their efficacy in producing FDCA and lactic acid from HMF and glycerol. In addition, helical coiled reactors were fabricated and employed to dehydrate fructose to HMF. The critical issues for producing all targeted products on a commercial scale are given below.

Competing Reactions: Fructose undergoes multiple reactions under the reaction conditions typically used for HMF production. These include forming levulinic acid and humins, which compete with the desired conversion to HMF. Minimizing these reactions to maximize HMF yield is a challenge.

Catalyst development and selectivity**:** An effective catalyst is crucial for promoting high lactic acid and HMF yields and achieving selective oxidation to FDCA under aqueous base-free conditions. Catalysts must be stable, selective, and be able to minimize by-products such as formic acid, levulinic acid, and humins.

Reaction conditions: Optimizing the reaction parameters such as temperature, pressure, solvent, pH, and catalyst loading is crucial. They affect the selectivity of the desired product (HMF, FDCA, lactic acid) formation, minimize side reactions, and enhance overall yield. Fine-tuning these conditions for commercial-scale processes demands extensive experimentation.

TH-3456_166107017

Feedstock quality and cost: The economic viability of desired product (HMF, FDCA, lactic acid) formation relies on the availability, purity, and cost of their corresponding raw material, crucial for large-scale manufacturing. Efficient biomass-based processes for HMF production are critical.

Scale-up challenges: Transitioning laboratory-scale synthesis to industrial-scale production involves addressing engineering challenges such as reactor design, heat and mass transfer efficiency, and process integration. Maintaining consistent product quality and optimizing production efficiency are key considerations.

Separation and purification: Efficient techniques are essential for separating and purifying desired products from the reaction mixture containing reactants, by-products, and catalyst residues. Developing cost-effective and environmentally sustainable separation techniques is critical for meeting commercial-scale demands.

Product stability: The HMF is susceptible to degradation during storage and handling, affecting product shelf-life and quality. Stabilization methods are needed to ensure product integrity and usability in various applications.

Economic viability: Efficiently producing FDCA from HMF without aqueous bases must be cost-effective, considering catalyst, feedstock, energy, and purification costs relative to market value. Sustainable processes with minimal waste and energy use are crucial, following green chemistry principles to reduce environmental impact. Economic viability depends on feedstock prices, operating conditions, desired product yields, catalyst expenses, energy requirements, and market demand.

TH-3456_166107017

Environmental impact: Developing environmentally sustainable processes with minimal waste generation, energy consumption, and environmental footprint is increasingly essential for commercial production.

1.4 Objectives of the Work

The thesis objectives were formulated to address specific knowledge gaps in the field. These objectives are structured to contribute valuable insights and advancements to the existing body of knowledge.

I. Continuous synthesis of 5-hydroxymethylfurfural from high-concentration fructose feedstock in a micro-helical coiled reactor using homogenous catalysts.

II. Catalytic conversion of 5-hydroxymethylfurfural (HMF) to 2,5-furandicarboxylic acid (FDCA) over activated carbon-supported ruthenium-vanadium bimetallic catalysts under base-free mild reaction conditions.

III. Selective aerobic oxidation of glycerol to lactic acid over ruthenium-vanadium bimetallic catalysts.

IV. Glycerol selective oxidation to lactic acid over platinum-vanadium bimetallic catalysts supported on activated carbon.

TH-3456_166107017

1.5 Organization of the Thesis

The thesis is structured into seven chapters strategically designed to comprehensively address and fulfill the proposed objectives.

CHAPTER 1: Background of the Work and Research Objectives

This chapter introduced the research problem and provided an overview of the relevant literature. Additionally, we have identified the knowledge gap in the existing body of work and outlined the specific research objectives this thesis aims to achieve. Finally, the organizational structure of the thesis is presented.

CHAPTER 2: Materials and Methods

In this chapter, the procedures employed for the preparation of activated carbon-supported monometallic Pt/AC, Ru/AC, V/AC, as well as bimetallic Pt-V/AC, Ru-V/AC, and Ru-Ni/AC catalysts utilizing the wet-impregnation method. The chapter comprehensively evaluates catalyst activity, explicitly focusing on producing lactic acid and 2,5-furandicarboxylic acid (FDCA) conducted in a high-pressure autoclave reactor. Furthermore, we expound upon the process involved in converting fructose to 5-HMF utilizing microreactor technology, incorporating homogeneous catalysts (H_2SO_4 and maleic acid) in dimethyl sulfoxide (DMSO) solvent. The methodologies adopted for the characterization of catalysts and the analysis of resultant products are also elucidated in this chapter.

CHAPTER 3: Continuous synthesis of 5-hydroxymethylfurfural from high-concentration fructose feedstock in a micro-helical coiled reactor using homogenous catalysts.

This chapter presents a comprehensive study on the catalytic dehydration of fructose to 5-hydroxymethylfurfural (HMF) using sulfuric acid and maleic acid as catalysts in helically coiled microreactors. Higher temperatures (180 ^{o}C), lower catalyst concentrations (0.2 wt%),

TH-3456_166107017

higher flow rates (5 mL min^{-1}), and higher fructose concentration (50 wt%) improved the reactor throughput with HMF space-time yield of 380 $g_{HMF}/g_{Cat}/h$. In addition, the dehydration reaction performance with maleic acid was compared with that of H_2SO_4. Interestingly, maleic acid exhibited good selectivity (83%) towards HMF compared to sulfuric acid (80%) due to reduced degradation of HMF to humins.

CHAPTER 4: Catalytic conversion of 5-hydroxymethylfurfural (HMF) to 2,5-furandicarboxylic acid (FDCA) over activated carbon-supported ruthenium-vanadium bimetallic catalysts under base-free mild reaction conditions.

This chapter synthesizes monometallic Ru and V and bimetallic Ru-V and Ru-Ni catalysts supported on activated carbon, characterization, and testing for HMF to FDCA. The synthesized catalysts were thoroughly characterized to obtain morphological and structural properties, elemental composition, and surface area. Further, the synthesized catalysts for 5-hydroxymethylfurfural (HMF) oxidation to FDCA under base-free mild reaction conditions. The 1.5wt%Ru-0.5wt%V/AC (% on a weight basis) bimetallic catalyst performed better than Ru-Ni bimetallic, other Ru-V bimetallic catalysts, and the monometallic Ru/AC, and V/AC. The molar yield of FDCA (74.4%) was the highest in a two-step, single-pot process at optimal conditions (100 ℃ for 2 h, 130 ℃, 2 h, 1.0 MPa O_2) over the 1.5%Ru-0.5%V/AC bimetallic catalyst. In contrast, a molar yield of 65.3% was achieved with 1.5%Ru-0.5%Ni/AC bimetallic catalyst (130 ^oC, 12 h, 1.0 MPa O_2). A simple acetone wash regenerates the 1.5Ru-0.5V/AC bimetallic catalyst nearly to its original performance. The acetone wash removed the humins deposited on the catalyst surface and exposed the active sites to the reaction mixture to regain complete activity.

CHAPTER 5: Selective aerobic oxidation of glycerol to lactic acid over ruthenium-vanadium bimetallic catalysts.

TH-3456_166107017

This chapter demonstrates the catalytic activity of monometallic Ru, V, and bimetallic Ru-V catalysts supported on activated carbon to produce lactic acid from glycerol through selective aerobic oxidation. The Ru-V/AC bimetallic catalyst containing 1.5 wt% Ru and 0.5 wt% V exhibited the best catalytic performance with a lactic acid yield of 75.5% at 98.7% glycerol conversion under mild operating conditions (1 NaOH/glycerol molar ratio, 4400 glycerol/metal molar ratio, 473 K temperature, 5 Bar air pressure and 3 h reaction time). The Ru-V_2O_5/AC (Ru-V/AC) bimetallic catalysts demonstrated superior performance to monometallic Ru and V catalysts, exhibiting a synergistic effect. The Ru-V/AC bimetallic catalyst showed good stability during the reaction with only a marginal loss in activity when reused for four consecutive cycles, suggesting that this catalyst can be recycled multiple times.

CHAPTER 6: Glycerol selective oxidation to lactic acid over platinum-vanadium bimetallic catalysts supported on activated carbon.

This chapter presents the synthesis, characterization, and evaluation of activated carbon-supported Pt-V bimetallic catalysts for selective glycerol oxidation to lactic acid. The physicochemical properties of the prepared catalysts were thoroughly evaluated using various advanced characterization techniques, such as field emission transmission electron microscopy (FETEM), high-resolution transmission electron microscopy (HRTEM), energy dispersive X-ray spectroscopy (EDX), X-ray diffraction (XRD), N_2-sorption analysis, and X-ray photoelectron spectroscopy (XPS). The bimetallic catalysts performed better than monometallic Pt and V catalysts, indicating the synergistic effect. The 1:1 weight ratio of Pt: V (1Pt-1V/AC) showed excellent activity towards lactic acid production from glycerol oxidation with a yield of 80% at 100% glycerol conversion under moderate reaction conditions (NaOH/glycerol = 1:1 mol/mol, 4400 glycerol/metal molar ratio, 473 K, 5 bar air, 12 h reaction time). The 1Pt-1V/C bimetallic catalyst also showed good stability up to four cycles with only minor activity loss in the first cycle.

TH-3456_166107017

CHAPTER 7: Conclusions and Future Work

This chapter briefly discusses the remarkable findings derived from the thesis work. Additionally, it offers recommendations for future research within the thesis field, highlighting the potential avenues for further exploration. To ensure a comprehensive understanding, the chapter acknowledges limitations inherent in the present thesis work, contributing to a nuanced perspective on the study's outcomes.

TH-3456_166107017

References

(1) Bozell, J. J.; Petersen, G. R. Technology Development for the Production of Biobased Products from Biorefinery Carbohydrates - The US Department of Energy's "Top 10" Revisited. Green Chemistry 2010, 12 (4), 539–554. https://doi.org/10.1039/b922014c.

(2) Sajid, M.; Zhao, X.; Liu, D. Production of 2,5-Furandicarboxylic Acid (FDCA) from 5-Hydroxymethylfurfural (HMF): Recent Progress Focusing on the Chemical-Catalytic Routes. Green Chemistry 2018, 20 (24), 5427–5453. https://doi.org/10.1039/c8gc02680g.

(3) J. J. Bozell; G. R. Petersen. Technology Development for the Production of Biobased Products from Biorefinery Carbohydrates—the US Department of Energy's "Top 10" Revisited. Green. Chem. 2010, 12, 539–554.

(4) Chheda, J. N.; Huber, G. W.; Dumesic, J. A. Liquid-Phase Catalytic Processing of Biomass-Derived Oxygenated Hydrocarbons to Fuels and Chemicals. Angew. Chem., Int. Ed. 2007, 46, 7164–7183.

(5) A. Corma; S. Iborra and; A. Velty. Chemical Routes for the Transformation of Biomass into Chemicals. Chem. Rev. 2007, 107, 2411–2502.

(6) P. Gallezot. Conversion of Biomass to Selected Chemical Products†. Chem. Soc. 2012, 41, 1538–1558.

(7) R.-J. van Putten; J. C. van der Waal; E. de Jong; C. B. Rasrendra; H. J. Heeres; J. G. de Vries. Hydroxymethylfurfural, A Versatile Platform Chemical Made from Renewable Resources. Chem. Rev. 2013, 113, 1499–1597.

TH-3456_166107017

(8) X. Cao; S. P. Teong; D. Wu; G. Yi; H. Su; Y. Zhang. An Enzyme Mimic Ammonium Polymer as a Single Catalyst for Glucose Dehydration to 5-Hydroxymethylfurfural†. Green. Chem. 2015, 17, 2348–2352.

(9) Dutta, S.; De, S.; Saha, B. A Brief Summary of the Synthesis of Polyester Building-Block Chemicals and Biofuels from 5-Hydroxymethylfurfural. ChemPlusChem. April 2012, pp 259–272. https://doi.org/10.1002/cplu.201100035.

(10) Lai, L.; Zhang, Y. The Production of 5-Hydroxymethylfurfural from Fructose in Isopropyl Alcohol: A Green and Efficient System. ChemSusChem 2011, 4 (12), 1745–1748. https://doi.org/10.1002/cssc.201100489.

(11) Peng, W. H.; Lee, Y. Y.; Wu, C.; Wu, K. C. W. Acid-Base Bi-Functionalized, Large-Pored Mesoporous Silica Nanoparticles for Cooperative Catalysis of One-Pot Cellulose-to-HMF Conversion. J Mater Chem 2012, 22 (43), 23181–23185. https://doi.org/10.1039/c2jm35391a.

(12) Teong, S. P.; Yi, G.; Zeng, H.; Zhang, Y. The Effects of Emulsion on Sugar Dehydration to 5-Hydroxymethylfurfural in a Biphasic System. Green Chemistry 2015, 17 (7), 3751–3755. https://doi.org/10.1039/c5gc00580a.

(13) Tuteja, J.; Choudhary, H.; Nishimura, S.; Ebitani, K. Direct Synthesis of 1,6-Hexanediol from HMF over a Heterogeneous Pd/ZrP Catalyst Using Formic Acid as Hydrogen Source. ChemSusChem 2014, 7 (1), 96–100. https://doi.org/10.1002/cssc.201300832.

(14) Xiao, B.; Zheng, M.; Li, X.; Pang, J.; Sun, R.; Wang, H.; Pang, X.; Wang, A.; Wang, X.; Zhang, T. Synthesis of 1,6-Hexanediol from HMF over Double-Layered Catalysts of Pd/SiO 2 + Ir-ReO x / SiO 2 in a Fixed-Bed Reactor †. Green. Chem. 2016, 18, 2175–2184. https://doi.org/10.1039/c5gc02228b.

TH-3456_166107017

(15) Wang, X.; Liu, Y.; Liang, X. Hydrogenolysis of 5-Hydroxymethylfurfural to 2,5-Dimethylfuran over Supported Pt-Co Bimetallic Catalysts under Mild Conditions †. Green. Chem. 2018, 20, 2894–2902. https://doi.org/10.1039/c8gc00716k.

(16) Lan, J.; Lin, J.; Chen, Z.; Yin, G. Transformation of 5-Hydroxymethylfurfural (HMF) to Maleic Anhydride by Aerobic Oxidation with Heteropolyacid Catalysts. ACS Catal 2015, 5 (4), 2035–2041. https://doi.org/10.1021/cs501776n.

(17) T. Werpy; G. Petersen. Top Value Added Chemicals from Biomass: Volume I – Results of Screening for Potential Candidates from Sugars and Synthesis Gas, Report DOE/GO-102004-1992; 2004.

(18) Zhang, Z.; Deng, K. Recent Advances in the Catalytic Synthesis of 2,5-Furandicarboxylic Acid and Its Derivatives. ACS Catalysis. American Chemical Society November 6, 2015, pp 6529–6544. https://doi.org/10.1021/acscatal.5b01491.

(19) Yi, G.; Teong, S. P.; Zhang, Y. Base-Free Conversion of 5-Hydroxymethylfurfural to 2,5-Furandicarboxylic Acid over a Ru/C Catalyst. Green. Chem. 2016, 18, 979–983. https://doi.org/10.1039/c5gc01584g.

(20) Yan, D.; Xin, J.; Shi, C.; Lu, X.; Ni, L.; Wang, G.; Zhang, S. Base-Free Conversion of 5-Hydroxymethylfurfural to 2,5-Furandicarboxylic Acid in Ionic Liquids. Chemical Engineering Journal 2017, 323. https://doi.org/10.1016/j.cej.2017.04.021.

(21) Gandini, A.; Silvestre, A. J. D.; Neto, C. P.; Sousa, A. F.; Gomes, M. The Furan Counterpart of Polyethylene Terephthalate An Alternative Material Based on Renewable Resources. J. Polym. Sci. A Polym. Chem., 47: 295-298.

(22) Kim, M.; Su, Y.; Fukuoka, A.; Hensen, E. J. M.; Nakajima, K. Aerobic Oxidation of 5-(Hydroxymethyl)Furfural Cyclic Acetal Enables Selective Furan-2,5-Dicarboxylic Acid

TH-3456_166107017

Formation with CeO2-Supported Gold Catalyst. Angewandte Chemie - International Edition 2018, 57 (27). https://doi.org/10.1002/anie.201805457.

(23) Casanova, O.; Iborra, S.; Corma, A. Biomass into Chemicals: Aerobic Oxidation of 5-Hydroxymethyl-2-Furfural into 2,5-Furandicarboxylic Acid with Gold Nanoparticle Catalysts. ChemSusChem 2009, 2 (12), 1138–1144. https://doi.org/10.1002/cssc.200900137.

(24) Zhang, Z.; Deng, K. Recent Advances in the Catalytic Synthesis of 2,5-Furandicarboxylic Acid and Its Derivatives. ACS Catal 2015, 5 (11), 6529–6544. https://doi.org/10.1021/acscatal.5b01491.

(25) Eerhart, A. J. J. E.; Faaij, A. P. C.; Patel, M. K. Replacing Fossil Based PET with Biobased PEF; Process Analysis, Energy and GHG Balance. Energy Environ Sci 2012, 5 (4), 6407–6422. https://doi.org/10.1039/c2ee02480b.

(26) Saha, B.; Gupta, D.; Abu-Omar, M. M.; Modak, A.; Bhaumik, A. Porphyrin-Based Porous Organic Polymer-Supported Iron(III) Catalyst for Efficient Aerobic Oxidation of 5-Hydroxymethyl-Furfural into 2,5-Furandicarboxylic Acid. J Catal 2013, 299, 316–320. https://doi.org/10.1016/j.jcat.2012.12.024.

(27) Gandini, A.; Silvestre, A. J. D.; Neto, C. P.; Sousa, A. F.; Gomes, M. The Furan Counterpart of Polyethylene Terephthalate: An Alternative Material Based on Renewable Resources. J Polym Sci A Polym Chem 2009, 47 (1), 295–298. https://doi.org/10.1002/pola.23130.

(28) Huang, Y.-T.; Wong, J.-J.; Huang, C.-J.; Li, C.-L.; Jang, G.-W. B. 2,5-Furandicarboxylic Acid Synthesis and Use. Chemicals and Fuels from Bio-Based Building Blocks 2016, 191–216. https://doi.org/10.1002/9783527698202.ch8.

TH-3456_166107017

(29) M. E. Davis. Heterogeneous Catalysis for the Conversion of Sugars into Polymers. Top. Catal. 2015, 58, 405–409.

(30) Pagliaro, M.; Ciriminna, R.; Kimura, H.; Rossi, M.; della Pina, C. From Glycerol to Value-Added Products. Angewandte Chemie - International Edition 2007, 46 (24), 4434–4440. https://doi.org/10.1002/anie.200604694.

(31) Kant, A.; He, Y.; Jawad, A.; Li, X.; Rezaei, F.; Smith, J. D.; Rownaghi, A. A. Hydrogenolysis of Glycerol over Ni, Cu, Zn, and Zr Supported on H-Beta. Chemical Engineering Journal. 2017, pp 1–8. https://doi.org/10.1016/j.cej.2017.02.064.

(32) Roy, D.; Subramaniam, B.; Chaudhari, R. v. Aqueous Phase Hydrogenolysis of Glycerol to 1,2-Propanediol without External Hydrogen Addition. Catal Today 2010, 156 (1–2), 31–37. https://doi.org/10.1016/j.cattod.2010.01.007.

(33) Qin, L. Z.; Song, M. J.; Chen, C. L. Aqueous-Phase Deoxygenation of Glycerol to 1,3-Propanediol over Pt/WO3/ZrO2 Catalysts in a Fixed-Bed Reactor. Green Chemistry 2010, 12 (8), 1466–1472. https://doi.org/10.1039/c0gc00005a.

(34) Corma, A.; Huber, G. W.; Sauvanaud, L.; O'Connor, P. Biomass to Chemicals: Catalytic Conversion of Glycerol/Water Mixtures into Acrolein, Reaction Network. J Catal 2008, 257 (1), 163–171. https://doi.org/10.1016/j.jcat.2008.04.016.

(35) Carrettin, S.; McMorn, P.; Johnston, P.; Griffin, K.; Hutchings, G. J. Selective Oxidation of Glycerol to Glyceric Acid Using a Gold Catalyst in Aqueous Sodium Hydroxide. Chemical Communications 2002, 7, 696–697. https://doi.org/10.1039/b201112n.

(36) Dimitratos, N.; Villa, A.; Bianchi, C. L.; Prati, L.; Makkee, M. Gold on Titania: Effect of Preparation Method in the Liquid Phase Oxidation. Applied Catalysis A: General. 2006, pp 185–192. https://doi.org/10.1016/j.apcata.2006.06.026.

TH-3456_166107017

(37) Zhou, C. H.; Beltramini, J. N.; Lu, G. Q. Chemoselective Catalytic Conversion of Glycerol as a Biorenewable Source to Valuable Commodity Chemicals. Chem Soc Rev 2008, 37 (3), 527–549. https://doi.org/10.1039/b707343g.

(38) Fan, Y.; Zhou, C.; Zhu, X. Catalysis Reviews Selective Catalysis of Lactic Acid to Produce Commodity Chemicals Selective Catalysis of Lactic Acid to Produce Commodity Chemicals. 2009. https://doi.org/10.1080/01614940903048513.

(39) Dusselier, M.; Wouwe, P. van; Dewaele, A.; Makshina, E.; Sels, B. F. Lactic Acid as a Platform Chemical in the Biobased Economy: The Role of Chemocatalysis. Energy Environ. Sci. 2013, 6, 1415–1442. https://doi.org/10.1039/c3ee00069a.

(40) Ivi Mä Ki-Arvela, P.; Simakova, I. L.; Salmi, T.; Murzin, D. Y. Production of Lactic Acid/Lactates from Biomass and Their Catalytic Transformations to Commodities. 2013. https://doi.org/10.1021/cr400203v.

(41) Pereira, C. S. M.; Silva, V. M. T. M.; Rodrigues, A. E. Ethyl Lactate as a Solvent: Properties, Applications and Production Processes – a Review. 2011. https://doi.org/10.1039/c1gc15523g.

(42) Li, R.; Greenchem, /; Sun, D.; Yamada, Y.; Sato, S.; Ueda, W. Glycerol as a Potential Renewable Raw Material for Acrylic Acid Production. Green Chemistry 2017, 19, 3186. https://doi.org/10.1039/c7gc00358g.

(43) Starr, J. N.; Westhoff, G. Lactic Acid. Lactic Acid. InUllmann's Encyclopediaof Industrial Chemistry; Wiley-VCH Verlag GmbH & Co. KGaA:Weinheim, Germany.DOI: 10.1002/14356007.a15_097.pub3.; 2014; pp 1–8.

TH-3456_166107017

(44) Kong, X.; Zhu, Y.; Fang, Z.; Kozinski, J. A.; Butler, I. S.; Xu, L.; Song, H.; Wei, X. Catalytic Conversion of 5-Hydroxymethylfurfural to Some Value-Added Derivatives. Green Chemistry 2018, 20 (16). https://doi.org/10.1039/c8gc00234g.

(45) Rosatella, A. A.; Simeonov, S. P.; Frade, R. F. M.; Afonso, C. A. M. 5-Hydroxymethylfurfural (HMF) as a Building Block Platform: Biological Properties, Synthesis and Synthetic Applications. Green Chemistry 2011, 13 (4). https://doi.org/10.1039/c0gc00401d.

(46) Baroncini, E. A.; Kumar Yadav, S.; Palmese, G. R.; Stanzione, J. F. Recent Advances in Bio-Based Epoxy Resins and Bio-Based Epoxy Curing Agents. Journal of Applied Polymer Science. 2016. https://doi.org/10.1002/app.44103.

(47) He, J.; Huang, K.; Barnett, K. J.; Krishna, S. H.; Alonso, D. M.; Brentzel, Z. J.; Burt, S. P.; Walker, T.; Banholzer, W. F.; Maravelias, C. T.; Hermans, I.; Dumesic, J. A.; Huber, G. W. New Catalytic Strategies for α,ω-Diols Production from Lignocellulosic Biomass. Faraday Discuss 2017, 202. https://doi.org/10.1039/c7fd00036g.

(48) He, J.; Burt, S. P.; Ball, M.; Zhao, D.; Hermans, I.; Dumesic, J. A.; Huber, G. W. Synthesis of 1,6-Hexanediol from Cellulose Derived Tetrahydrofuran-Dimethanol with Pt-WOx/TiO2 Catalysts. ACS Catal 2018, 8 (2). https://doi.org/10.1021/acscatal.7b03593.

(49) Hu, L.; Li, T.; Xu, J.; He, A.; Tang, X.; Chu, X.; Xu, J. Catalytic Transfer Hydrogenation of Biomass-Derived 5-Hydroxymethylfurfural into 2,5-Dihydroxymethylfuran over Magnetic Zirconium-Based Coordination Polymer. Chemical Engineering Journal 2018, 352. https://doi.org/10.1016/j.cej.2018.07.007.

TH-3456_166107017

(50) Román-Leshkov, Y.; Barrett, C. J.; Liu, Z. Y.; Dumesic, J. A. Production of Dimethylfuran for Liquid Fuels from Biomass-Derived Carbohydrates. Nature 2007, 447 (7147). https://doi.org/10.1038/nature05923.

(51) Girisuta, B.; Janssen, L. P. B. M.; Heeres, H. J. A Kinetic Study on the Decomposition of 5-Hydroxymethylfurfural into Levulinic Acid. Green Chemistry 2006, 8 (8). https://doi.org/10.1039/b518176c.

(52) Dutta, S.; Yu, I. K. M.; Tsang, D. C. W.; Ng, Y. H.; Ok, Y. S.; Sherwood, J.; Clark, J. H. Green Synthesis of Gamma-Valerolactone (GVL) through Hydrogenation of Biomass-Derived Levulinic Acid Using Non-Noble Metal Catalysts: A Critical Review. Chemical Engineering Journal 2019, 372. https://doi.org/10.1016/j.cej.2019.04.199.

(53) Alonso, D. M.; Wettstein, S. G.; Dumesic, J. A. Gamma-Valerolactone, a Sustainable Platform Molecule Derived from Lignocellulosic Biomass. Green Chemistry. 2013. https://doi.org/10.1039/c3gc37065h.

(54) Wang, Z.; Chen, Q. Conversion of 5-Hydroxymethylfurfural into 5-Ethoxymethylfurfural and Ethyl Levulinate Catalyzed by MOF-Based Heteropolyacid Materials. Green Chemistry 2016, 18 (21). https://doi.org/10.1039/c6gc01206j.

(55) Chithra, P. A.; Darbha, S. Catalytic Conversion of HMF into Ethyl Levulinate – A Biofuel over Hierarchical Zeolites. Catal Commun 2020, 140. https://doi.org/10.1016/j.catcom.2020.105998.

(56) Chheda, J. N.; Román-Leshkov, Y.; Dumesic, J. A. Production of 5-Hydroxymethylfurfural and Furfural by Dehydration of Biomass-Derived Mono- and Poly-Saccharides. Green Chemistry 2007, 9 (4). https://doi.org/10.1039/b611568c.

TH-3456_166107017

(57) Daorattanachai, P.; Khemthong, P.; Viriya-Empikul, N.; Laosiripojana, N.; Faungnawakij, K. Conversion of Fructose, Glucose, and Cellulose to 5-Hydroxymethylfurfural by Alkaline Earth Phosphate Catalysts in Hot Compressed Water. Carbohydr Res 2012, 363. https://doi.org/10.1016/j.carres.2012.09.022.

(58) Kumar Yedla, S.; Velaga, B.; Choudhury, S.; Namdeo, A.; Kumar Golder, A.; Rao Peela, N. -Butyl-3-Methylimidazolium Bromide Functionalized Zeolites: Nature of Interactions and Catalytic Activity for Carbohydrate Conversion to Platform Chemicals †. Cite this: React. Chem. Eng 2020, 5, 1738. https://doi.org/10.1039/d0re00277a.

(59) Peela, N. R.; Yedla, S. K.; Velaga, B.; Kumar, A.; Golder, A. K. Choline Chloride Functionalized Zeolites for the Conversion of Biomass Derivatives to 5-Hydroxymethylfurfural. Appl Catal A Gen 2019, 580, 59–70. https://doi.org/10.1016/J.APCATA.2019.05.005.

(60) Velaga, B.; Peela, N. R. Seed-Assisted and OSDA-Free Synthesis of H-Mordenite Zeolites for Efficient Production of 5-Hydroxymethylfurfural from Glucose. Microporous and Mesoporous Materials 2019, 279, 211–219. https://doi.org/10.1016/J.MICROMESO.2018.12.028.

(61) Kuster, B. F. M. 5-Hydroxymethylfurfural (HMF). A Review Focussing on Its Manufacture. Starch - Stärke 1990, 42 (8). https://doi.org/10.1002/star.19900420808.

(62) Zakrzewska, M. E.; Bogel-Łukasik, E.; Bogel-Łukasik, R. Ionic Liquid-Mediated Formation of 5-Hydroxymethylfurfural-A Promising Biomass-Derived Building Block. Chem Rev 2011, 111 (2). https://doi.org/10.1021/cr100171a.

(63) Kruger, J. S.; Choudhary, V.; Nikolakis, V.; Vlachos, D. G. Elucidating the Roles of Zeolite H-BEA in Aqueous-Phase Fructose Dehydration and HMF Rehydration. ACS Catal 2013, 3 (6). https://doi.org/10.1021/cs4002157.

TH-3456_166107017

(64) León, M.; Swift, T. D.; Nikolakis, V.; Vlachos, D. G. Adsorption of the Compounds Encountered in Monosaccharide Dehydration in Zeolite Beta. Langmuir 2013, 29 (22). https://doi.org/10.1021/la401138g.

(65) Moliner, M.; Román-Leshkov, Y.; Davis, M. E. Tin-Containing Zeolites Are Highly Active Catalysts for the Isomerization of Glucose in Water. Proc Natl Acad Sci U S A 2010, 107 (14). https://doi.org/10.1073/pnas.1002358107.

(66) Swift, T. D.; Nguyen, H.; Erdman, Z.; Kruger, J. S.; Nikolakis, V.; Vlachos, D. G. Tandem Lewis Acid/Brønsted Acid-Catalyzed Conversion of Carbohydrates to 5-Hydroxymethylfurfural Using Zeolite Beta. J Catal 2016, 333. https://doi.org/10.1016/j.jcat.2015.10.009.

(67) Dutta, S.; De, S.; Patra, A. K.; Sasidharan, M.; Bhaumik, A.; Saha, B. Microwave Assisted Rapid Conversion of Carbohydrates into 5-Hydroxymethylfurfural Catalyzed by Mesoporous TiO2 Nanoparticles. Appl Catal A Gen 2011, 409–410. https://doi.org/10.1016/j.apcata.2011.09.037.

(68) Qi, X.; Watanabe, M.; Aida, T. M.; Smith, R. L. Catalytical Conversion of Fructose and Glucose into 5-Hydroxymethylfurfural in Hot Compressed Water by Microwave Heating. Catal Commun 2008, 9 (13). https://doi.org/10.1016/j.catcom.2008.04.025.

(69) Watanabe, M.; Aizawa, Y.; Iida, T.; Aida, T. M.; Levy, C.; Sue, K.; Inomata, H. Glucose Reactions with Acid and Base Catalysts in Hot Compressed Water at 473 K. Carbohydr Res 2005, 340 (12). https://doi.org/10.1016/j.carres.2005.06.017.

(70) Qi, X.; Watanabe, M.; Aida, T. M.; Smith, R. L. Sulfated Zirconia as a Solid Acid Catalyst for the Dehydration of Fructose to 5-Hydroxymethylfurfural. Catal Commun 2009, 10 (13). https://doi.org/10.1016/j.catcom.2009.05.029.

TH-3456_166107017

(71) Shimizu, K. ichi; Uozumi, R.; Satsuma, A. Enhanced Production of Hydroxymethylfurfural from Fructose with Solid Acid Catalysts by Simple Water Removal Methods. Catal Commun 2009, 10 (14). https://doi.org/10.1016/j.catcom.2009.06.012.

(72) Ordomsky, V. v.; van der Schaaf, J.; Schouten, J. C.; Nijhuis, T. A. Fructose Dehydration to 5-Hydroxymethylfurfural over Solid Acid Catalysts in a Biphasic System. ChemSusChem 2012, 5 (9). https://doi.org/10.1002/cssc.201200072.

(73) Lansalot-Matras, C.; Moreau, C. Dehydration of Fructose into 5-Hydroxymethylfurfural in the Presence of Ionic Liquids. Catal Commun 2003, 4 (10). https://doi.org/10.1016/S1566-7367(03)00133-X.

(74) Aellig, C.; Hermans, I. Continuous D-Fructose Dehydration to 5-Hydroxymethylfurfural under Mild Conditions. ChemSusChem 2012, 5 (9). https://doi.org/10.1002/cssc.201200279.

(75) Desir, P.; Vlachos, D. G. Intensified Reactive Extraction for the Acid-Catalyzed Conversion of Fructose to 5-Hydroxymethyl Furfural. Chemical Engineering Journal 2022, 428, 132556. https://doi.org/10.1016/J.CEJ.2021.132556.

(76) Desir, P.; Saha, B.; Vlachos, D. G. Ultrafast Flow Chemistry for the Acid-Catalyzed Conversion of Fructose. Energy Environ Sci 2019, 12 (8). https://doi.org/10.1039/c9ee01189g.

(77) Tuercke, T.; Panic, S.; Loebbecke, S. Microreactor Process for the Optimized Synthesis of 5-Hydroxymethylfurfural: A Promising Building Block Obtained by Catalytic Dehydration of Fructose. Chem Eng Technol 2009, 32 (11). https://doi.org/10.1002/ceat.200900427.

TH-3456_166107017

(78) Román-Leshkov, Y.; Chheda, J. N.; Dumesic, J. A. Phase Modifiers Promote Efficient Production of Hydroxymethylfurfural from Fructose. https://www.science.org.

(79) Guo, W.; Zhang, Z.; Hacking, J.; Heeres, H. J.; Yue, J. Selective Fructose Dehydration to 5-Hydroxymethylfurfural from a Fructose-Glucose Mixture over a Sulfuric Acid Catalyst in a Biphasic System: Experimental Study and Kinetic Modelling. Chemical Engineering Journal 2021, 409. https://doi.org/10.1016/j.cej.2020.128182.

(80) Shimanouchi, T.; Kataoka, Y.; Tanifuji, T.; Kimura, Y.; Fujioka, S.; Terasaka, K. Chemical Conversion and Liquid-Liquid Extraction of 5-Hydroxymethylfurfural from Fructose by Slug Flow Microreactor. AIChE Journal 2016, 62 (6), 2135–2143. https://doi.org/10.1002/AIC.15201.

(81) Guo, W.; Heeres, H. J.; Yue, J. Continuous Synthesis of 5-Hydroxymethylfurfural from Glucose Using a Combination of AlCl3 and HCl as Catalyst in a Biphasic Slug Flow Capillary Microreactor. Chemical Engineering Journal 2020, 381, 122754. https://doi.org/10.1016/J.CEJ.2019.122754.

(82) Gorbanev, Y. Y.; Klitgaard, S. K.; Woodley, J. M.; Christensen, C. H.; Riisager, A. Gold-Catalyzed Aerobic Oxidation of 5-Hydroxymethylfurfural in Water at Ambient Temperature. ChemSusChem 2009, 2 (7), 672–675. https://doi.org/10.1002/cssc.200900059.

(83) Davis, S. E.; Houk, L. R.; Tamargo, E. C.; Datye, A. K.; Davis, R. J. Oxidation of 5-Hydroxymethylfurfural over Supported Pt, Pd and Au Catalysts. Catal Today 2011, 160 (1), 55–60. https://doi.org/10.1016/j.cattod.2010.06.004.

(84) Leandro Ardemani; Giannantonio Cibin; Andrew J. Dent; Mark A. Isaacs; Georgios Kyriakou; Adam F. Lee; Christopher M. A. Parlett; Stephen A. Parry; Karen Wilson.

TH-3456_166107017

Solid Base Catalysed 5-HMF Oxidation to 2,5-FDCA over Au/Hydrotalcites: Fact or Fiction?†. Chem. Sci. 2015, 6, 4940–4945.

(85) Ait Rass, H.; Essayem, N.; Besson, M. Selective Aerobic Oxidation of 5-HMF into 2,5-Furandicarboxylic Acid with Pt Catalysts Supported on TiO2- and ZrO2-Based Supports. ChemSusChem 2015, 8 (7), 1206–1217. https://doi.org/10.1002/cssc.201403390.

(86) Chen, C. T.; van Nguyen, C.; Wang, Z. Y.; Bando, Y.; Yamauchi, Y.; Bazziz, M. T. S.; Fatehmulla, A.; Farooq, W. A.; Yoshikawa, T.; Masuda, T.; Wu, K. C. W. Hydrogen Peroxide Assisted Selective Oxidation of 5-Hydroxymethylfurfural in Water under Mild Conditions. ChemCatChem 2018, 10 (2), 361–365. https://doi.org/10.1002/cctc.201701302.

(87) Yanbing Wang; Kai Yu; da Lei; Wei Si; Yajun Feng; Lan-Lan Lou; Shuangxi Liu. Basicity-Tuned Hydrotalcite-Supported Pd Catalysts for Aerobic Oxidation of 5-Hydroxymethyl-2-Furfural under Mild Conditions. ACS Sustainable Chem. Eng. 2016, 4 (9), 4752–4761.

(88) HaoChen; JinshanShen; KequanChen; YongQin; XiuyangLu; Pingkai Ouyanga; JieFu. Atomic Layer Deposition of Pt Nanoparticles on Low Surface Area Zirconium Oxide for the Efficient Base-Free Oxidation of 5-Hydroxymethylfurfural to 2,5-Furandicarboxylic Acid. Appl Catal A Gen 2018, 555, 98–107.

(89) Zhou, C.; Deng, W.; Wan, X.; Zhang, Q.; Yang, Y.; Wang, Y. Functionalized Carbon Nanotubes for Biomass Conversion: The Base-Free Aerobic Oxidation of 5-Hydroxymethylfurfural to 2,5-Furandicarboxylic Acid over Platinum Supported on a Carbon Nanotube Catalyst. ChemCatChem 2015, 7 (18), 2853–2863. https://doi.org/10.1002/cctc.201500352.

TH-3456_166107017

(90) Xuewang Han; Liang Geng; Yong Guo; Rong Jia; Xiaohui Liu; Yongguang Zhang; Yanqin Wang. Base-Free Aerobic Oxidation of 5-Hydroxymethylfurfural to 2,5-Furandicarboxylic Acid over a Pt_C–O–Mg Catalyst. Green Chem. 2016, 18, 1597–1604.

(91) Wan, X.; Zhou, C.; Chen, J.; Deng, W.; Zhang, Q.; Yang, Y.; Wang, Y. Base-Free Aerobic Oxidation of 5-Hydroxymethyl-Furfural to 2,5-Furandicarboxylic Acid in Water Catalyzed by Functionalized Carbon Nanotube-Supported Au-Pd Alloy Nanoparticles. ACS Catal 2014, 4 (7), 2175–2185. https://doi.org/10.1021/cs5003096.

(92) Zhi Gao; Renfeng Xie; Guoli Fan; Lan Yang; Feng Li. Highly Efficient and Stable Bimetallic AuPd over La-Doped Ca–Mg–Al Layered Double Hydroxide for Base-Free Aerobic Oxidation of 5-Hydroxymethylfurfural in Water. ACS Sustainable Chem. Eng. 2017, 5 (7), 5852–5861.

(93) Bonincontro, D.; Lolli, A.; Villa, A.; Prati, L.; Dimitratos, N.; Veith, G. M.; Chinchilla, L. E.; Botton, G. A.; Cavani, F.; Albonetti, S. AuPd-NNiO as an Effective Catalyst for the Base-Free Oxidation of HMF under Mild Reaction Conditions †. Green. Chem. 2019, 21, 4090–4099. https://doi.org/10.1039/c9gc01283d.

(94) Jinshan Shen; Hao Chen; Kequan Chen; Yong Qin§Orcid; Xiuyang Lu; Pingkai Ouyang; Jie Fu. Atomic Layer Deposition of a Pt-Skin Catalyst for Base-Free Aerobic Oxidation of 5-Hydroxymethylfurfural to 2,5-Furandicarboxylic Acid. Ind. Eng. Chem. Res. 2018, 57 (8), 2811–2818.

(95) Yury Y. Gorbanev; Słren Kegnæs; Anders Riisager. Effect of Support in Heterogeneous Ruthenium Catalysts Used for the Selective Aerobic Oxidation of HMF in Water. Top. Catal. 2011, 54, 1318–1324.

TH-3456_166107017

(96) Artz, J.; Palkovits, R. Base-Free Aqueous-Phase Oxidation of 5-Hydroxymethylfurfural over Ruthenium Catalysts Supported on Covalent Triazine Frameworks. ChemSusChem 2015, 8 (22), 3832–3838. https://doi.org/10.1002/cssc.201501106.

(97) TianyuGao; YongxuanYin; WenhaoFang; QiueCao. Highly Dispersed Ruthenium Nanoparticles on Hydroxyapatite as Selective and Reusable Catalyst for Aerobic Oxidation of 5-Hydroxymethylfurfural to 2,5-Furandicarboxylic Acid under Base-Free Conditions. Mol. Catal. 2018, 450, 55–64.

(98) Dinesh Kumar Mishra; Hye Jin Lee; Jinsung Kim; Hong-Shik Lee; Jin Ku Cho; Young-Woong Suh; Yongjin Yid; Yong Jin Kim. MnCo2O4 Spinel Supported Ruthenium Catalyst for Air-Oxidation of HMF to FDCA under Aqueous Phase and Base-Free Conditions†. Green Chem. 2017, 19, 1619–1623.

(99) Pichler, C. M.; Al-Shaal, M. G.; Gu, D.; Joshi, H.; Ciptonugroho, W.; Schüth, F. Ruthenium Supported on High-Surface-Area Zirconia as an Efficient Catalyst for the Base-Free Oxidation of 5-Hydroxymethylfurfural to 2,5-Furandicarboxylic Acid. ChemSusChem 2018, 11 (13), 2083–2090. https://doi.org/10.1002/cssc.201800448.

(100) Lai, J.; Liu, K.; Zhou, S.; Zhang, D.; Liu, X.; Xu, Q.; Yin, D. Selective Oxidation of 5-Hydroxymethylfurfural into 2,5-Diformylfuran over VPO Catalysts under Atmospheric Pressure †. RSC Adv. 2019, 9, 14242–14246. https://doi.org/10.1039/c9ra02213a.

(101) Lai, J.; Zhou, S.; Cheng, F.; Guo, D.; Liu, X.; Xu, Q.; Yin, D. Efficient and Selective Oxidation of 5-Hydroxymethylfurfural into 2, 5-Diformylfuran Catalyzed by Magnetic Vanadium-Based Catalysts with Air as Oxidant. Catal Letters 2020, 3, 1301–1308. https://doi.org/10.1007/s10562-019-03041-w.

(102) Gao, T.; Zhang, H.; Hu, C.; Jing, F.; Fang, W. Base-Free Aerobic Oxidation of 5-Hydroxymethylfurfural on a Ru(0) Center in Cooperation with a Co(II)/Co(III) Redox

TH-3456_166107017

Pair over the One-Pot Synthesized Ru−Co Composites. Cite This: Ind. Eng. Chem. Res 2020, 59, 17200–17209. https://doi.org/10.1021/acs.iecr.0c00937.

(103) Tirsoaga, A.; Fergani, M. el; Parvulescu, V. I.; Coman, S. M. Upgrade of 5-Hydroxymethylfurfural to Dicarboxylic Acids onto Multifunctional-Based Fe 3 O 4 @SiO 2 Magnetic Catalysts. ACS Sustainable Chem. Eng. 2018, 6,11, 14292–14301. https://doi.org/10.1021/acssuschemeng.8b02962.

(104) Ghaffar, T.; Irshad, M.; Anwar, Z.; Aqil, T.; Zulifqar, Z.; Tariq, A.; Kamran, M.; Ehsan, N.; Mehmood, S. Recent Trends in Lactic Acid Biotechnology: A Brief Review on Production to Purification. J Radiat Res Appl Sci 2014, 7 (2), 222–229. https://doi.org/10.1016/J.JRRAS.2014.03.002.

(105) Corma Canos, A.; Iborra, S.; Velty, A. Chemical Routes for the Transformation of Biomass into Chemicals. Chemical Reviews. 2007, pp 2411–2502. https://doi.org/10.1021/cr050989d.

(106) Ramírez-López, C. A.; Ochoa-Gómez, J. R.; Fernández-Santos, M.; Gómez-Jiménez-Aberasturi, O.; Alonso-Vicario, A.; Torrecilla-Soria, J. Synthesis of Lactic Acid by Alkaline Hydrothermal Conversion of Glycerol at High Glycerol Concentration. Industrial and Engineering Chemistry Research. 2010, pp 6270–6278. https://doi.org/10.1021/ie1001586.

(107) Kishida, H.; Jin, F.; Zhou, Z.; Moriya, T.; Enomoto, H. Conversion of Glycerin into Lactic Acid by Alkaline Hydrothermal Reaction. Chem Lett 2005, 34 (11), 1560–1561. https://doi.org/10.1246/cl.2005.1560.

(108) Shen, Z.; Jin, F.; Zhang, Y.; Wu, B.; Kishita, A.; Tohji, K.; Kishida, H. Effect of Alkaline Catalysts on Hydrothermal Conversion of Glycerin into Lactic Acid. Industrial and

TH-3456_166107017

Engineering Chemistry Research. 2009, pp 8920–8925. https://doi.org/10.1021/ie900937d.

(109) Chen, L.; Ren, S.; Ye, X. P. Lactic Acid Production from Glycerol Using CaO as Solid Base Catalyst. Fuel Processing Technology. 2014, pp 40–47. https://doi.org/10.1016/j.fuproc.2013.11.019.

(110) Haixu Yin; Changhua Zhang; Hengbo Yin⇑; Dezhi Gao; Lingqin Shen; Aili Wang. Hydrothermal Conversion of Glycerol to Lactic Acid Catalyzed by Cu_hydroxyapatite, Cu_MgO, and Cu_ZrO2 and Reaction Kinetics. Chemical Engineering Journal 2016, No. 288, 333–342.

(111) Maris, E. P.; Ketchie, W. C.; Murayama, M.; Davis, R. J. Glycerol Hydrogenolysis on Carbon-Supported PtRu and AuRu Bimetallic Catalysts. Journal of Catalysis. 2007, pp 281–294. https://doi.org/10.1016/j.jcat.2007.08.007.

(112) J. ten Dam; F. Kapteijn; K. Djanashvili; U. Hanefeld. Tuning Selectivity of Pt/CaCO3 in Glycerol Hydrogenolysis — A Design of Experiments Approach. Catal Commun 2011, 13 (1), 1–5.

(113) Maris, E. P.; Davis, R. J. Hydrogenolysis of Glycerol over Carbon-Supported Ru and Pt Catalysts. Journal of Catalysis. 2007, pp 328–337. https://doi.org/10.1016/j.jcat.2007.05.008.

(114) Xu, J.; Zhang, H.; Zhao, Y.; Yu, B.; Chen, S.; Li, Y.; Hao, L.; Liu, Z. Selective Oxidation of Glycerol to Lactic Acid under Acidic Conditions Using AuPd/TiO2 Catalyst. Green Chemistry. 2013, pp 1520–1525. https://doi.org/10.1039/c3gc40314a.

TH-3456_166107017

(115) Hong Je Cho; Chun-Chih Changa; Wei Fan. Base Free, One-Pot Synthesis of Lactic Acid from Glycerol Using a Bifunctional Pt/Sn-MFI Catalyst. Green Chemistry 2014, 16 (7), 3428–3433. https://doi.org/10.1039/c4gc00723a.

(116) Shen, Y.; Zhang, S.; Li, H.; Ren, Y.; Liu, H. Efficient Synthesis of Lactic Acid by Aerobic Oxidation of Glycerol on Au-Pt/TiO2 Catalysts. Chemistry - A European Journal. 2010, pp 7368–7371. https://doi.org/10.1002/chem.201000740.

(117) Purushothaman, R. K. P.; van Haveren, J.; van Es, D. S.; Melián-Cabrera, I.; Meeldijk, J. D.; Heeres, H. J. An Efficient One Pot Conversion of Glycerol to Lactic Acid Using Bimetallic Gold-Platinum Catalysts on a Nanocrystalline CeO2 Support. Appl Catal B 2014, 147, 92–100. https://doi.org/10.1016/j.apcatb.2013.07.068.

(118) Nagorski, R. W.; Richard, J. P. Mechanistic Imperatives for Aldose - Ketose Isomerization in Water: Specific, General Base- and Metal Ion-Catalyzed Isomerization of Glyceraldehyde with Proton and Hydride Transfer. J Am Chem Soc 2001, 123 (5). https://doi.org/10.1021/ja003433a.

(119) Yan, H.; Yao, S.; Yin, B.; Liang, W.; Jin, X.; Feng, X.; Liu, Y.; Chen, X.; Yang, C. Synergistic Effects of Bimetallic PtRu/MCM-41 Nanocatalysts for Glycerol Oxidation in Base-Free Medium: Structure and Electronic Coupling Dependent Activity. Appl Catal B 2019, 259, 118070. https://doi.org/10.1016/J.APCATB.2019.118070.

(120) Yan, H.; Zhao, M.; Feng, X.; Zhao, S.; Zhou, X.; Li, S.; Zha, M.; Meng, F.; Chen, X.; Liu, Y.; Chen, D.; Yan, N.; Yang, C. PO43− Coordinated Robust Single-Atom Platinum Catalyst for Selective Polyol Oxidation**. Angewandte Chemie - International Edition 2022, 61 (21). https://doi.org/10.1002/anie.202116059.

TH-3456_166107017

(121) Jin, M.; Wang, C.; Song, X.; Song, Y.; Shen, Z.; Zhang, Y. Dehydrogenation of Glycerol for CO2 Reduction in One-Pot Production of Lactic Acid and Formic Acid with Ru-MACHO. ChemCatChem 2023. https://doi.org/10.1002/cctc.202201541.

(122) Shen, L.; Zhou, X.; Zhang, C.; Yin, H.; Wang, A.; Wang, C. Functional Characterization of Bimetallic CuPdx Nanoparticles in Hydrothermal Conversion of Glycerol to Lactic Acid. Journal of Food Biochemistry. 2019. https://doi.org/10.1111/jfbc.12931.

(123) Zhang, G.; Jin, X.; Guan, Y.; Yin, B.; Chen, X.; Liu, Y.; Feng, X.; Shan, H.; Yang, C. Toward Selective Dehydrogenation of Glycerol to Lactic Acid over Bimetallic Pt-Co/CeOx Catalysts. Ind Eng Chem Res 2019, 58 (31), 14548–14558. https://doi.org/10.1021/ACS.IECR.9B01918.

(124) Zhang, G.; Jin, X.; Li, X.; Meng, K.; Wang, J.; Zhang, Q.; Chen, X.; Liu, Y.; Feng, X.; Yang, C. Electronic Coupling Enhanced PtCo/CeO2 Hybrids as Highly Active Catalysts for the Key Dehydrogenation Step in Conversion of Bio-Derived Polyols. Chem Eng Sci 2021, 229, 116060. https://doi.org/10.1016/J.CES.2020.116060.

(125) Zhang, C.; Wang, T.; Liu, X.; Ding, Y. Cu-Promoted Pt/Activated Carbon Catalyst for Glycerol Oxidation to Lactic Acid. J Mol Catal A Chem 2016, 424, 91–97. https://doi.org/10.1016/J.MOLCATA.2016.08.018.

(126) Mimura, N.; Muramatsu, N.; Hiyoshi, N.; Sato, O.; Yamaguchi, A. Continuous Production of Glyceric Acid and Lactic Acid by Catalytic Oxidation of Glycerol over an Au–Pt/Al2O3 Bimetallic Catalyst Using a Liquid-Phase Flow Reactor. Catalysis Today. 2020. https://doi.org/10.1016/j.cattod.2020.03.029.

(127) Shuguang Xu; Qing Tian; Yuan Xiao; Wenyu Zhang; Shengqi Liao; Jianmei Li; Changwei Hu. Regulating the Competitive Reaction Pathway in Glycerol Conversion to Lactic Acid-Glycolic Acid Selectively. J Catal 2022, 413, 407–416.

TH-3456_166107017

(128) Xu, S.; Xiao, Y.; Zhang, W.; Liao, S.; Yang, R.; Li, J.; Hu, C. Relay Catalysis of Copper-Magnesium Catalyst on Efficient Valorization of Glycerol to Glycolic Acid. Chemical Engineering Journal 2022, 428. https://doi.org/10.1016/j.cej.2021.132555.

(129) Dawang Chu; Hui Zhou; Zhicheng Luo. CrOx Decoration on Fe TiO2 with Tunable and Stable Oxygen Vacancies for Selective Oxidation of Glycerol to Lactic Acid†. New J. Chem. 2022, 46, 18744–18750.

(130) Liao, S.; Tian, Q.; Xiao, Y.; Qin, D.; Li, J.; Hu, C. Glycerol Valorization Towards Glycolic Acid Production Over Cu-Based Biochar Catalyst. ChemSusChem 2022, 15 (23), e202201537. https://doi.org/https://doi.org/10.1002/cssc.202201537.

(131) Yin, H.; Yin, H.; Wang, A.; Shen, L. Catalytic Conversion of Glycerol to Lactic Acid over Graphite-Supported Nickel Nanoparticles and Reaction Kinetics. Journal of Industrial and Engineering Chemistry 2018, 57. https://doi.org/10.1016/j.jiec.2017.08.028.

(132) Zhang, J.; Wu, X.; Chen, J.; Wang, X.; Mai, Y. Efficient and Stable Cu-Cu2O@NC Catalysts for Selective Catalytic Conversion of Glycerol to Lactic Acid. ChemCatChem 2022. https://doi.org/10.1002/cctc.202201139.

(133) Shen, L.; Yin, H.; Wang, A.; Lu, X.; Zhang, C. Gas Phase Oxidehydration of Glycerol to Acrylic Acid over Mo/V and W/V Oxide Catalysts. Chemical Engineering Journal 2014, 244, 168–177. https://doi.org/10.1016/J.CEJ.2014.01.051.

(134) Huang, H.; Jiang, B.; Gu, L.; Qi, Z.; Lu, H. Promoting Effect of Vanadium on Catalytic Activity of Pt/Ce–Zr–O Diesel Oxidation Catalysts. Journal of Environmental Sciences 2015, 33, 135–142. https://doi.org/10.1016/J.JES.2014.10.026.

TH-3456_166107017

(135) Garcia, T.; Agouram, S.; Taylor, S. H.; Morgan, D.; Dejoz, A.; Vázquez, I.; Solsona, B. Total Oxidation of Propane in Vanadia-Promoted Platinum-Alumina Catalysts: Influence of the Order of Impregnation. Catal Today 2015, 254, 12–20. https://doi.org/10.1016/J.CATTOD.2015.01.038.

(136) Pestana, C. F. M.; Guerra, A. C. O.; Ferreira, G. B.; Turci, C. C.; Mota, C. J. A. Oxidative Dehydration of Glycerol to Acrylic Acid over Vanadium-Impregnated Zeolite Beta. J Braz Chem Soc 2013, 24 (1), 100–105. https://doi.org/10.1590/S0103-50532013000100014.

(137) Mitran, G.; Neațu, F.; Neațu, Ștefan; Trandafir, M. M.; Florea, M. VAlPOs as Efficient Catalysts for Glycerol Conversion to Methanol. Catalysts 2020, 10 (7), 728. https://doi.org/10.3390/catal10070728.

(138) Tang, Z.; Cao, H.; Tao, Y.; Heeres, H. J.; Pescarmona, P. P. Transfer Hydrogenation from Glycerol over a Ni-Co/CeO2 Catalyst: A Highly Efficient and Sustainable Route to Produce Lactic Acid. Appl Catal B 2020, 263, 118273. https://doi.org/10.1016/J.APCATB.2019.118273.

(139) Chinchilla, L. E.; Olmos, C. M.; Villa, A.; Carlsson, A.; Prati, L.; Chen, X.; Blanco, G.; Calvino, J. J.; Hungría, A. B. Ru-Modified Au Catalysts Supported on Ceria–Zirconia for the Selective Oxidation of Glycerol. Catal Today 2015, 253, 178–189. https://doi.org/10.1016/J.CATTOD.2015.02.030.

(140) TakatoMitsudome; KazuyaMiyagawa; ZenMaeno; TomooMizugaki; KoichiroJitsukawa; JunYamasaki; YasutakaKitagawa; KiyotomiKaneda. Mild Hydrogenation of Amides to Amines over a Platinum-Vanadium Bimetallic Catalyst. Angew. Chem., Int. Ed. 2017, 56, 9381–9385.

TH-3456_166107017

(141) Jin, Y. MnCo2O4 Spinel Supported Ruthenium Catalyst for Air-Oxidation of HMF to FDCA under Aqueous Phase and Base-Free Conditions. 2017, 19 (7), 4–9. https://doi.org/10.1039/c7gc00027h.

भारतीय प्रौद्योगिकी संस्थान गुवाहाटी • Indian Institute of Technology Guwahati •

TH-3456_166107017

TH-3456_166107017

Chapter 2

Materials and Methods

This chapter outlines the experimental design, techniques, and analytical methods used in the study. It gives the detailed experimental methods followed for the preparation of catalysts and their characterization for physicochemical properties, such as particle size, shape, elemental composition, chemical states, and N_2 sorption capacity, using advanced characterization techniques such as field emission transmission electron microscopy (FETEM), high-resolution transmission electron microscopy (HRTEM), energy dispersive X-ray spectroscopy (EDX), X-ray diffraction (XRD), N2-sorption analysis, and X-ray photoelectron spectroscopy (XPS).

The chapter also provides a detailed explanation of the experimental procedures used to evaluate the catalytic activity of the synthesized catalysts in the oxidation of glycerol (GL) and 5-hydroxymethylfurfural (5-HMF) to lactic acid (LA) and 2,5-furandicarboxylic acid (FDCA), respectively. The process of synthesizing 5-hydroxymethylfurfural (5-HMF) from D-Fructose and analyzing its products is also discussed in detail. The chapter contains a list of the specifications for all chemicals and reagents used in the study. Any modifications or deviations from the described procedures are noted in the appropriate section (s) or chapter (s).

TH-3456_166107017

2.1 Materials and Reagents

The materials used in the study were sourced from various suppliers without undergoing any purification. Oxygen, air, and nitrogen (99.99%) gases were obtained from Assam Air Products Pvt. Ltd., India. Deionized water, with a conductivity of 0.055 μS cm^{-1}, was used to prepare all solutions and was obtained from the Millipore Filtration Unit (Model: Elix-3, Make: Millipore, USA). The plastic wares used were polypropylene and procured from Tarson Products Pvt. Ltd., Kolkata (India). The glassware, which had a low thermal expansion coefficient, was mainly obtained from Borosil and JSGW, India. The materials used and their information can be found in Table 2.1.

Table 2.1: List of materials, chemicals/reagents used for the catalyst preparation, and their activity testing.

Reagents/Chemicals	**Purity (%)**	**Grade**	**Make**
Glycerol ($C_3H_8O_3$)	99	Hi-AR	HiMedia
Lactic acid ($C_3H_6O_3$)	85-90	Hi-AR	HiMedia
1,2-Propanediol ($C_3H_8O_2$)	99	AR	Avra
Acetic acid (CH_3COOH)	99.6	AR	Finar Ltd
Formic acid (CH_2O_2)	85	AR	Merck
Glycolic acid ($C_2H_4O_3$)	99	AR	Sigma-Aldrich
Ethylene Glycol ($C_2H_6O_2$)	≥99	AR	Sigma-Aldrich
Hexachloroplatinic acid solution (H_2PtCl_6)	8	AR	Sigma-Aldrich
Ruthenium (III) chloride hydrate ($RuCl_3.xH_2O$)	99.98	AR	Sigma-Aldrich
Vanadium (III) Chloride	97	AR	Sigma-Aldrich
Nickel nitrate hexahydrate ($Ni(NO_3)_2.6H_2O$)	99	AR	Alfa Aesar
Titanium dioxide (TiO_2)	99.5	AR	Sigma-Aldrich

TH-3456_166107017

Activated Charcoal (AC)	>99.9	AR	Sigma-Aldrich
Sodium borohydride ($NaBH_4$)	>98	AR	HiMedia
Sodium hydroxide (NaOH)	>98	AR	HiMedia
Potassium hydroxide (KOH)	≥85	AR	HiMedia
D-Fructose ($C_6H_{12}O_6$)	≥99	AR	HiMedia
D-Glucose ($C_6H_{12}O_6$)	≥99.5	AR	HiMedia
5-Hydroxymethylfurfural ($C_6H_6O_3$)	≥99	FR	Sigma-Aldrich
Furfural ($C_5H_4O_2$)	99	AR	Sigma-Aldrich
Sulphuric acid (H_2SO_4)	98	AR	Finar Ltd
Maleic acid ($C_4H_4O_4$)	>99	AR	HiMedia
Levulinic acid ($C_3H_8O_3$)	97	GR	Merck
2,5-Furandicarboxlic acid ($C_6H_4O_5$)	98	AR	Alfa Aesar
2,5-diformylfuran ($C_6H_4O_{3)}$	98	AR	TCI
5-Formyl-2-furancarboxylic acid ($C_6H_4O_4$)	98	AR	Sigma-Aldrich
5-Hydroxymethyl-2-furancarboxylic acid ($C_6H_6O_4$)	98	AR	Sigma-Aldrich
Dimethyl sulfoxide (C_2H_6OS)	98	AR	Finar Ltd
Acetone (C_3H_6O)	98	AR	Finar Ltd
Methanol (CH_3OH)	98	AR	Finar Ltd
Ethanol (C_2H_5OH)	98	AR	Finar Ltd
Silicone oil	-	-	HiMedia

TH-3456_166107017

2.2 Methodology

2.2.1 Preparation of monometallic (Ru, Pt, and V) and bimetallic (Pt-V, Ru-V, and Ru-Ni) catalysts on activated carbon

Monometallic (Pt/AC, V/AC, and Ru/AC) and bimetallic (Pt-V/AC, Ru-VAC, and Ru-Ni/AC) catalysts supported on activated carbon were prepared using the simple wet impregnation method. 1.96 g of activated carbon was suspended in 200 mL of milli-Q-water, and the suspension was stirred at 600 rpm for 2 h using a magnetic stirrer. The required amounts of hexachloroplatinic acid solution or ruthenium chloride hydrate ($RuCl_3.xH_2O$, 99.98% trace metal basis) were taken as primary metal, and vanadium (III) chloride or nickel nitrate hexahydrate (Ni $(NO_3)_2.6H_2O$) were taken as secondary metal and were dissolved in 50 mL milli-Q-water under sonication for 1 h.

Subsequently, the metal precursor solution was added to the activated carbon solution dropwise under stirring at 600 rpm. The resulting solution was kept under sonication for 1 h for proper dispersion of metals on the support. The metals were reduced using a 10 M $NaBH_4$ aqueous solution, which was added dropwise under stirring. The slurry was stirred for 12 h. Subsequently, the slurry was filtered and dried at 110 °C under vacuum overnight (12 h). The schematic representation of the catalyst synthesis process is shown in Fig. 2.1. A similar procedure was used to prepare 2 wt% monometallic (Pt, Ru, and V) and Pt-V, Ru-V, and Ru-V/TiO_2 bimetallic catalysts with different compositions of Pt, Ru, and V (Table 2.2).

TH-3456_166107017

Table 2.2: List of catalysts and their nominal compositions.

S.No.	Catalyst	Nominal catalyst composition (W%)			
		Pt	V	Ru	Ni
1	1Pt-1V/AC	1	1	N/A	N/A
2	1.5Pt-0.5V/AC	1.5	0.5	N/A	N/A
3	0.5Pt-1.5V/AC	0.5	1.5	N/A	N/A
4	2V/AC	0	2	N/A	N/A
5	2Pt/AC	2	0	N/A	N/A
6	1Ru-1V/AC	N/A	1	1	N/A
7	1.5Ru-0.5V/AC	N/A	0.5	1.5	N/A
8	0.5Ru-1.5V/AC	N/A	1.5	0.5	N/A
9	2Ru/AC	N/A	0	2	N/A
10	1.5Ru-0.5Ni/AC	N/A	N/A	1.5	0.5
11	1.5Ru-0.5V/TiO_2	N/A	0.5	1.5	N/A

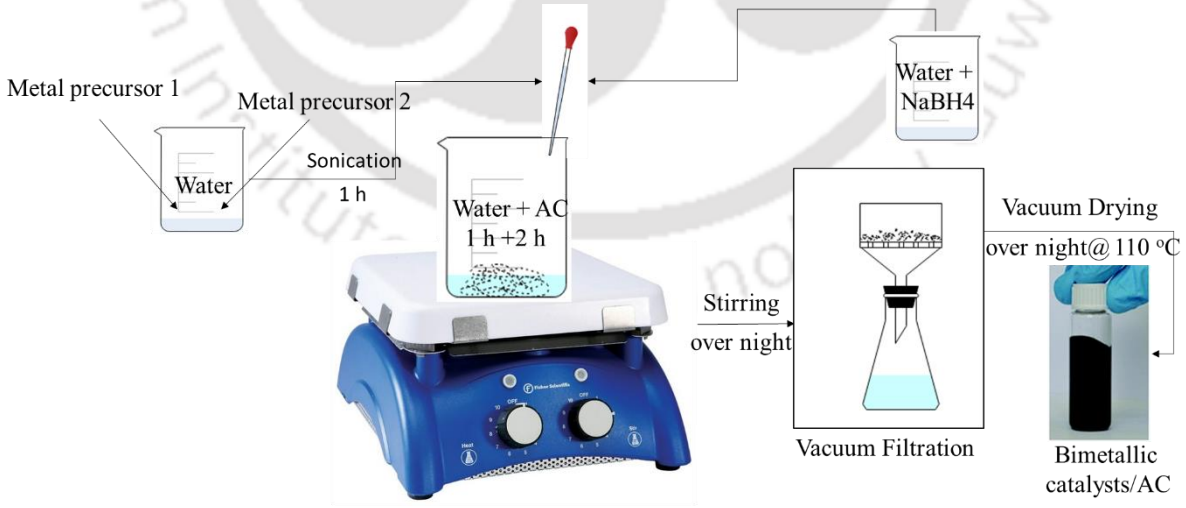

Figure 2.1: Schematic representation of monometallic and bimetallic catalysts synthesis process.

TH-3456_166107017

2.2.2 Catalysts characterization

The synthesized materials were thoroughly analyzed to assess their physical and chemical properties. This was done by employing a range of characterization techniques such as powder X-ray diffraction (XRD), N_2 sorption, electron microscopy (FETEM/HRTEM/EDX), and X-ray photoelectron spectroscopy (XPS). The XRD was utilized to evaluate the crystal structure, phase formation, purity, and size of the crystallites in the material. The N_2-sorption was employed to determine the surface area, pore volume, and distribution of pores. Electron microscopy (FETEM/HRTEM/EDX) was used to study surface morphology. The XPS was utilized to examine the chemical states of the material. The specific methodology for each of these techniques is described in the analysis procedure.

2.2.2.1 BET surface area analyzer

The N_2 sorption study (Tristar-II 3020, Micromeritics, USA) was used to determine surface area, pore volume, and pore size distribution (PSD) at 77K. Samples were degassed under vacuum (200°C, 6 h) to remove moisture and volatiles. The multi-point BET method calculated BET surface area (p/p_o: 0.05-0.3). Micro and mesopore analysis was performed using t-plot (p/p_o: 0.08-0.3) and BJH methods (p/p_o: 0.35-1), respectively. BJH model was used to calculate the average pore diameter (APD). Isotherms and hysteresis were classified by following the IUPAC nomenclature.

2.2.2.2 X-Ray Diffraction

The XRD patterns and crystallinity of Pt, Ru, V monometallic and Pt-V, Ru-V, Ru-Ni bimetallic catalysts were recorded on an X-ray diffractometer (Model: Smartlab, Make: Rigaku, Japan) using Cu Kα radiation (λ = 0.1578 nm). 20 mg dried sample was used, and

TH-3456_166107017

XRD patterns were recorded between 5-50° 2θ angle. XRD parameters: step size: 0.01°, step speed: 20°/min.

2.2.2.3 Electron microscopic analysis

The particle size, morphology, and elemental composition were determined using field emission transmission electron microscopy (FETEM) and energy dispersive X-ray (EDX) spectroscopy (Model: JEM-2100F, Make: JEOL, Japan). With the same instrument, the interplanar spacing and crystal planes were determined using high-resolution TEM (HRTEM) and selected area diffraction patterns (SAED). The sample was prepared for FETEM and EDX using the following procedure: A small amount of catalyst was dispersed in acetone using sonication, drop-casted onto the carbon-coated copper grid, and vacuum-dried at ambient temperature. The ImageJ software was used to analyze the particle size distribution using the following formula.

$$\text{Average particle size (nm)} = \frac{N_1 d_1 + N_2 d_2 + \cdots + N_n d_n}{N_1 + N_2 + \cdots + N_n} \text{ x } 100$$

N_1: number of particles, d_1: diameter of the particle.

2.2.2.4 X-ray photoelectron spectroscopy

The X-ray photoelectron spectroscopy (XPS) was used to study the chemical states of monometallic (Pt/AC, Ru/AC, and V/AC) and bimetallic Pt-V/AC, and Ru-V/AC catalysts with a monochromatic X-ray source (ESCALAB Xi+, Thermo Fisher Scientific, UK). Samples were prepared by dispersing catalytic powders on copper tape. Argon pressure was ~3×10^{-9} mbar, pass energy was 20 eV, and electron take-off angle was 55°. The XPS data were analyzed using XPSPEAK 4.1 software, and peak fitting was performed.

TH-3456_166107017

Table 2. 3: Instruments used in this thesis, along with their specifications and availability.

S. No.	Instrument Name	Make, model, and origin	Pre-treatment conditions and specifications	Availability
1	X-ray powder diffraction (XRD)	Smartlab, Rigaku, Japan	CuKα source; 5KW, scan speed-20°/min, Dried at 110 °C	CIF, IITG
2	Surface area analysis (BET)	Tristar-II Micromeritics, USA	200°C for 6h	Analytical lab, Chemical Engg. Dept., IITG
3	Field Emission Transmission Electron Microscope (FETEM)	JEM-2100F, JEOL, Japan	Sonicated with ethanol and drop cast over the copper grid	CIF, IITG
4	High-Performance Liquid Chromatography (HPLC)	SPD-M30A, Shimadzu, Japan	RID, PDA autosampler, Aminex-87H column, Biorod column, and the sample is filtered using 0.2 m filter	Analytical lab, Chemical Engg. Dept., IITG
5	X-ray photoelectron spectroscopy	ESCALAB Xi+, Thermo Fisher Scientific, UK		CSIR-NEIST, Jorhat

TH-3456_166107017

2.3 Catalytic testing experiments and product analysis

2.3.1 Conversion of fructose dehydration to 5-HMF in a helically coiled reactor

Fig.2.2 shows the experimental setup for synthesizing HMF using a helical coiled microreactor (HCMR). The HCMR was designed and fabricated in-house using SS316-grade stainless steel tubing and fittings. Typically, the feed, consisting of fructose, solvent (DMSO), and homogenous catalyst (SA or MA), was pumped into a microreactor using a high-performance liquid chromatography (HPLC) pump. This study calculated the fructose and catalyst concentrations (expressed in wt%) based on the solvent's mass but not the solution's mass. For example, the concentration of fructose was calculated as follows:

$$C_F(\text{wt\%}) = \frac{\text{mass of fructose}}{\text{mass of DMSO}} \text{ X } 100$$

The HCMR was heated using heating tape with insulation, and the heating was controlled using a PID controller and monitored with the help of thermocouples. The length of the microreactor (i.e., excluding sections outside the heating system, which were kept at room temperature) was 2 and 3 m. The internal diameter of the coil was 1.76 mm. The outlet of the microreactor was connected to another coiled tube, which was immersed in a cold-water bath (ca. 25 °C) to cool the reaction mass. After the system reached the steady state (i.e., after approximately 4 times the residence time in the microreactor), the product samples were collected and filtered using a 0.2 µm nylon filter under vacuum. The samples were diluted and analyzed using high-performance liquid chromatography (HPLC) equipped with a refractive index (RID) and photodiode array (PDA) detectors (Model: RID 20A, Make: Shimadzu, USA).

TH-3456_166107017

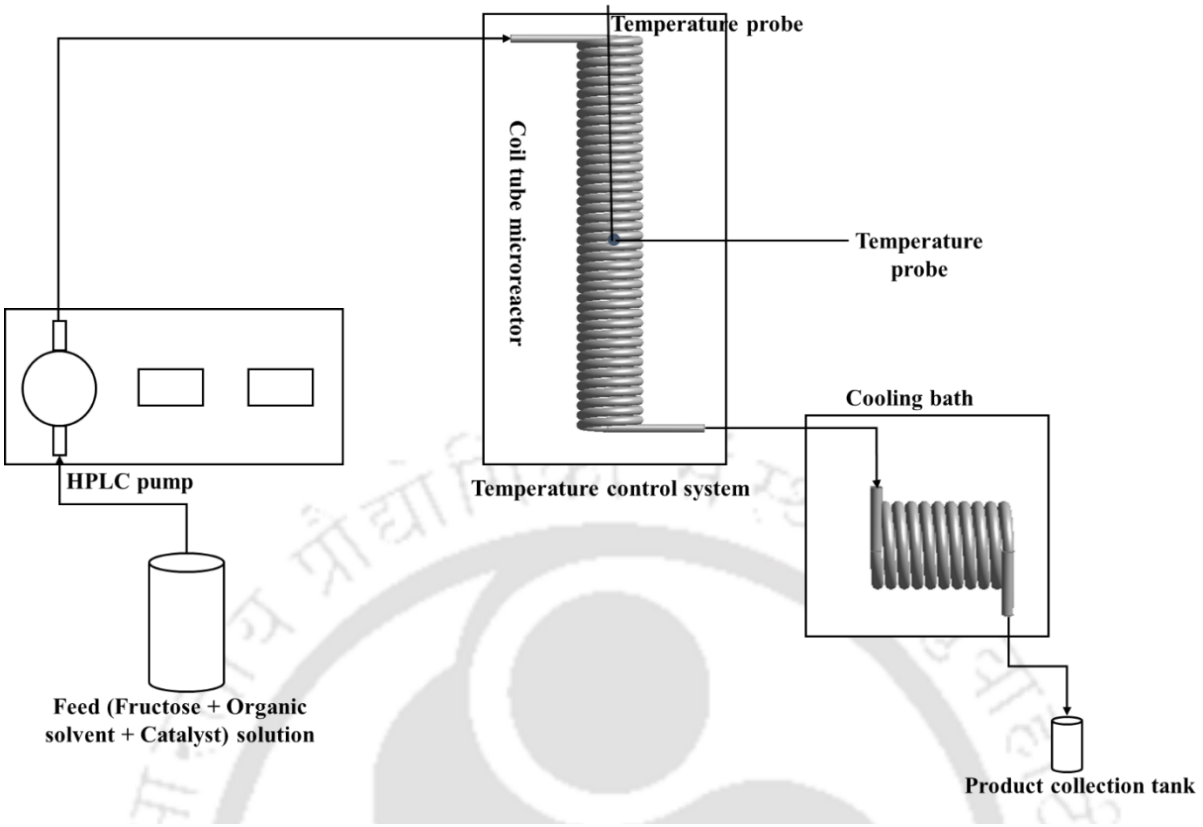

Figure 2.2: Schematic diagram of the coil tube microreactor system for continuously synthesizing 5-HMF from fructose.

2.3.2 Conversion of 5-Hydroxymethylfurfural (HMF) to 2,5-Furandicarboxlic acid (FDCA)

The synthesized catalysts underwent testing for the conversion of 5-HMF to 2,5-FDCA. Catalytic experiments were conducted in a 50 mL Teflon-lined stainless steel (SS316) high-pressure autoclave from Amar Equipment Private Limited in Mumbai, India. The autoclave was initially loaded with a 25 mL aqueous 5-HMF solution (0.08 mmol). Subsequently, the catalyst was introduced into the autoclave, which was then sealed, purged with O_2, and pressurized to the desired level (5-15 bar O_2). The autoclave was immersed in an oil bath pre-stabilized at the specified temperature (100-140 °C) and stirred using a magnetic stirring bar (600 rpm). The reaction time commenced after the reactor reached the set temperature. The autoclave remained in the oil bath for the designated reaction period (1-12 h), then was

TH-3456_166107017

removed, promptly cooled to room temperature with a cold-water bath, and depressurized. Solid catalyst separation from the liquid phase was achieved through vacuum filtration using a 200 nm nylon membrane filter. The liquid samples were diluted with milli-Q water and analyzed using High-Performance Liquid Chromatography (HPLC). A schematic representation of the experimental setup for the oxidation of HMF to FDCA is shown in Fig. 2.3.

2.3.3 Conversion of glycerol to lactic acid

The synthesized catalysts were tested for converting biomass-derived glycerol to lactic acid. The catalytic experiments were performed in a 50 mL Teflon-lined stainless steel (SS316) high-pressure autoclave (Amar Equipment Private Limited, Mumbai, India). The autoclave was charged with 25 mL aqueous glycerol solution (Molarity: 7.2-10.9 M), KOH or NaOH (base/glycerol molar ratio of 0.5-1 mol/mol), and catalyst (glycerol to metal ratio of 4400-17600 mol/mol). Subsequently, the autoclave was closed, flushed with air, and pressurized at the desired pressure (5-15 bar air). The autoclave was then immersed in an oil bath pre-stabilized at the desired temperature (160-180 °C) and kept under stirring with a magnetic stirring bar (600 rpm). The reaction time counting was started after the reactor reached the set temperature. The autoclave was kept in the oil bath for the specified reaction time (1–12 h), removed from the oil bath, cooled immediately to room temperature using a cold-water bath, and depressurized. The solid catalyst was separated from the liquid by vacuum filtration using a 200 nm nylon membrane filter. The liquid samples were neutralized with H_2SO_4 solution, diluted with milli-Q water, and analyzed in HPLC. The schematic representation of the experimental setup for the oxidation of glycerol and the 5-HMF process is shown in Fig. 2.3.

TH-3456_166107017

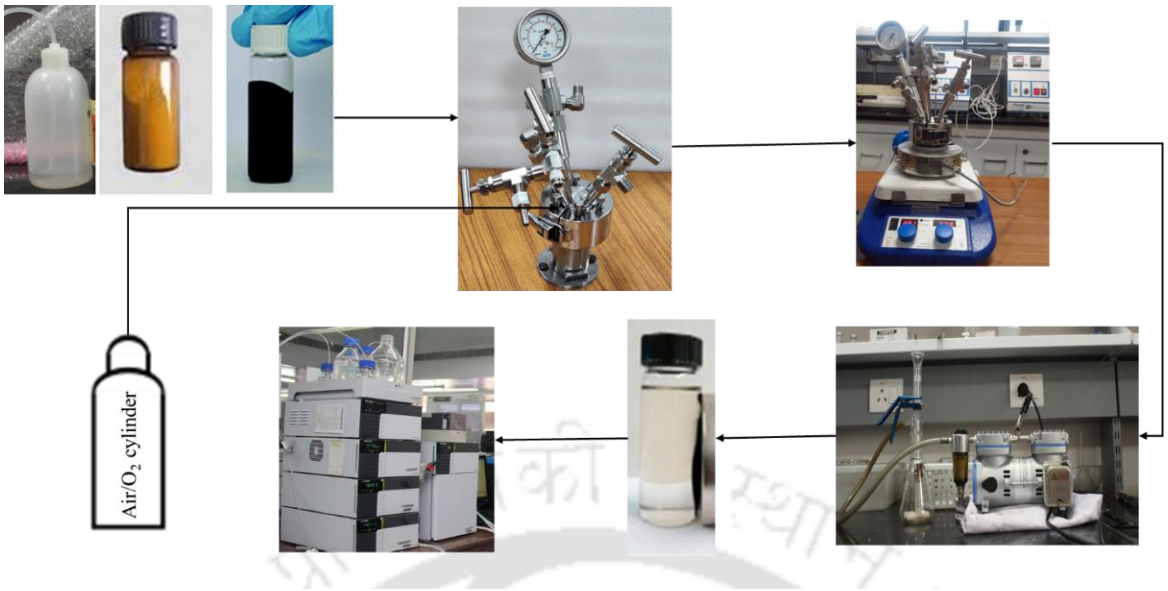

Figure 2.3: Schematic representation of experimental setup for oxidation reactions.

2.3.4 Catalyst Stability Test

The stability of the bimetallic catalyst was tested by reusing the same catalyst sample for four to six cycles. After each cycle, the catalyst was recovered by vacuum filtration, rinsed with excess water, and dried in a vacuum at 110 °C overnight. The investigation examined the impact of humins or coke deposition on the catalyst surface. Humins, undesirable by-products of the reaction, can accumulate on the catalyst, diminishing its effectiveness. The study also assessed the influence of washing the catalyst with water and acetone on its performance. The spent catalyst was re-used under the same reaction conditions in the next cycle. A minimal quantity of fresh catalyst (3-5 mg) was introduced into each successive batch to offset the weight loss incurred during handling.

2.3.5 Analysis procedure for estimation of product concentration

To determine the concentration of the reaction products and unreacted reactants in a liquid mixture, a high-performance liquid chromatography (HPLC) system was employed. The HPLC system was a Shimadzu SPD-M30A and RID-20A model, equipped with photodiode array (PDA) and refractive index (RI) detectors. The mobile phase used in the analysis was a 5 mM

TH-3456_166107017

aqueous solution of sulfuric acid (H_2SO_4) with a flow rate of 0.6 mL min^{-1} (Chapters 3 and 4) and 0.3 mL min^{-1} (Chapters 5 and 6). An HPLC column (Model: Aminex HPX-87H, Make: BIO-RAD, USA) separated the sample mixture's components. The column temperature was kept at 60 °C (Chapters 3 and 4) and 40 °C (Chapters 5 and 6) throughout the analysis to maintain column stability and accuracy. Initially, the sample mixtures containing different known compositions of compounds (glycerol (GL), lactic acid (LA), 1,2-propanediol (1,2-PDO), ethylene glycol (EG), formic acid (FA), acetic acid (AA), glycolic acid (GLA), 5-hydroxymethylfurfural (5-HMF), 2,5-diformylfuran (DFF), 5-hydroxymethyl-2-furan carboxylic acid (HMFCA), and 5-formyl-2-furan carboxylic acid (FFCA), 2,5-furandicarboxylic acid (FDCA), maleic acid (MA), and fructose) were injected for the calibration to determine the calibration factor or slope for the estimation of the actual concentration of these compounds in the experimental samples. The HPLC system effectively separated these components and determined their concentrations, providing valuable insights into the reaction process using the calibration curves (Fig. 2.4). Each experiment was carried out twice, and averaged data was presented.

$$\text{Conversion of i (\%)} = \frac{moles\ i\ reacted}{initial\ moles\ of\ i} \times 100$$

$$\text{The yield of product k (\%)} = \frac{moles\ k\ formed}{initial\ moles\ of\ i} \times 100$$

$$\text{Carbon balance (\%)} = \frac{moles\ of\ C_{out}}{moles\ of\ C_{in}} \times 100$$

Where i is GL, Fructose, 5-HMF, and k are LA, GLA, FA, AA, 1,2-PDO, EG, 5-HMF, DFF, HMFCA, FFCA, FDCA.

TH-3456_166107017

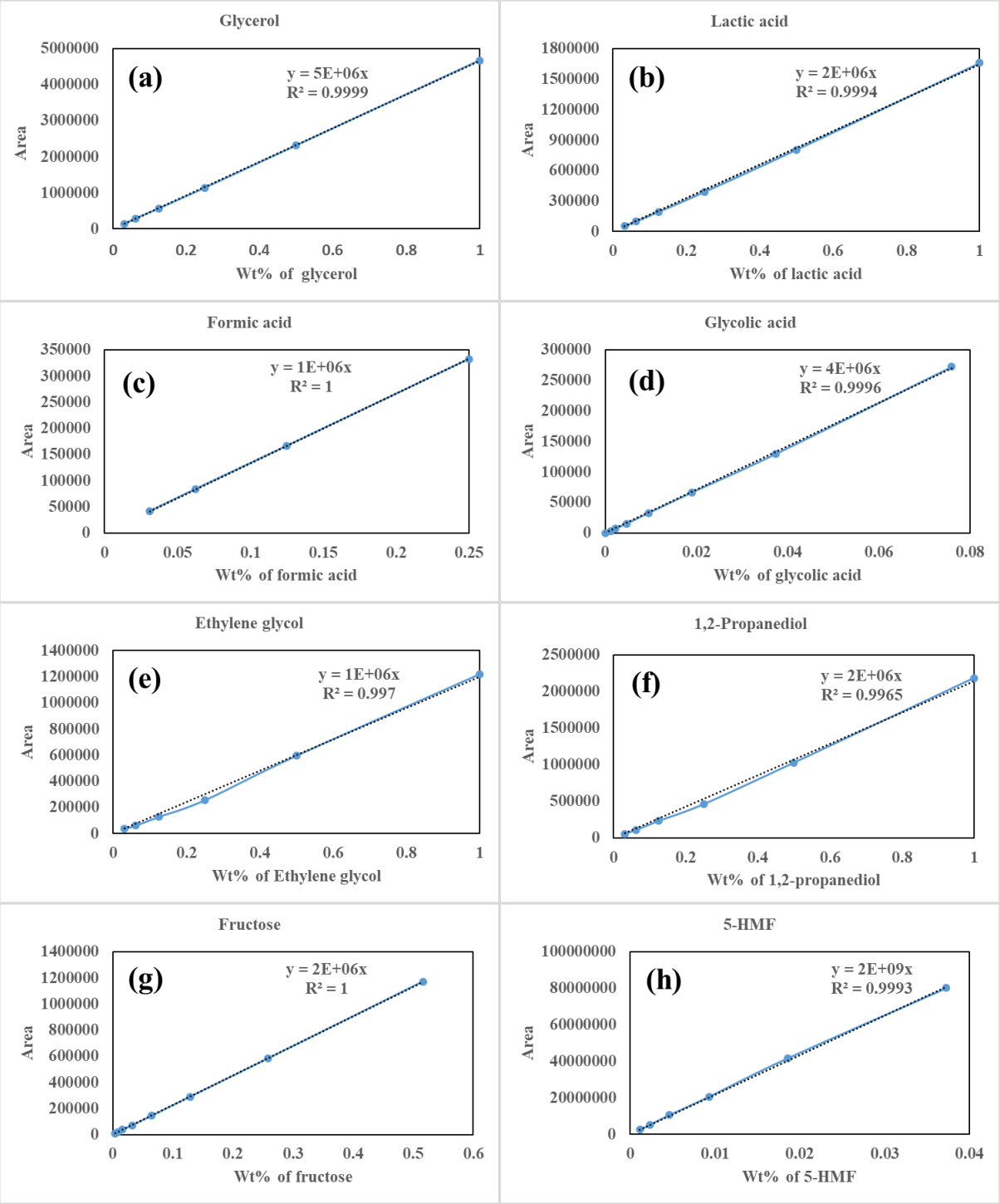

TH-3456_166107017

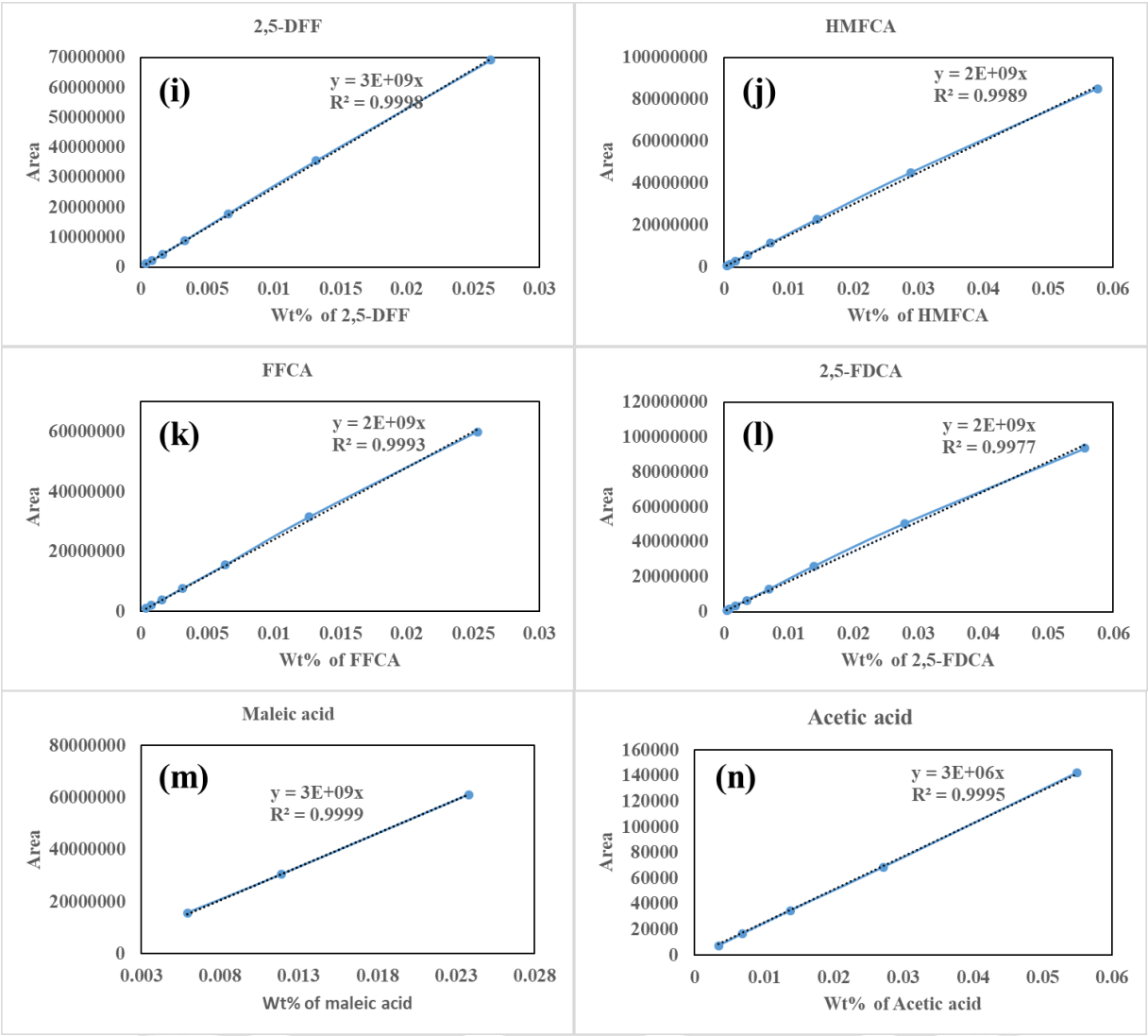

Figure 2.4: Calibration curves of (a) glycerol, (b) lactic acid, (c) formic acid, (d) glycolic acid, (e) ethylene glycol, (f) 1,2-propanediol, (g) fructose, (h) 5-HMF, (i) 2,5-diformylfuran (DFF), (j) 5-hydroxymethyl-2-furan carboxylic acid (HMFCA), (k) 5-formyl-2-furan carboxylic acid (FFCA), (l) 2,5-Furandicarboxlic acid (FDCA), (m) maleic acid and (n) acetic acid obtained from HPLC.

TH-3456_166107017

TH-3456_166107017

Chapter 3

Continuous synthesis of 5-hydroxymethylfurfural from high-concentration fructose feedstock in a micro-helical coiled reactor using homogenous catalysts

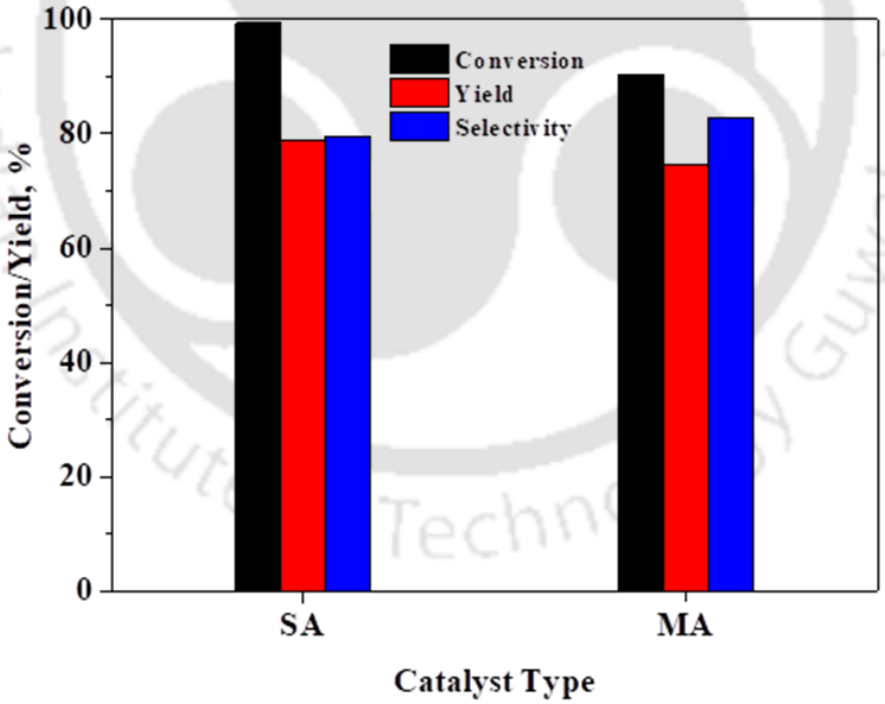

TH-3456_166107017

3.1 Objectives

This study describes a systematic experimental investigation to synthesize HMF from fructose in a single-phase system using DMSO as a solvent and a micro helical coiled reactor using different Brønsted acid catalysts such as H_2SO_4 (SA) and maleic acid (MA). A stainless-steel helical coiled microreactor was used in this study, with an inner diameter of 1.76 mm and a total length of 2 and 3 m. The microreactor was equipped with heating tape, insulation, thermocouples, and a PID temperature controller to control the reactor's temperature. The effect of temperature, catalyst concentration, flow rate, and fructose concentration on fructose conversion and HMF yield was studied. The role of DMSO in enhancing the selectivity to HMF was also studied by investigating the conversion of fructose to HMF without a catalyst. The results of this study were then compared with well-accepted literature to evaluate the importance of using microreactor systems for producing HMF.

3.2 Results and Discussion

3.2.1 HMF synthesis from fructose dehydration using SA as a catalyst

A series of experiments were conducted to study the effect of flow rate and SA concentration on the HMF yield and fructose conversion in a DMSO solvent at a specific temperature (100 ^{o}C) using 3.5 wt% and 10 wt% of fructose concentration (Fig. 3.1). With the increase of flow rate from 0.1 to 0.5 mL min^{-1}, the HMF yield was decreased from 94.5 to 81.6%, along with a decrease in fructose conversion from 100 to 89.6% at a SA concentration of 0.25 wt% and a fructose concentration of 3.5 wt% (Fig. 3.1a). A similar trend was observed for HMF yield as a function of flow rate when the SA concentration of 0.5 and 0.75 wt% (Fig. 3.1b and Fig. 3.1c) were used at a fructose concentration of 10 wt%. The study also investigated the effect of SA concentration on the HMF yield with 10 wt% of fructose and at a flow rate of 0.1 mL min^{-1}

TH-3456_166107017

(Fig. 3.1d). With the increased SA concentration, the HMF yield was increased first and then decreased marginally. The HMF yield passed through a maximum (86.7%) at a catalyst concentration of 0.76 wt%. Further increasing the SA concentration to 1.51 wt% resulted in a marginal decrease in the HMF yield to 84.9%. At a specified temperature, catalyst concentration, and fructose concentration, the conversion and HMF yield decrease were solely influenced by the residence time, as illustrated in Figure 3.1. However, at elevated temperatures (e.g., 180 °C), the impact of residence time, flow rate, and catalyst concentration on conversion and HMF yield becomes negligible. At this point, it is primarily a temperature-driven effect, as demonstrated in Fig. 3.3b. The significant error bars primarily stem from temperature fluctuations within the reactor. Such instability has been noted to introduce variability in the yield of HMF at lower fructose concentrations. The reproducibility can be achieved by maintaining consistent temperature within the reactor, as illustrated in the figures (e.g., Figs. 3.4 and 3.6).

TH-3456_166107017

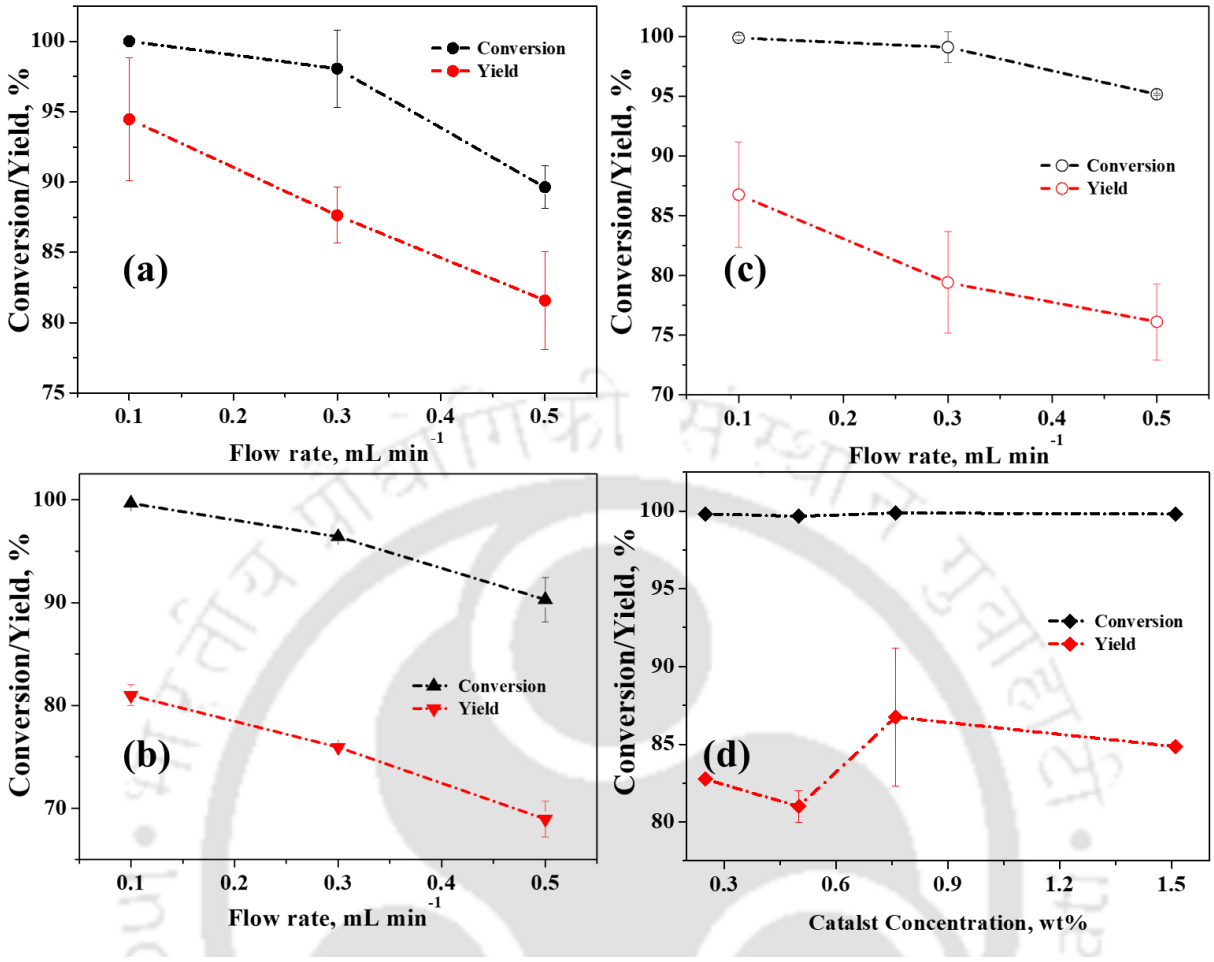

Figure 3.1: Effect of flow rate (a, b & c) and SA concentration on the fructose conversion and HMF yield; Reaction conditions (a) 3.5 wt% fructose, 0.25% SA (b) 10 wt% fructose, 0.5% SA (c) 10 wt% fructose, 0.76% SA (d) 10 wt% fructose, 0.1 mL min^{-1} flow rate. All the experiments presented in this figure were conducted at 100 ℃ temperature and in a reactor of length 2 m.

The study also investigated the effect of temperature on fructose conversion and HMF yield using different fructose concentrations, acid concentrations, and flow rates. Four parameters were used: 3.5 wt% fructose concentration with 0.25 wt% SA and 0.1 mL min^{-1} flow rate; 10 wt% fructose concentration with 0.5 wt% SA and 1 mL min^{-1} flow rate; 10 wt% fructose concentration with 0.5 wt% SA and 0.1 mL min^{-1} flow rate; and 20 wt% fructose concentration with 0.76 wt% SA and 1 mL min^{-1} flow rate. The results indicate that at 3.5 wt% fructose concentration, the HMF yield increased with increasing temperature up to 100 ℃. Further, an

TH-3456_166107017

increase in temperature to 106 ℃ resulted in a marginal decrease in HMF yield (Fig. 3.2a). The fructose conversion reached full completion (100%) at all tested temperatures. The study explored the impact of temperature on fructose conversion and HMF yield while adjusting the other variables, including fructose concentration, SA concentration, and flow rate, and comparing Figs. 3.2b and 3.2c, it is evident that the flow rate significantly influences both fructose conversion and HMF yield. The findings indicate that at lower rates (0.1 mL min^{-1}), the HMF yield was higher than at higher flow rates (1 mL min^{-1}), while fructose conversion remained nearly constant. We have not seen any significant effect on fructose conversion and HMF yield concerning reactor length (e.g., 2 and 3 m), and other factors (Temperature, fructose concentration, SA concentration, etc.) significantly affect HMF yield. Based on Fig.3.3b, we concluded that residence time does not influence the fructose conversion and HMF yield.

At higher fructose concentrations of 10 wt% and lower (0.1 mL min^{-1}) and higher (1 mL min^{-1}) flow rates, the yield of HMF was monotonically increased with temperature (Figs. 3.2b and 3.2c). However, it was observed that at a higher flow rate (1 mL min^{-1}) and the operating temperatures used in this study, the catalyst concentration needed to be increased to achieve higher yields of HMF. To investigate the effect of temperature on HMF yield, the study was further extended to a fructose concentration of 20 wt% and higher catalyst concentration (0.76 wt%) with a flow rate of 0.1 mL min^{-1} at different temperatures. This investigation showed that the yield of HMF increased marginally with increasing temperature from 90 ℃ (83.5%) to 100 ℃ (85.1%). It decreased to 78.4% with a further increase in temperature to 110 ℃ (Fig. 3.2d). Temperature has a more pronounced effect on the yield of HMF from fructose at lower concentrations (e.g., 3.5%) than at higher concentrations (e.g., 10%). Differences in kinetic and thermodynamic factors can explain this.

Reaction Kinetics: At lower fructose concentrations, the reaction rate for converting fructose to HMF is more sensitive to temperature changes. With less substrate, the reaction relies more

TH-3456_166107017

heavily on temperature to supply the necessary activation energy. As the temperature rises, the kinetic energy of the molecules increases, resulting in more frequent and effective collisions between reactants, which boosts the conversion rate to HMF.

Equilibrium Considerations: The conversion of fructose to HMF, an endothermic dehydration reaction, is influenced by thermodynamics and kinetics. Higher temperatures generally favour HMF formation by making the reaction more thermodynamically favorable. However, the system may approach equilibrium at higher fructose concentrations, where side reactions like humin polymerization become more significant, potentially masking the temperature effect observed at lower concentrations. This can lead to a plateau in HMF yield due to increased by-product formation and possible saturation with HMF, slowing further production.

In summary, the reaction of fructose to HMF is not purely thermodynamically limited, but temperature plays a crucial role in both the thermodynamic favourability and the kinetics of the reaction. At lower fructose concentrations, the effect of temperature is more pronounced because side reactions hinder the system and are more sensitive to changes in kinetic energy provided by temperature. As concentration increases, other factors come into play, diminishing the temperature effect.

TH-3456_166107017

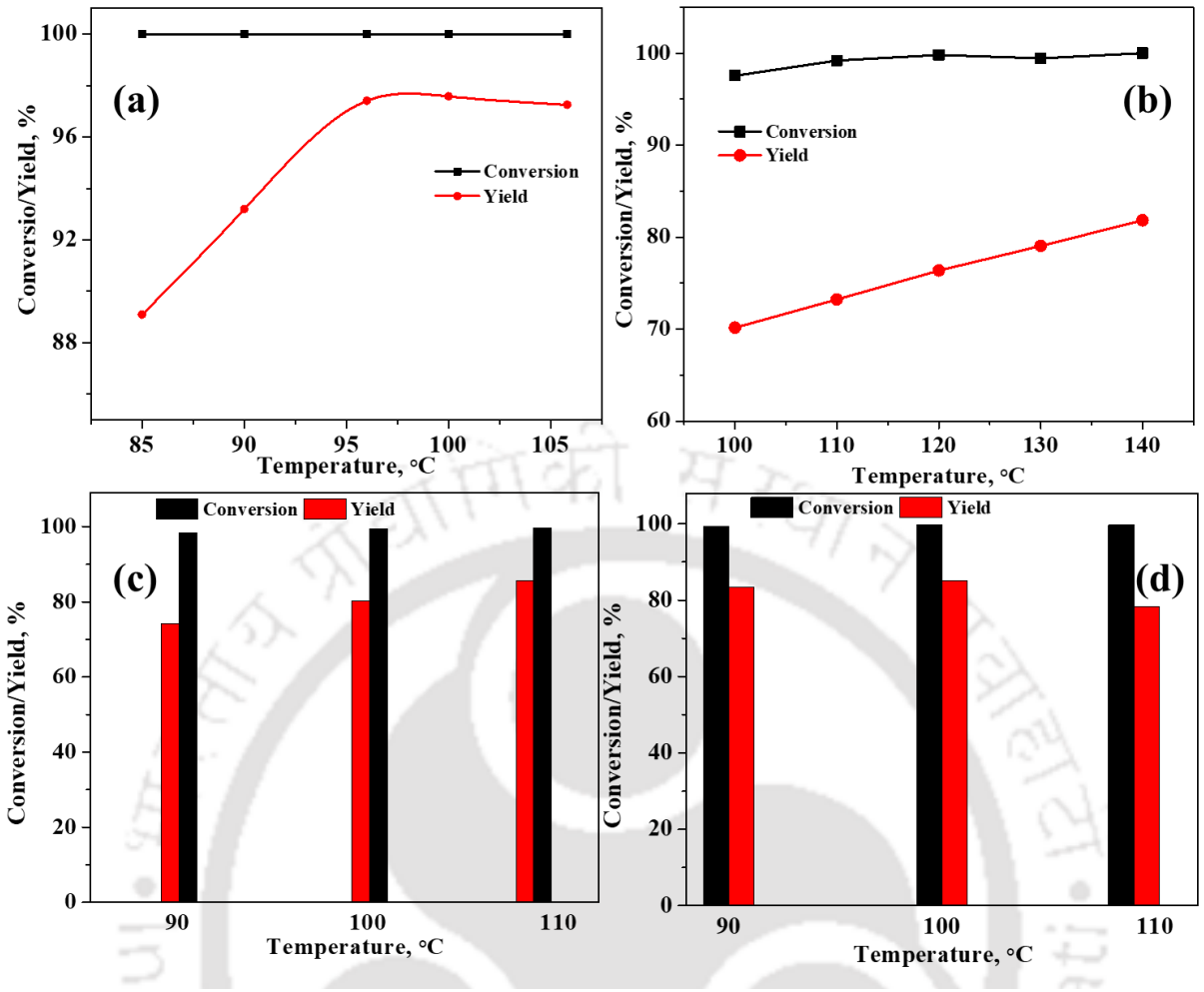

Figure 3.2: Effect of temperature on the fructose conversion and HMF yield at reaction conditions (a) 0.1 mL min^{-1} flow rate, 3.5 wt% fructose, and 0.25 wt% SA; (b) 1 mL min^{-1} flow rate, 10 wt% fructose and 0.5 wt% SA (reactor length: 3 m) (c) 0.1 mL min^{-1} flow rate, 10 wt% fructose and 0.5 wt% SA; and (d) 0.1 mL min^{-1} flow rate, 20 wt% fructose and 0.76 wt% SA. All the experiments presented in this figure were conducted in a reactor of length 2 m.

Further, the study aimed to enhance the HMF space-time yield or productivity by increasing the reactor throughput with a higher (50 wt%) fructose concentration. First, the effect of temperature on HMF yield was examined by fixing the flow rate at 5 mL min^{-1} and catalyst concentration at 0.5 wt% SA. As shown in Fig. 3.3a, the temperature increases from 120-180 °C increased the fructose conversion from 86.0 to 100% and HMF yield from 44.3 to 89.0%. The effect of flow rate (residence time) on HMF yield was also studied at two different flow rates while keeping the temperature at 180 °C and catalyst concentration at 0.5 wt% H_2SO_4.

TH-3456_166107017

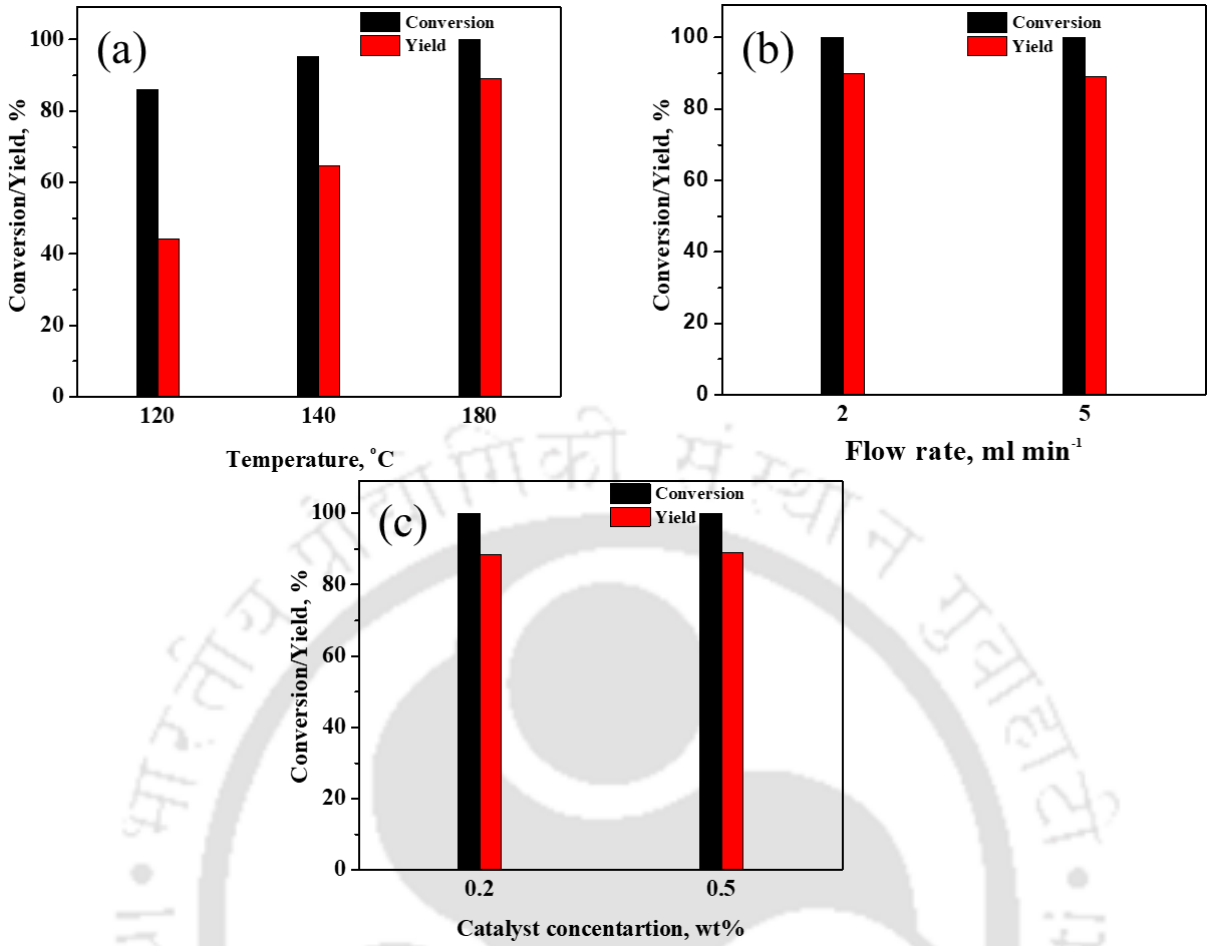

Figure 3.3: Effect of (a) temperature, (b) flow rate, (c) SA concentration on the fructose conversion and HMF yield. Other reaction conditions: 0.5 wt% SA, 5 mL min^{-1} flow rate, 50 wt% fructose, 180 ^{o}C temperature, and 3 m reactor length.

(Fig. 3.3b), A marginal decrease in HMF yield from 90.0 to 89.0% was observed with an increase in flow rate from 2 to 5 mL min^{-1}. Furthermore, the impact of catalyst concentration on HMF yield was investigated by decreasing the concentration from 0.5 to 0.2 wt% SA (Fig. 3.3c), revealing a slight reduction in HMF yield from 89.0% to 88.4%. However, we attained the highest HMF production rate when employing a 0.2 wt% SA concentration, reaching 379.9 $g_{HMF}/g_{Cat}/h$, surpassing the production rates achieved with other catalyst concentrations. Without a catalyst, the control experiment showed a 12.2% HMF yield with 54.5% fructose conversion (Table 3.1, Entry 1) through the solvation effect.[1] Moreover, the investigation assessed the influence of lower flow rates, temperatures, and higher catalyst concentration

TH-3456_166107017

while maintaining a fructose concentration of 50 wt% on the HMF yield. Further studies to understand the residence time effect (10, 15, and 20 mL min^{-1}) are being carried out in our research group.

Fig. 3.4 describes the effect of flow rate on fructose conversion and HMF yield at 100 ^{o}C reaction temperature with 1.5 wt% catalyst concentration. Due to insufficient catalyst concentration, reaction time, and temperature, the fructose conversions (96.1 to 88.3%) and HMF yields (65.2 to 44.1%) decreased with increasing flow rates. To gain further insight, the impact of catalyst concentration was further explored by varying it both upwards and downwards at a temperature of 100 °C and a flow rate of 0.1 mL min-1 (Fig. 3.5a). The findings indicated that higher catalyst concentrations (0.82 to 3.1 wt%) improved fructose conversion (95.0 to 97.5%) and enhanced HMF yields (62.0 to 79.7%). Conversely, decreasing the catalyst concentration reduced fructose conversion and diminished HMF yields. Moreover, a similar effect was further investigated by raising the temperature to 110 °C (Fig. 3.5b), aiming to comprehend the reaction kinetics' dependence on temperature.[2,3] The outcomes demonstrated an improved HMF yield (93.5%) while maintaining nearly identical fructose conversion (98.1%). Nevertheless, lower temperatures were not conducive to higher HMF yields with higher fructose concentrations, as highlighted in Table 3.1. At a higher flow rate (0.3 mL min^{-1}), achieving higher HMF yields (58.0 to 64.2%) with high fructose concentration requires a rise in temperatures (110 ^{o}C) (Table 3.1, Entry 2). Further extensive studies are being carried out in our research group to understand the effect of various parameters.

TH-3456_166107017

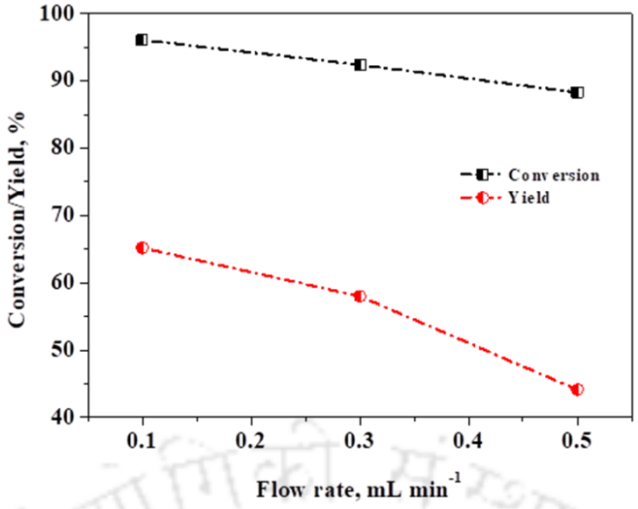

Figure 3.4: Effect of flow rate on fructose conversion to HMF. Reaction Conditions: 1.5 wt% SA concentration, 50 wt% fructose, 100 ^{o}C temperature (reactor length: 3 m).

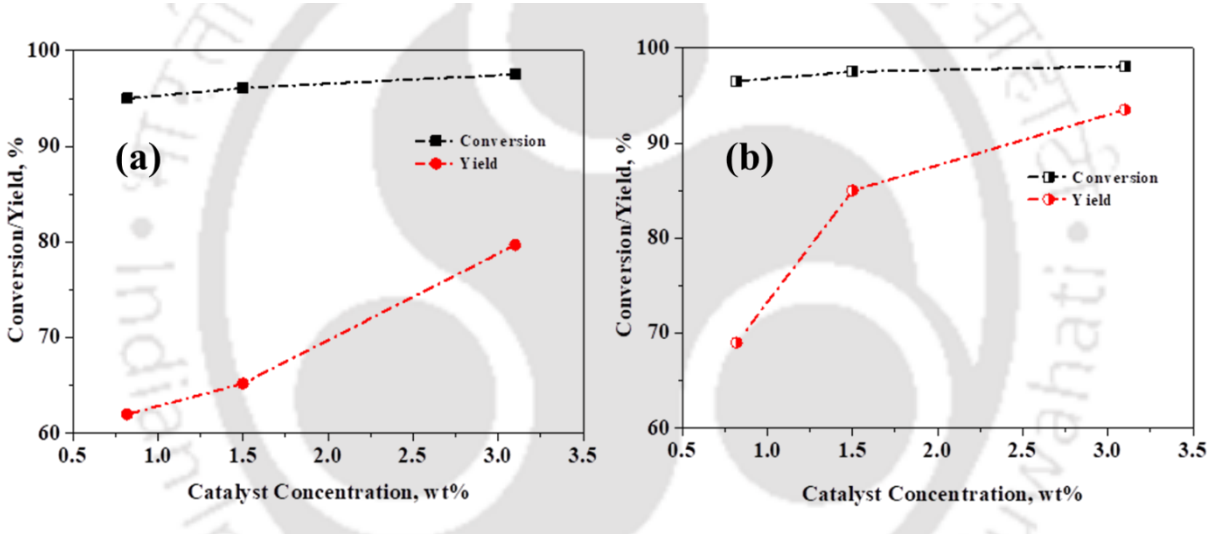

Figure 3.5: Effect of catalyst concentration on fructose conversion to HMF. (a) 100 ^{o}C (b) 110 ^{o}C Reaction Conditions: 1.5 wt% SA concentration, 50 wt% fructose, and flow rate: 0.1 mL min^{-1} (reactor length: 3 m).

TH-3456_166107017

Table 3.1: Fructose dehydration to HMF using SA as a catalyst.

Entry No.	Fructose concentration (wt.%)	Catalyst concentration (wt.%)	Flow rate (mL min^{-1})	Temperature (^oC)	Fructose conversion (%)	HMF yield (%)
1	50	blank	2	180	54.5	12.2
2	50	1.5	0.3	110	95.8	64.2
3	50	1.5	0.1	90	93.6	52.1
4	50	3.1	0.1	110	100	83.7
5	20	0.81	0.5	105	95.5	64.9
6	20	0.81	1	97	78.0	51.2
7	20	0.25	0.1	100	100	46.2
8	10	0.76	0.2	100	100	85.5
9	10	0.76	0.4	100	100	81.4

TH-3456_166107017

3.2.2 HMF synthesis from fructose dehydration using maleic acid (MA) as a catalyst

Maleic acid, an organic acid, was investigated as a potential catalyst for the dehydration of fructose to HMF in the continuous microreactor system using DMSO as a solvent. Organic acids, such as maleic acid (MA), work as catalysts and stabilizers for HMF in the DMSO solvent. MA has a unique nature; it reduces the humins formation by reacting with oligomers of humins and suppressing further reaction.[4,5] Maleic acid stabilizes the intermediate species formed during the reaction by leveraging its dicarboxylic acid structure, which forms an internal hydrogen bond with transition-state intermediates. This interaction increases the activation energy barrier for further degradation.[6] This mechanism helps prevent undesired side reactions and promotes the desired pathway leading to HMF. This could lead to improved yields and reaction kinetics compared to the mineral acids reported in the literature.[4,5] At a fructose concentration of 10 wt%, the temperature and catalyst concentrations were varied to understand their impact on the HMF yield and fructose conversion. In the first set of experiments, the temperature was varied from 100 to 130 ℃ at a catalyst (MA) concentration of 1.5 wt%. The increase in temperature significantly increased the fructose conversion from 58.5 to 98.9% and HMF yield from 35.4 to 78.2% (Fig. 3.6a). In the next set of experiments, the temperature variation effect was studied at a higher catalyst concentration of 3 wt%. The trends were similar at lower and higher concentrations of catalysts. However, at higher catalyst concentrations, the fructose conversion and HMF yield were significantly higher than those at lower catalyst concentrations. For example, the fructose conversion and HMF yield increased from 58.5 to 73% and 35.4 to 48.1% at 100 ℃ as catalyst concentration increased from 1.5 to 3 wt% (Fig. 3.6b). When the temperature was increased to 130 ℃, the fructose conversion and HMF yield were found to be 98.7% and 79.4%, respectively, at 3 wt% catalyst concentration. The effect of temperature variation at higher fructose concentrations of 20 wt.% and 1.5 wt%

TH-3456_166107017

MA concentration was studied. The trend of HMF yield and fructose conversion variation with temperature was similar to that at lower fructose concentrations. However, at higher fructose concentrations, the HMF yield, and fructose conversion were lower than those at lower fructose concentrations at any temperature studied (Fig. 3.6c). The maximum HMF yield and fructose concentration were obtained at 130 °C and were 97.2% and 70.6%, respectively (Fig. 3.6c).

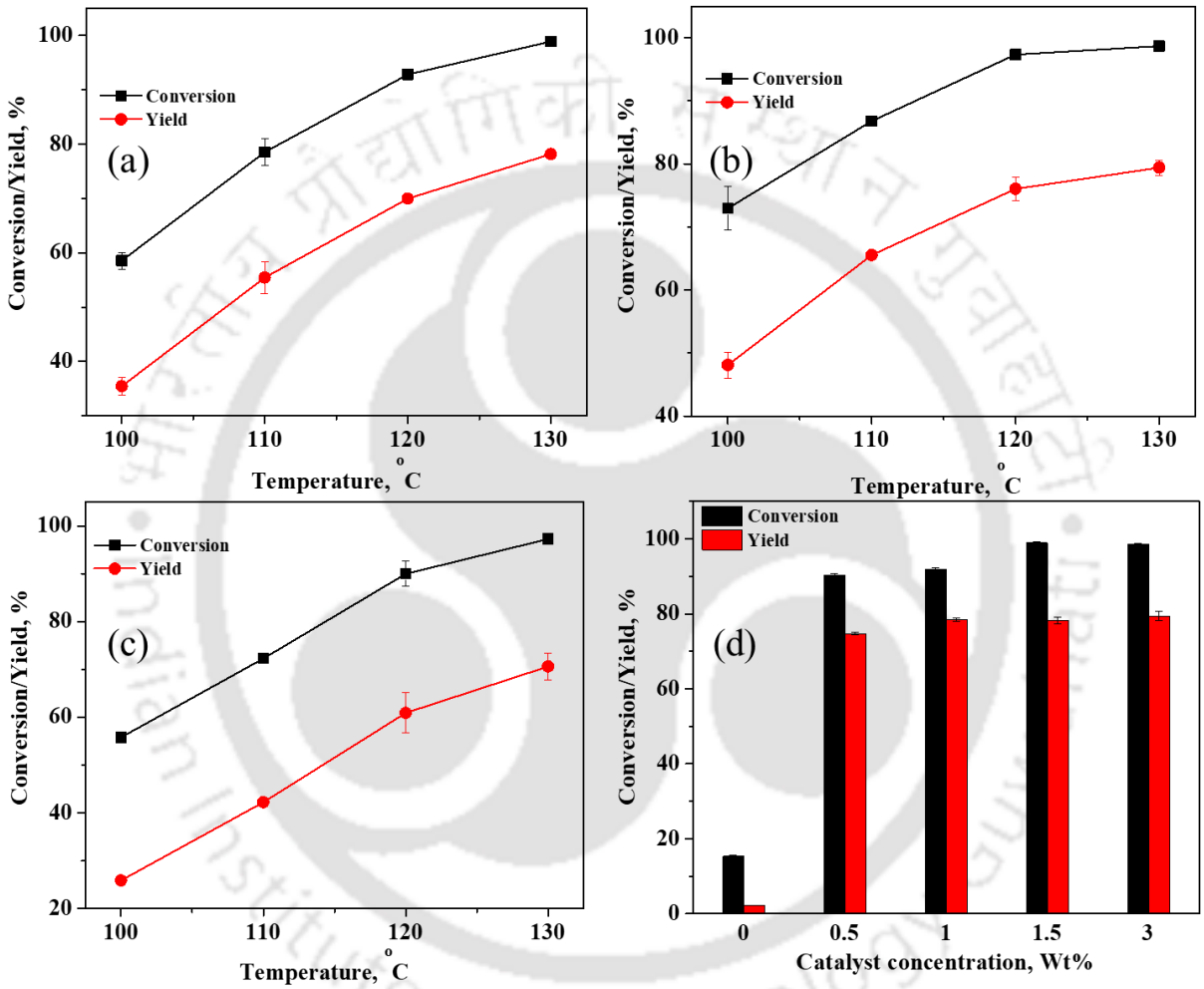

Figure 3.6: Effect of temperature (a, b & c) and MA concentration on the fructose conversion and HMF yield. Reaction conditions: (a)1.5 wt% MA, 10 wt% fructose (b) 3 wt% MA, 10 wt% fructose (c) 1.5 wt% MA, 20 wt% fructose (d) 10 wt% fructose, 130 °C temperature. All the experiments presented in this figure were conducted at 1 mL min^{-1} flow rate and in a reactor of length 3 m.

TH-3456_166107017

Furthermore, the impact of MA concentration was examined on fructose conversion and HMF yield at 130 °C using a 10 wt% fructose concentration. The results indicated no significant influence of MA concentration on HMF yield beyond 1 wt% at ≥ 130 °C (Fig. 3.6d). In conclusion, the study found that higher temperatures with lower MA concentrations or those with high MA concentrations were necessary for achieving higher fructose conversion and HMF yields. Furthermore, a comparison was conducted between the performance of SA and MA with fructose conversion and HMF yield, as depicted in Fig. 3.7. The outcomes indicated that SA exhibited slightly superior performance to MA regarding fructose conversion and HMF yield. However, MA displayed better performance in HMF selectivity when compared to SA, and it also effectively managed to control the formation of humins through degradation.[4,5]

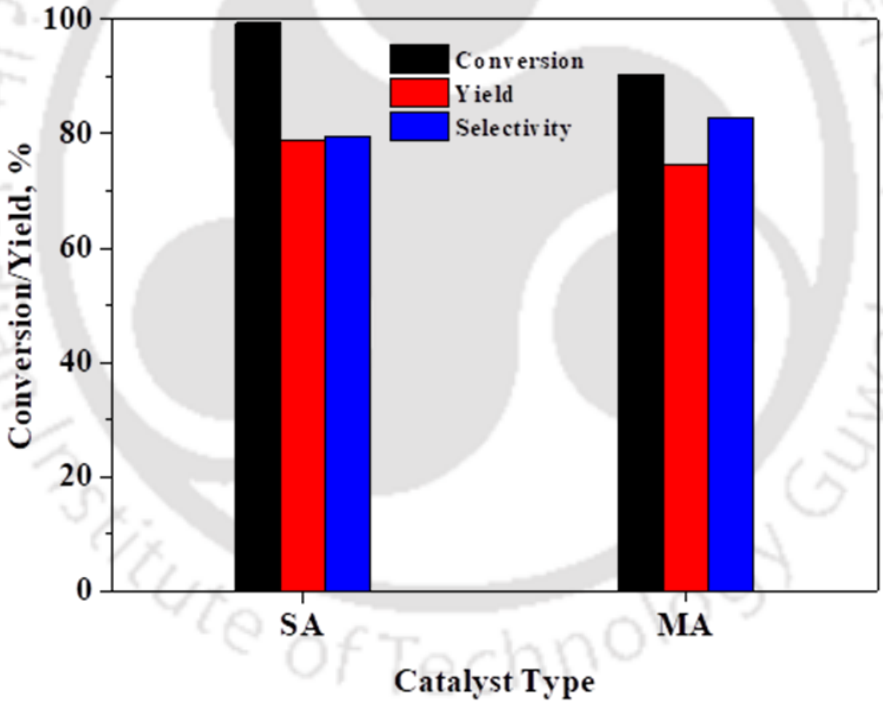

Figure 3.7: Effect of catalyst type on fructose conversion to HMF. Reaction Conditions: 130 °C temperature, 0.5 wt% catalyst concentration, 10 wt% fructose, and flow rate: 1 mL min^{-1} (reactor length: 3 m).

TH-3456_166107017

The effects of reaction kinetics and thermodynamic equilibrium were discussed above. Apart from this, concentration dependency is discussed below.

- At lower concentrations, the reaction is less likely to be limited by factors such as substrate availability or side reactions, allowing the effect of temperature to be more pronounced. The system is more "dilute," meaning that the fructose molecules are more spread out, reducing the likelihood of intermolecular interactions that could lead to side reactions at higher temperatures than lower temperatures, thus making temperature a more critical factor in determining the reaction rate and yield.
- At higher concentrations, the proximity of fructose molecules increases the chance of side reactions, reducing the overall yield of HMF and making the effect of temperature less apparent.
- Higher flow rates reduce the HMF yield compared to lower flow rates due to slower reaction rates at lower temperatures compared to higher temperatures.
- At higher flow rates, the system lacks sufficient time to reach thermodynamic equilibrium, resulting in products and reactants not being in equilibrium proportions. This leads to lower conversion or yield than lower flow rates, where the system has enough time to reach equilibrium and maximize yield.
- While flow rate only does not affect the position of thermodynamic equilibrium, it impacts whether the system can achieve equilibrium within the reactor's residence time, as equilibrium is determined by temperature, pressure, and composition.
- In Summary, the flow rate in a reactor significantly affects both reaction kinetics and the approach to thermodynamic equilibrium. High flow rates reduce residence time, which can lower conversion and yield due to insufficient time to reach equilibrium. In contrast, low flow rates increase residence time, improving conversion and yield, but may also introduce

TH-3456_166107017

issues like increased side reactions. As discussed in the chapter, finding the optimal flow rate is essential for balancing reaction kinetics with thermodynamic efficiency.

3.3 Summary

In this study, a helically coiled reactor was designed, fabricated, and tested for producing chemicals at high-yield productivity from renewable sources in an organic solvent. Specifically, using sulfuric acid (SA) and maleic acid (MA) as catalytic systems, the fructose dehydration to 5-hydroxymethylfurfural (HMF) was demonstrated. The highest HMF yield of 95% was achieved at 100 ^{o}C, with a flow rate of 0.1 mL min^{-1} and a fructose concentration of 3.5 wt% using SA as the catalyst. This result represents the highest productivity in the experiments in short residence times (1.46 min) and high temperatures (180 ^{o}C). Productivity could be further enhanced by increasing the temperature and lowering the catalyst concentration. At 180 ^{o}C, an HMF yield of 90.0% was achieved with a flow rate of 2 mL min^{-1} and a catalyst concentration of 0.5 wt% SA. Similarly, an HMF yield of 89.0% was achieved at the same temperature with a flow rate of 5 mL min^{-1} and the same catalyst concentration. The highest HMF productivity (380 g_{HMF}/g_{Cat}/h) was achieved with 0.2 wt% SA concentration at 180 °C, employing a flow rate of 5 mL min^{-1} and 50 wt% fructose concentration (HMF yield was 88%). Using 3 wt% MA as a catalyst, a maximum HMF yield of 80% was obtained with a fructose concentration of 10 wt%, temperature 130 °C, and flow rate of 1 mL min^{-1}. Moreover, maleic acid plays a critical role in mitigating the degradation of HMF and preventing the formation of humins. The study demonstrates the potential of the helically coiled reactor to produce chemicals at high-yield productivity from renewable feedstocks.

TH-3456_166107017

References

(1) Whitaker, M. R.; Parulkar, A.; Ranadive, P.; Joshi, R.; Brunelli, N. A. Examining Acid Formation During the Selective Dehydration of Fructose to 5-Hydroxymethylfurfural in Dimethyl Sulfoxide and Water. ChemSusChem 2019, 12 (10). https://doi.org/10.1002/cssc.201803013.

(2) Tuercke, T.; Panic, S.; Loebbecke, S. Microreactor Process for the Optimized Synthesis of 5-Hydroxymethylfurfural: A Promising Building Block Obtained by Catalytic Dehydration of Fructose. Chem Eng Technol 2009, 32 (11). https://doi.org/10.1002/ceat.200900427.

(3) Desir, P.; Saha, B.; Vlachos, D. G. Ultrafast Flow Chemistry for the Acid-Catalyzed Conversion of Fructose. Energy Environ Sci 2019, 12 (8). https://doi.org/10.1039/c9ee01189g.

(4) Zhang, X.; Hewetson, B. B.; Mosier, N. S. Kinetics of Maleic Acid and Aluminum Chloride Catalyzed Dehydration and Degradation of Glucose. Energy and Fuels 2015, 29 (4), 2387–2393. https://doi.org/10.1021/ef502461s.

(5) Istasse, T.; Bockstal, L.; Richel, A. Production of 5-Hydroxymethylfurfural from D-Fructose in Low-Transition-Temperature Mixtures Enhanced by Chloride Anions and Low Amounts of Organic Acids. Chempluschem 2018, 83 (12), 1135–1143. https://doi.org/10.1002/cplu.201800416.

(6) Lu, Y.; Mosier, N. S. Kinetic Modeling Analysis of Maleic Acid-Catalyzed Hemicellulose Hydrolysis in Corn Stover. Wiley InterScience (www.interscience.wiley.com). Biotechnol. Bioeng 2008, 101, 1170–1181. https://doi.org/10.1002/bit.22008.

TH-3456_166107017

TH-3456_166107017

Chapter 4

Catalytic conversion of 5-hydroxymethylfurfural to 2,5-furandicarboxylic acid over carbon-supported ruthenium-vanadium bimetallic catalysts under base-free mild reaction conditions

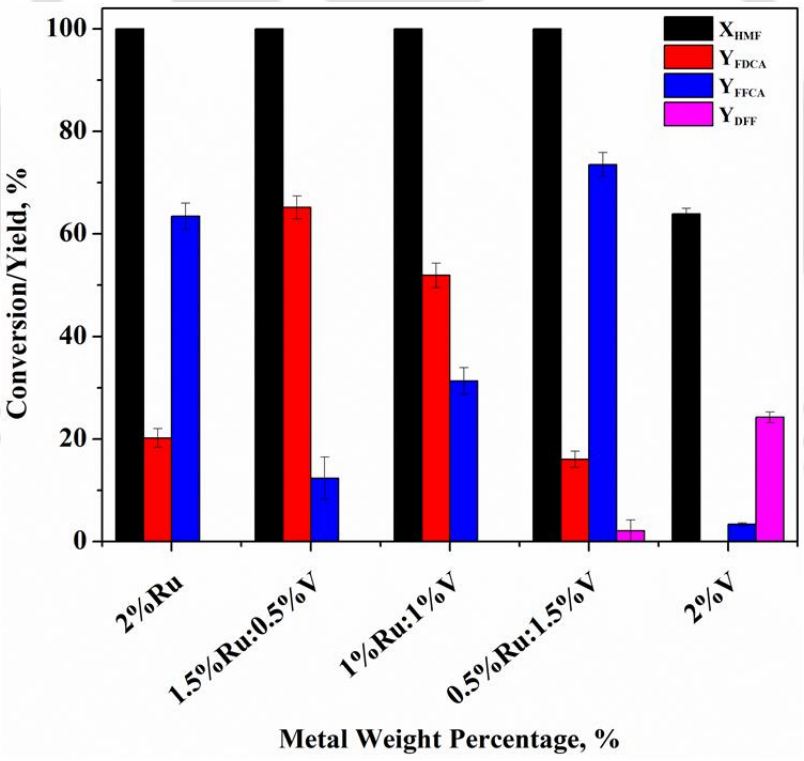

TH-3456_166107017

4.1 Objectives

This study delved into examining novel Ru-V and Ru-Ni bimetallic catalysts, explicitly focusing on their application in the base-free oxidation of HMF to FDCA and the associated intermediates within an aqueous phase reaction. To comprehensively understand and elucidate the catalyst characteristics, advanced characterization techniques were employed, including powder X-ray diffraction (XRD), BET surface area analysis, field emission transmission electron microscopy (FETEM), high-resolution transmission electron microscopy (TEM), energy-dispersive X-ray spectroscopy (EDX), and X-ray photoelectron spectroscopy (XPS). These methodologies unraveled the developed catalyst intricacies, providing insights into their structural, surface, and compositional attributes. Additionally, monometallic catalysts were synthesized and subjected to testing to facilitate a comparative evaluation. This approach aimed to establish a contextual framework for assessing the performance and catalytic properties of the bimetallic catalysts in comparison to their monometallic counterparts.

4.2 Results and Discussion

4.2.1 Characterization of the Catalysts

The field emission transmission electron microscope (FETEM) imaging, high-resolution TEM (HRTEM) imaging, selected area electron diffraction (SAED), and energy-dispersive X-ray spectroscopy (EDX) elemental mapping (Fig. 4.1) was used to understand the particle size, crystal phases and elemental distribution of Ru-V/AC catalyst. The TEM images in Fig. 4.1a confirm that the metal particles were well dispersed on the surface of activated carbon support and exhibited different particle sizes with an average particle diameter of 1.05 nm (as analyzed using ImageJ software). The particle size distribution of Ru-V/AC was in the range of 0.71-2.27 nm (counted approximately 322 particles, inset of Fig. 4.1a). The Ru and V components

TH-3456_166107017

were evenly distributed throughout the catalyst, as indicated by EDX elemental mapping (Figs. 4.1b and 4.1c).

The HRTEM image of the 1.5Ru-0.5V/AC bimetallic catalyst revealed a crystalline structure with well-defined fringes (Fig. 4.1d). The average distance (lattice spacing) between neighboring planes was 0.21 nm (for ten fringes: 2.1 nm), which corresponds to the (101) crystal plane of ruthenium. The average lattice spacing of 0.57 nm (for ten fringes: 5.7 nm) corresponds to the (001) crystal plane of vanadium pentoxide (V_2O_5)[1]. The SAED pattern of the 1.5Ru-0.5V/AC catalyst demonstrated that most ruthenium nanoparticles were crystalline, with a cubic phase structure of Ru (101). The distinct ring pattern in SAED (Fig. 4.1e) indicates the polycrystalline nature of the bimetallic catalyst.

All the synthesized catalysts exhibited the combined Type I and Type IV N_2-sorption isotherms with H_4 hysteresis loop (Fig. 4.2a), demonstrating that the catalysts possess both micro and mesopores with slit-pore geometry. The BET-specific surface area (BET-SA) of the bare AC support was 775 m^2/g, with a pore volume of 0.51 cm^3/g and an average pore diameter (APD) of 2.63 nm (Table 4.1). The structure of the pores in the AC support remained intact upon metal impregnation. A decrease in BET-SA (from 775 to a minimum of 572 m^2/g) and in micropore SA (from 543 to a minimum of 373 m^2/g) and a marginal increase of APD (from 2.63 to a maximum of 3.02 nm) upon metal impregnation were observed. The decrease of BET-SA could be attributed to Ru and V_2O_5 species on the support surface. Meanwhile, the decrease in micropore SA could be attributed to the occupation of micropores with metal particles and possibly the blocking of micropores. The maximum decrease in micropore surface area was observed with the V/AC catalyst. The more significant decrease in micropore surface area with V/AC could be attributed to larger V_2O_5 particle size. The surface area of 1Ru-1V/AC is higher than 2Ru/AC, depending on the specific structural and compositional properties of the

TH-3456_166107017

materials involved. Here are some possible reasons for the enhancement of surface area in 1Ru-1V/AC compared to 2Ru/AC:

- Dispersion of Metal Particles: In 1Ru-1V/AC, the addition of vanadium (V) might lead to a better dispersion of ruthenium (Ru) particles on the activated carbon (AC) support. Better dispersion means smaller metal particles and more uniform coverage, increasing the accessible surface area.
- Modification of Support Structure: Vanadium might interact with the activated carbon support to create additional porosity or modify existing pores, thereby increasing the overall surface area[2].
- Formation of Ru-V alloy nanoparticles: The formation of Ru-V alloy nanoparticles on the support could lead to a different morphology with a higher surface area than the support with only ruthenium.
- Stabilization of the Support: Adding vanadium might stabilize the carbon support against structural collapse or sintering during preparation or usage, thus preserving the high surface area.

TH-3456_166107017

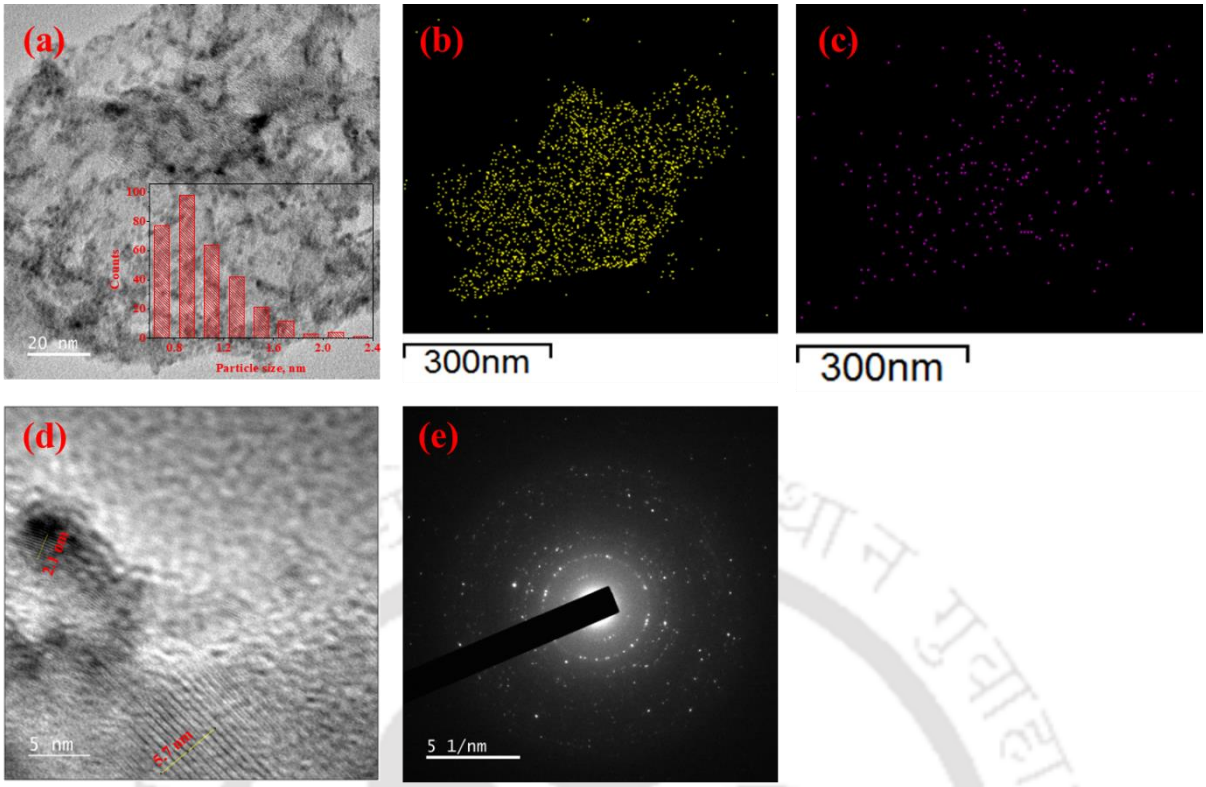

Figure 4.1: (a) FETEM image (inset: particle size distribution of the fresh catalyst) (b) XEDS image of Ru element (c) XEDS image of V element (d) HRTEM image with fringes and lattice spacing (e) SAED pattern (f) N_2 sorption isotherms of various Ru-V bimetallic catalysts supported on activated carbon.

The XRD patterns of activated carbon-supported Ru and V_2O_5 catalysts exhibited diffraction planes, (002) at 27° and (100) at 43° (JCPDS card No. 00-056-0159), corresponding to carbon with graphitic nature (Fig. 4.2b). The planes corresponding to Ru and V_2O_5 species were not visible, indicating low Ru and V species concentration and significant dispersion; however, for 2 wt.% Ru/AC catalyst, the diffraction plane of Ru (101) was observed at 43.3° (JCPDS card number 006-0663).

TH-3456_166107017

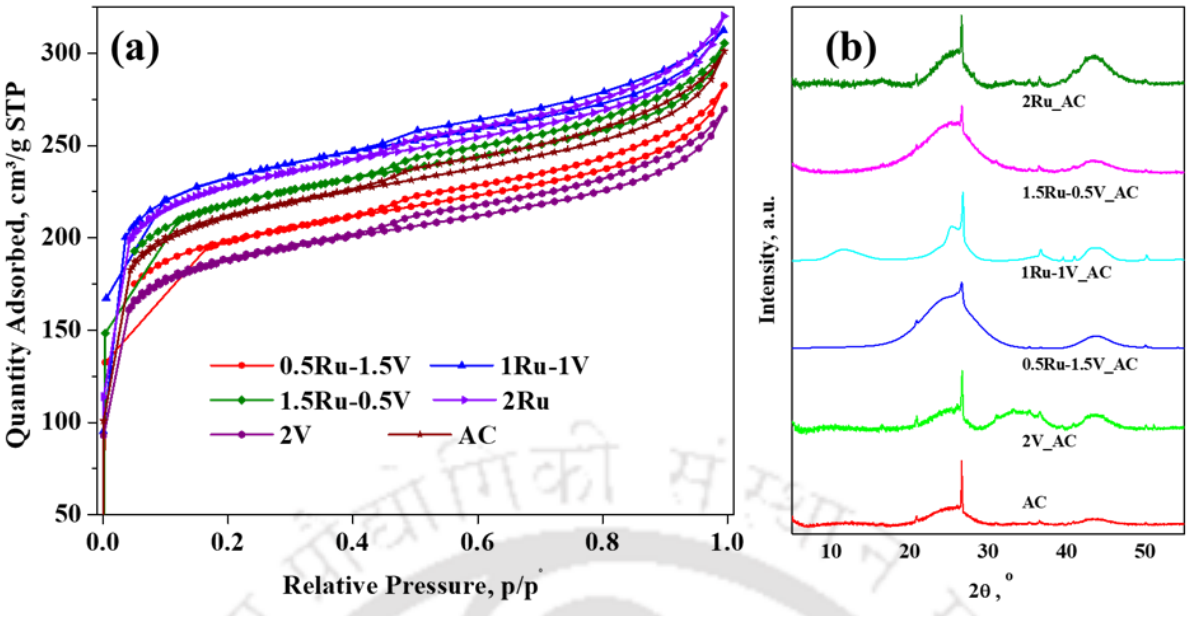

Figure 4.2: (a) BET N_2 sorption isotherms and (b) XRD patterns of various activated carbon-supported Ru-V bimetallic catalysts synthesized in this study. The data for bare activated carbon support was also included for the comparison.

The X-ray photoelectron spectroscopy (XPS) is used on Ru/AC, V/AC, and Ru-V/AC catalysts to understand their chemical state (Fig.4.3). The XPS survey spectra of 2Ru/AC, 2V/AC, and 1.5Ru-0.5V/AC are shown in Fig. 4.3a, while the high-resolution spectra of Ru 3d and V 2p are shown in Figs. 4.3b and 4.3c, respectively. The survey spectrum of the 1.5Ru-0.5V/AC catalyst shows peaks corresponding to Ru 3d, V2p, and C 1s orbitals, indicating that the bimetallic catalyst was effectively synthesized. By employing the peak fitting method, the Ru 3d and V2p core-level spectra of the 1.5Ru-0.5V/AC catalyst were deconvoluted into two significant Ru peaks (Ru $3d_{5/2}$ and Ru $3d_{3/2}$), and two significant V peaks ($V2p_{1/2}$ and $V2p_{3/2}$). The deconvolution verifies that the peaks with binding energies of 285.0 and 281.2 eV correspond to the Ru $3d_{3/2}$ and Ru $3d_{5/2}$ of the ruthenium metallic phase[3,4] of monometallic Ru/AC catalyst. According to Fig. 4.3b, the peak at 284.7 eV is related to activated carbon (C 1s) support used in the catalyst synthesis. Similar XPS peaks of metallic Ru (282.0 eV for Ru $3d_{5/2}$ and 285.0 eV for Ru $3d_{5/2}$) were observed for the Ru-V/AC catalyst (Fig. 4.3b). From the V2p high-resolution XPS spectrum (Fig. 4.3c) of Ru-V/AC and V/AC, two peaks

TH-3456_166107017

corresponding to the pentavalent oxidation state of vanadium were observed. The peaks at 517.4 and 523.2 eV binding energies correspond to the $V2p_{3/2}$ and $V2p_{1/2}$, respectively[5,6]. After adding V to the Ru catalysts, the binding energies of V in the R-V/AC catalyst show a negative shift compared to the corresponding value published in the literature.[5] The binding energies of V in Ru-V/AC catalysts were 516.7 and 523.9 eV are represented by high-resolution spectra of V2p as shown in Fig. 4.3c. The strong electronic interaction between Ru and V may alter the Ru electrical structure. The difference in binding energies of $V2p_{3/2}$ and $V2p_{1/2}$ indicates the creation of alloy nanoparticles between Ru and V species. As a result, catalyst activity could be increased.

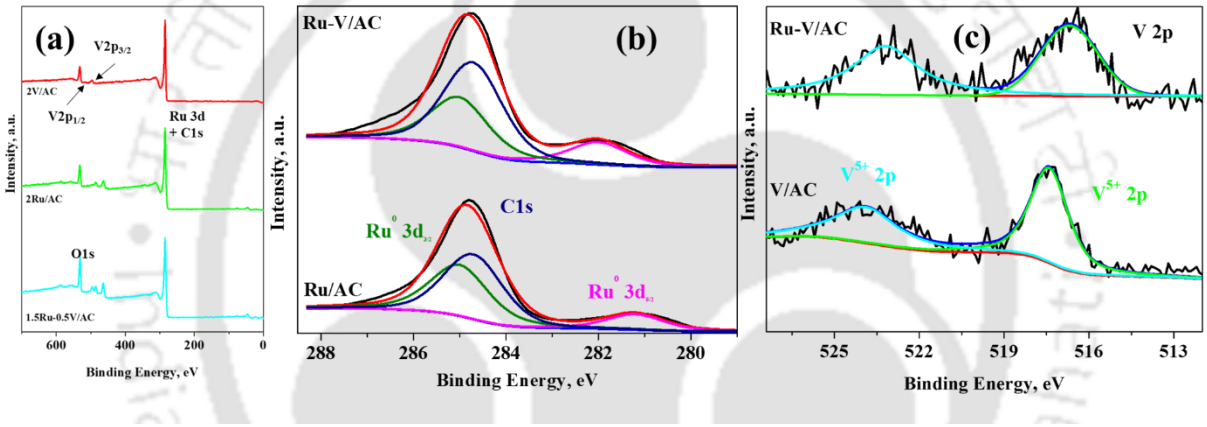

Figure 4.3: X-ray photoelectron spectroscopy (XPS) spectra: (a) Survey plots comparison of Ru-V/AC, Ru/AC, and V/AC catalysts; High-resolution XPS spectra of (b) Ru 3d spectra comparison of Ru-V/AC and Ru/AC catalysts and (c) V2p spectra comparison of Ru-V/AC and V/AC catalysts.

TH-3456_166107017

Table 4.1: Specific surface area, pore volume, and average pore size of various Ru-V bimetallic catalysts supported on activated carbon.

Catalyst code	Nominal catalyst composition		S_{BET} (m^2/g)	Pore volume (cm^3/g)	Pore size (nm)	Micropore area (m^2/g)	Micropore volume (cm^3/g)	Meso pore area (m^2/g)	Meso pore volume (cm^3/g)
	Ru%	V%[#]							
1Ru-1V/AC	1	1	744	0.480	2.59	508	0.26	89.0	0.132
1.5Ru-0.5V/AC	1.5	0.5	652	0.47	2.87	438.2	0.244	89.40	0.150
0.5Ru-1.5V/AC	0.5	1.5	572	0.370	3.02	384.0	0.224	86.0	0.144
2V/AC	0	2	592	0.340	2.785	373	0.194	154	0.153
2Ru/AC	2	0	715	0.410	2.74	468	0.244	90.6	0.160
AC	0	0	775	0.51	2.63	543	0.273	83.0	0.135
1.5Ru-0.5V/TiO_2	1.5	0.5	76.0	0.23	12.3	n/d	n/d	100.7	0.23
1.5Ru-0.5V/AC*	1.5	0.5	3.0	0.02	22.40	n/d	n/d	2.90	0.015

#Vanadium wt% in the form of V_2O_5; AC: Activated carbon, *Spent catalyst after four cycles; n/d: not determined.

TH-3456_166107017

4.3 Catalyst Activity Tests

4.3.1 Effect of metal weight ratio on HMF oxidation to FDCA

The effect of the metal weight ratio (Ru: V w/w; wt% of vanadium in the form of V_2O_5) of Ru-V/AC bimetallic catalysts on the conversion of HMF to FDCA was investigated (Fig. 4.4). Additionally, the performance of bimetallic catalysts was compared to that of monometallic catalysts (Ru/AC and V/AC). The conversion of HMF was only 64% with the V/AC monometallic catalysts. It was 100% over Ru-V/AC bimetallic and Ru/AC monometallic catalysts. FDCA was not observed over the V/AC catalyst, and the reaction mostly stopped at DFF (yield 24.2%) and FFCA (yield 3.4%). The FDCA yield initially increased with Ru content and passed through a maximum (with an FDCA yield of 65.2%) at 1.5 wt% Ru in the bimetallic catalyst. The DFF yield decreased with increased Ru content in the bimetallic catalyst and became 0% at higher Ru contents (≥ 1 wt%). Without vanadium, the monometallic Ru/AC catalyst exhibited FDCA and FFCA yields of 20.2% and 63.5%, respectively, and no DFF formed. This indicates a synergism between V_2O_5 and ruthenium in enhancing the catalytic performance of Ru-V/AC bimetallic catalyst in HMF conversion to FDCA.

4.3.2 Effect of temperature and time on HMF oxidation to FDCA

The selective oxidation of HMF to FDCA was studied using Ru-V bimetallic catalysts supported on activated carbon. The effect of temperature on the reaction was evaluated using 1%Ru-1%V/AC bimetallic catalyst at 1 MPa O_2 for a reaction time of 4 h. The yield of FDCA increased from 51.9 to 61.8% with increasing temperature from 110 to 120 °C. Further increases in temperature to 130 and 140 °C decreased the FDCA yield to 59.7% and 52.9%, respectively (Fig. 4.5). The conversion of HMF was 100% at all temperatures. Increasing the reaction temperature enhances the formation of humins (undesirable by-products) from HMF

TH-3456_166107017

with water as a solvent due to condensation reactions. At elevated temperatures, DFF and FFCA intermediates demonstrate reduced stability compared to FDCA and convert to FDCA. As a result, the yield of FFCA decreased significantly relative to FDCA (Fig.4.5). The base-free oxidation of HMF using molecular oxygen with heterogeneous monometallic and bimetallic catalysts involves several key steps. Initially, HMF is converted to DFF, which rapidly transforms into FFCA. The subsequent conversion of FFCA to FDCA represents the rate-limiting step in the process. Achieving this step efficiently requires higher temperatures or longer reaction times at lower temperatures (Figs. 4.6 and 4.7).

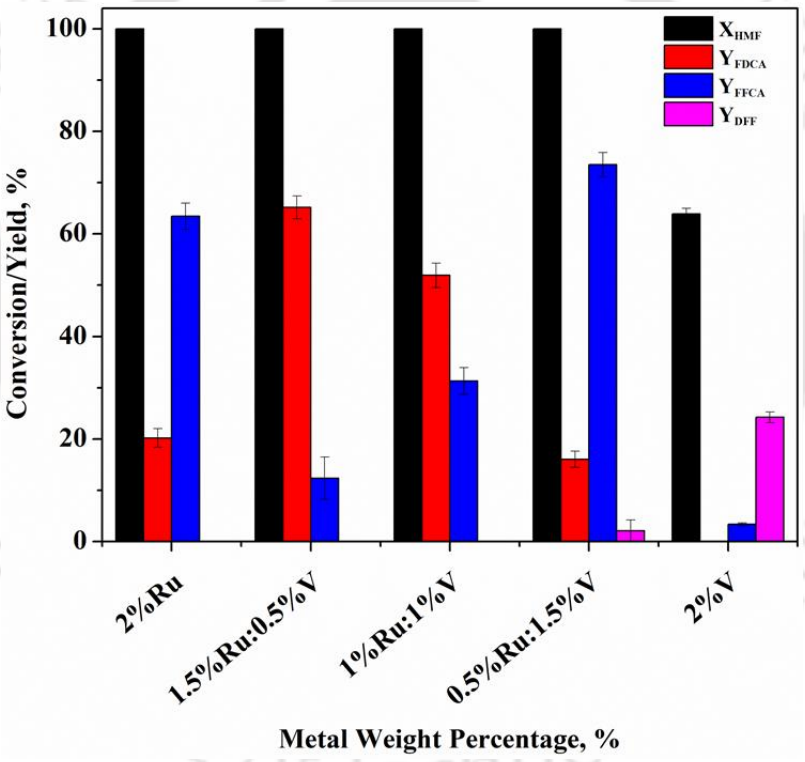

Figure 4.4: Effect of metal weight percentage (total metal loading: 2 wt%) on the conversion of HMF to FDCA. Reaction conditions: temperature 110 °C, pressure 1.0 MPa O_2, reaction time 4 h.

TH-3456_166107017

Table 4.2: Carbon balance at various process conditions in 5-HMF oxidation to FDCA.

S.No.	Catalyst	T (°C)	P (bar)	Time (h)	CB (%)
1	2%Ru/AC	110	10	4	85.2
2	1.5%Ru-0.5%V/AC	110	10	4	80.3
3	1.0%Ru-1.0%V/AC	110	10	4	85.6
4	0.5%Ru-1.5%V/AC	110	10	4	94.5
5	2%V/AC	110	10	4	65.3
6*	1.5%Ru-0.5%V/AC	110	10	4	91.6
7$	1.5%Ru-0.5%V/AC	110	10	4	90.3
8	1.5%Ru-0.5%Ni/AC	110	10	12	97.3
9	1.5%Ru-0.5%Ni/AC	120	10	12	97.0
10	1.5%Ru-0.5%Ni/AC	130	10	12	97.0
11	1.5%Ru-0.5%Ni/AC	140	10	12	79.2
12	1.5%Ru-0.5%Ni/AC	140	5	12	78.6
13	1.5%Ru-0.5%Ni/AC	140	15	12	74.1
14	1.5%Ru-0.5%V/AC	100 + 100	10	2 + 2	85.0
15	1.5%Ru-0.5%V/AC	100 + 110	10	2 + 2	80.9
16	1.5%Ru-0.5%V/AC	100 + 120	10	2 + 2	88.6
17	1.5%Ru-0.5%V/AC	100 + 130	10	2 + 2	82.2
18	1.5%Ru-0.5%V/AC	100 + 140	10	2 + 2	68.5
19	1.5%Ru-0.5%V/AC	100 + 150	10	2 + 2	54.5
20	1.0%Ru-1.0%V/AC	120	10	4	75.3
21	1.0%Ru-1.0%V/AC	130	10	4	64.9
22	1.0%Ru-1.0%V/AC	140	10	4	54.7

*DMSO, $ DMSO + Water

TH-3456_166107017

The FFCA yield was the highest (31.3%) at a lower temperature (110 °C), decreased monotonically with temperature, and was approximately 0% at 140 °C. A negligible amount of DFF formed at all temperatures studied. The lower carbon balance (Table 4.2, Entry 22) can be attributed to the formation of humins, an undesired material, from the HMF through condensation reactions.[7] The effect of reaction time on the conversion of HMF to FDCA was studied using the 1.5%Ru-0.5%V/AC bimetallic catalyst at 100 °C and 1 MPa O_2 (Fig. 4.6). 100% HMF conversion was observed at all reaction times studied. The FDCA yield was lower at lower reaction times and increased with reaction time, with a maximum yield of 71.0% achieved at 12 h with a 78.3% carbon mass balance. The DFF yield was the highest at lower reaction times (1 h), decreased with reaction time, and became 0 % at higher reaction times (>4 h). The FFCA yield first increased from 50.6% to 53.6% with an increase of reaction time from 1 h to 2 h. Further increase in reaction time resulted in the monotonic decrease of FFCA.

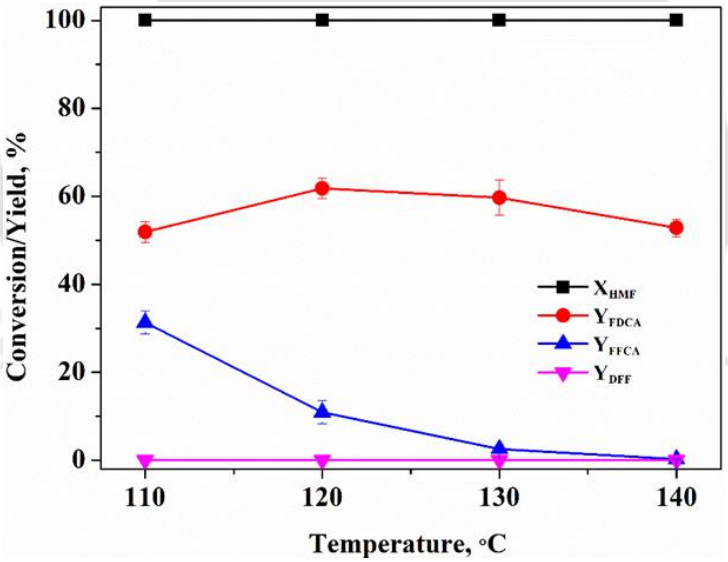

Figure 4.5: Effect of temperature on the conversion of HMF and yields of FDCA, FFCA, and DFF over 1Ru-1V/AC bimetallic catalyst. Other reaction conditions: reaction time: 4 h, HMF/metal molar ratio: 5.8 (mol/mol), pressure: 1.0 MPa O_2.

TH-3456_166107017

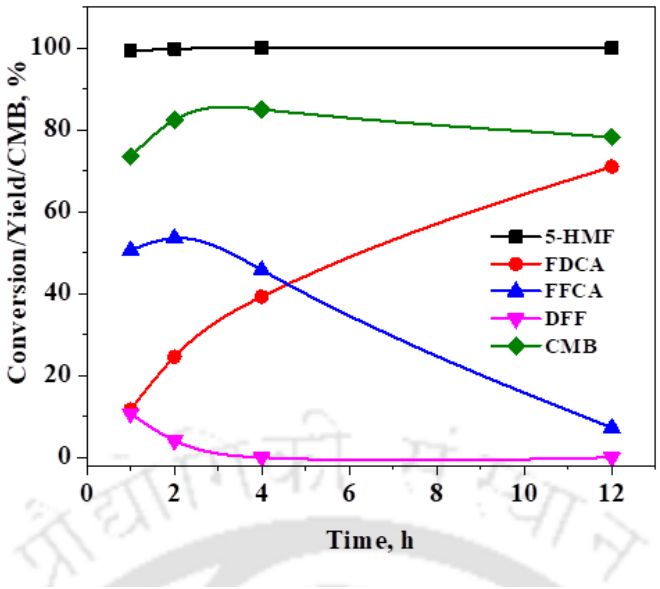

Figure 4.6: Effect of reaction time on the conversion of HMF and yields of FDCA, FFCA, and DFF over 1.5Ru-0.5V/AC bimetallic catalyst. Other reaction conditions: temperature: 100 ℃, HMF/metal molar ratio: 8.3 (mol/mol), pressure: 1.0 MPa O_2.

A combination of two different temperatures was used to understand the effect of two-step temperature on the conversion of HMF to FDCA in a single pot. The reaction temperature was kept constant at 100 ℃ for 2 h in the first step. This initial step ensured 100% conversion of HMF to other products, such as FFCA and DFF, before moving on to the next step. Due to milder conditions in this step, the humins formation was minimized. In the second step, the reaction temperature was varied from 100 to 150 ℃ for 2 h reaction time at each temperature (Fig. 4.7a). A single step at high temperature converts some of the HMF to humins, resulting in lower FDCA yield. Therefore, converting HMF to a relatively stable product (FFCA or DFF) selectively at low temperatures reduces the humins formation. Then, converting FFCA/DFF to FDCA at high temperatures yields higher FDCA and speeds up the process. Following this strategy, the FDCA yield was increased with increasing temperature, and the FFCA yield decreased at 130 ℃. The FDCA yield decreased at higher temperatures, and the FFCA yield was approximately constant. A maximum FDCA yield of 74.4% was achieved at a second-step temperature of 130 ℃ (2 h reaction time) after an initial 2 h reaction at 100 ℃. The carbon

TH-3456_166107017

mass balance decreased (82.2% to 68.5%) as the temperature increased from 130 to 140 °C, indicating that more of the starting material was converted into undesired products at high temperatures.

4.3.3 Effect of solvent type and combination of solvents on HMF oxidation to FDCA

The effect of solvent and combination of solvents on the conversion of HMF to FDCA was studied over the 1.5%Ru-0.5%V/AC catalyst (Fig. 4.7b). The results indicate that while complete conversion of HMF was achieved in pure water and DMSO, the combination of water and DMSO (1:2 volume ratio) resulted in a lower conversion of HMF (88.7%). Additionally, the yield of FDCA was higher, and FFCA was lower in water than in DMSO. With water as a solvent, the yields of FDCA and FFCA were 65.2 and 12.4%, and those with DMSO as a solvent were 57.7 and 32.9%, respectively. The DFF was not observed in either case. In the mixed water + DMSO solvent, the FDCA yield was meager (1.1%), the FFCA yield was 61.4%, and the DFF yield was 14.7%. The carbon mass balance was higher in DMSO (91.6%) and the mixed solvent (90.2%) than in water (80.3%). The lower carbon balance in water could be due to the formation of humins, which form from condensation and degradation reactions of HMF. The aprotic solvent, DMSO, helps stabilize the charged starting materials, intermediates, and transition states during oxidation, potentially enhancing the reaction rate and yield[8–10]. The increase in selectivity towards FFCA in the presence of DMSO can be attributed to several factors related to the solvent's interaction with HMF and the reaction intermediates. Based on the literature, it can be explained by different factors:

Solubility and stability of HMF**:** DMSO is known to solvate HMF effectively due to its polarity and ability to form hydrogen bonds. This solvation stabilizes HMF, preventing its further

TH-3456_166107017

degradation or side reactions, and provides more scope to convert the HMF to FFCA with more selectivity.

Effect on reaction intermediates: DMSO can preferentially solvate reaction intermediates such as DFF and FFCA during oxidation. This preferential solvation may stabilize these intermediates, reducing their tendency to undergo side reactions or decomposition pathways.

Catalyst interaction: DMSO may also interact with the catalyst surface differently than other solvents, influencing the catalyst's activity and selectivity towards FFCA. This interaction can enhance the catalyst's ability to promote the oxidation of DFF to FFCA, thereby increasing FFCA selectivity.

Reaction kinetics: The presence of DMSO may alter the reaction kinetics by affecting the transition states involved in the oxidation steps leading to FFCA. This can lead to a more favorable pathway toward FFCA formation, increasing its selectivity. In summary, the enhanced selectivity towards FFCA in the presence of DMSO can be explained by its ability to stabilize HMF and reaction intermediates, influence catalyst behavior, and potentially alter reaction kinetics favorably. These factors collectively contribute to a higher FFCA yield than other solvents (Fig. 4.7b).

TH-3456_166107017

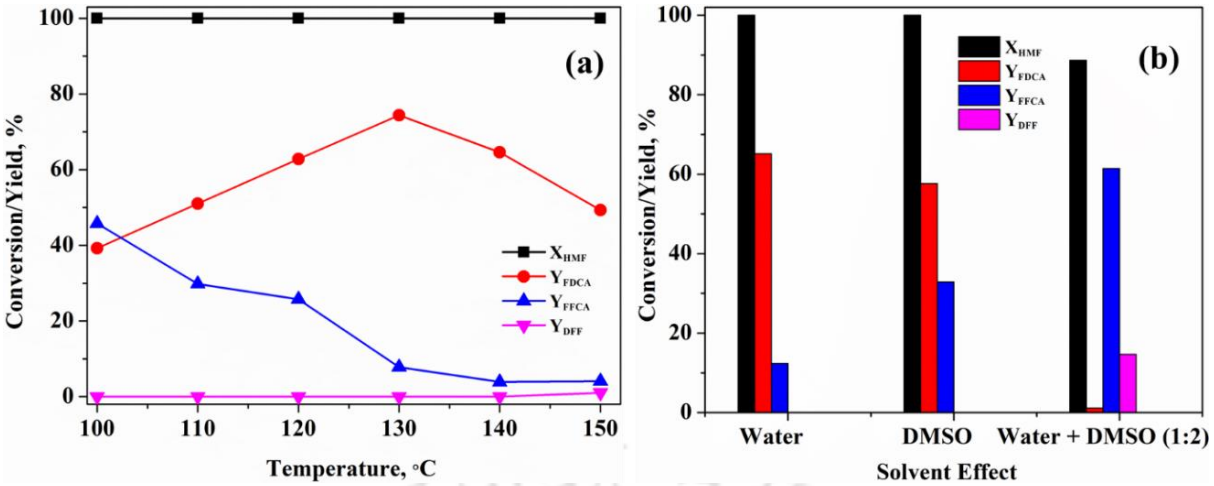

Figure 4.7: Conversion of HMF to FDCA over 1.5%Ru-0.5%V/AC bimetallic catalyst. (a) Two-step process (Kept for 2 h at 100 ℃ and then for 2 h at varying temperatures), (b) Solvent effect. Other reaction conditions: HMF/metal molar ratio 8.3 (mol/mol), pressure 1.0 MPa O_2, temperature 110 ℃, reaction time 4 h.

4.3.4 Effect of temperature and pressure on HMF conversion to FDCA over Ru-Ni/AC bimetallic catalyst

This work also studied the performance of 1.5Ru-0.5Ni/AC bimetallic catalyst (the effect of temperature and pressure) to convert HMF to FDCA with a 12 h reaction time. The HMF conversion was 100% at all temperatures and pressures, as shown in Figs 4.8a and 8b. The yield of FDCA increased first and then decreased with the temperature increase from 110 to 140 ℃, reaching a peak at 130 ℃ with a maximum FDCA yield of 63.6%. It suggests higher temperatures (140 ℃) lead to HMF degradation or the formation of humins. The yield of the intermediate product, FFCA, decreased monotonically as the temperature increased from 110 to 140 ℃. The yield of another intermediate DFF was close to 0% at all temperatures studied. The carbon mass balance was similar (97.0%) at all temperatures except at 140 ℃ (79.2%). With increased O_2 pressure from 0.5 to 1.5 MPa, the yield of FDCA increased (from 54.3 to 65.3%), and the FFCA yield decreased from 21.5 to 4.4%. The carbon mass balance was slightly decreased from 79.2% to 74.1% with increasing pressure from 1.0 to 1.5 MPa O_2.

TH-3456_166107017

These results suggest that the 1.5Ru-0.5Ni/AC bimetallic catalyst can be an excellent alternative to the Ru-V/AC bimetallic catalyst to oxidize HMF to FDCA. However, these catalysts required a higher reaction time (12 h) than the Ru-V/AC catalyst (4 h).

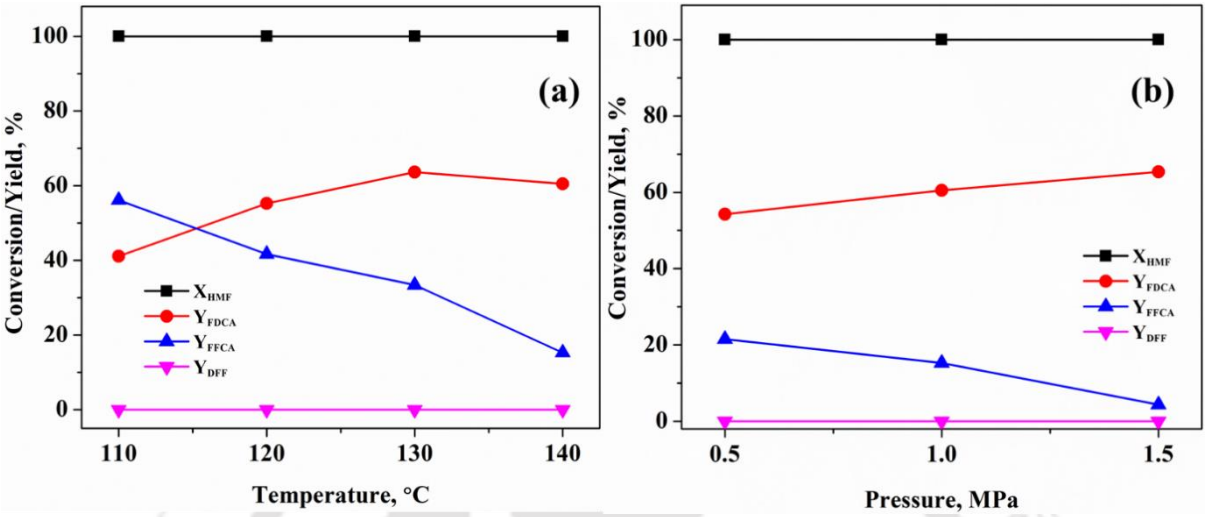

Figure 4.8: Conversion of HMF to FDCA over 1.5Ru-0.5Ni/AC bimetallic catalyst: Effect of (a) temperature and (b) pressure. Reaction conditions: HMF/metal molar ratio 5.3 mol/mol, pressure 1.0 MPa O_2 for (a), temperature 140 ℃ for (b) and reaction time 12 h.

4.3.5 Catalyst stability and reusability study

The stability and recyclability of a catalyst are essential to evaluate its potential for industrial use. The 1.5%Ru-0.5%V/AC catalyst was tested for its stability by conducting multiple experiments to convert HMF to FDCA by using the same catalyst from the previous cycle (Fig. 9a). The study looked at the effect of humins or coke deposition on the catalyst surface. The humins are unwanted by-products of the reaction that can accumulate on the catalyst and reduce its effectiveness. The effect of washing the catalyst with water and acetone on the performance was tested. The results showed that the conversion of HMF decreased from 100% in cycle 1 to 96.4% in cycle 4. The yield of FDCA decreased monotonically from 37.5% to 12.0% from cycle 1 to cycle 4. The FDCA yield was lower due to humins formation caused by the condensation of HMF in water and their subsequent deposition on the catalyst surface.[7] The FFCA yield increased gradually from 25.0 to 47.1% from cycles 1 to 3 and decreased in cycle

TH-3456_166107017

4 (39.8%). The DFF yield increases monotonically from 0.6% in cycle 1 to 25.5% in cycle 4. After washing the catalyst with acetone, the FDCA yield increased significantly from 12.0% to 42.7% from cycle 4 to cycle 5. The change in FFCA yield was negligible between cycle 4 and cycle 5. The DFF yield decreased from 25.5% in cycle 4 to 4.1% in cycle 5 due to improved catalyst activity after removing humins from the surface by acetone wash. After cycle 5, the catalyst was washed with only water and tested in cycle 6. A decrease in FDCA yield from 42.7% in cycle 5 to 31.1% in cycle 6 and an increase in FFCA yield from 39.6% in cycle 5 to 52.8% in cycle 6 were observed. The DFF yield increased from 4.1 to 15.5% in cycle 6 because humins were not entirely removed just by water wash. FETEM analysis performed on the spent catalyst (Fig. 9b) shows an average particle size of 0.7 nm and a particle size distribution of 0.37–1.62 nm. The number of particles counted was approximately 1780. The average particle size decreased from 1.1 nm for the fresh catalyst to 0.7 nm for the used catalyst, as shown in the inset of Fig. 9b.

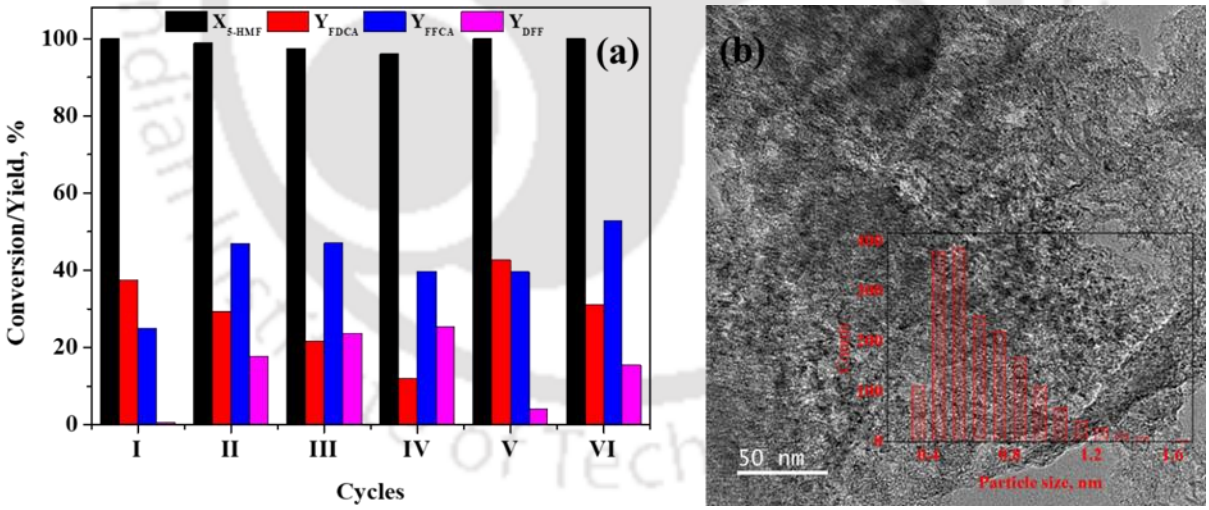

Figure 4.9: (a) Stability studies of 1.5Ru-0.5V/AC catalyst for conversion of HMF to FDCA, (b) FETEM image of the used catalyst (inset: Metal particle size distribution). Reaction conditions: 130 ^{o}C temperature, HMF/metal: 8.3 (mol/mol), pressure: 1.0 MPa O_2, 4 h reaction time.

TH-3456_166107017

4.4 Summary

Bimetallic and monometallic catalysts were successfully synthesized using wet impregnation and chemical reduction. These catalysts were used in the base-free oxidation of 5-hydroxymethylfurfural (HMF) to FDCA in aqueous, DMSO, and combined solvents. Due to the synergism between Ru and V_2O_5 in Ru-V_2O_5/AC and Ru and Ni in Ru-Ni bimetallic catalysts, they exhibit excellent performance compared to their monometallic counterparts for oxidizing HMF to FDCA. The highest FDCA yield of 74.4% and 65.3% was observed with the Ru-V_2O_5/AC and Ru-Ni/AC bimetallic catalysts. The Ru-V_2O_5/AC bimetallic catalyst was stable after washing with the acetone.

TH-3456_166107017

References

(1) Kumar, N. S.; Chang, J. H.; Ho, M. S.; Balraj, B.; Chandrasekar, S.; Mohanbabu, B.; Gowtham, M.; Guo, D.; Mohanraj, K. Impact of Zn2+ Doping on the Structural, Morphological and Photodiode Properties of V2O5 Nanorods. J Inorg Organomet Polym Mater 2021, 31 (3), 1066–1078. https://doi.org/10.1007/s10904-020-01751-y.

(2) Hu, P.; Lang, W.-Z.; Yan, X.; Chen, X.-F.; Guo, Y.-J. Vanadium-Doped Porous Silica Materials with High Catalytic Activity and Stability for Propane Dehydrogenation Reaction. 2018. https://doi.org/10.1016/j.apcata.2018.01.014.

(3) Kandasamy, P.; Gogoi, P.; Venugopalan, A. T.; Raja, T. A Highly Efficient and Reusable Ru-NaY Catalyst for the Base Free Oxidation of 5-Hydroxymethylfurfural to 2,5-Furandicarboxylic Acid. Catal Today 2021, 375, 145–154. https://doi.org/10.1016/J.CATTOD.2020.05.009.

(4) Morgan, D. J. Resolving Ruthenium: XPS Studies of Common Ruthenium Materials. Surface and Interface Analysis 2015, 47 (11). https://doi.org/10.1002/sia.5852.

(5) Romanyuk, A.; Oelhafen, P. Oxidation of Vanadium with Reactive Oxygen Plasma: A Photoelectron Spectroscopy Study of the Initial Stages of the Oxide Growth Process. Thin Solid Films 2007, 515 (16), 6544–6547. https://doi.org/10.1016/J.TSF.2006.11.055.

(6) Niu, C.; Huang, M.; Wang, P.; Meng, J.; Liu, X.; Wang, X.; Zhao, K.; Yu, Y.; Wu, Y.; Lin, C.; Mai, L.; Berlin, S.-V. Carbon-Supported and Nanosheet-Assembled Vanadium Oxide Microspheres for Stable Lithium-Ion Battery Anodes. https://doi.org/10.1007/s12274-015-0896-6.

TH-3456_166107017

(7) Xuewang Han; Liang Geng; Yong Guo; Rong Jia; Xiaohui Liu; Yongguang Zhang; Yanqin Wang. Base-Free Aerobic Oxidation of 5-Hydroxymethylfurfural to 2,5-Furandicarboxylic Acid over a Pt_C–O–Mg Catalyst. Green Chem. 2016, 18, 1597–1604.

(8) Lai, J.; Liu, K.; Zhou, S.; Zhang, D.; Liu, X.; Xu, Q.; Yin, D. Selective Oxidation of 5-Hydroxymethylfurfural into 2,5-Diformylfuran over VPO Catalysts under Atmospheric Pressure †. 2019. https://doi.org/10.1039/c9ra02213a.

(9) Chen, G.; Wu, L.; Fan, H.; Li, B. Highly Efficient Two-Step Synthesis of 2,5-Furandicarboxylic Acid from Fructose without 5-Hydroxymethylfurfural (HMF) Separation: In Situ Oxidation of HMF in Alkaline Aqueous H 2 O/DMSO Mixed Solvent under Mild Conditions. Ind. Eng. Chem. Res 2018, 57, 58. https://doi.org/10.1021/acs.iecr.8b03589.

(10) Liu, H.; Cao, X.; Wang, T.; Wei, J.; Tang, X.; Zeng, X.; Sun, Y.; Lei, T.; Liu, S.; Lin, L. Efficient Synthesis of Bio-Monomer 2,5-Furandicarboxylic Acid from Concentrated 5-Hydroxymethylfurfural or Fructose in DMSO/H 2 O Mixed Solvent. 2019. https://doi.org/10.1016/j.jiec.2019.04.038.

TH-3456_166107017

TH-3456_166107017

Chapter 5

Selective aerobic oxidation of glycerol to lactic acid over ruthenium-vanadium bimetallic catalysts

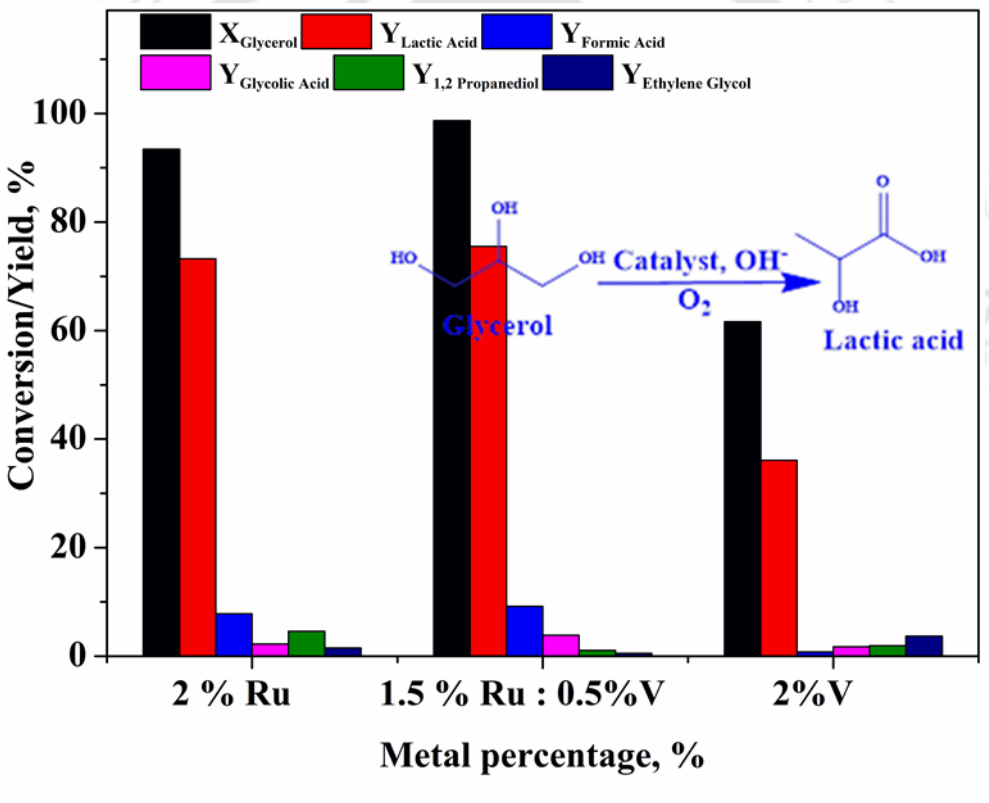

TH-3456_166107017

5.1 Objectives

In this work, for the first time, a unique Ru-V bimetallic catalyst on activated carbon support has been studied for its effectiveness in GL conversion to LA. Advanced characterization techniques such as powder XRD, BET surface area analysis, FETEM, high-resolution TEM, EDX, and XPS were used to characterize the developed catalysts. The catalysts were tested for the selective oxidation of glycerol to lactic acid at high glycerol concentration (40 wt%) in the temperature and O_2/air pressure ranges of 160-200 ^oC and 5-15 bar, respectively, and glycerol to the metal molar ratio of 4400-8800 mol/mol. The monometallic catalysts were also prepared and tested for comparative assessment.

5.2 Results and Discussion

The previous chapter thoroughly characterized the catalysts used in this chapter (i.e., Chapter 4). Therefore, the catalyst activity test results for glycerol to lactic acid conversion are presented here.

5.2.1 Catalyst Activity Tests

5.2.1.1 Effect of the base type and catalyst loading

The selective oxidation of glycerol (GL) to lactic acid (LA) was investigated over 1.5Ru:0.5V/AC bimetallic catalyst in the presence of base materials (NaOH and KOH) to understand their influence on the activity and selectivity of the desired product. In the presence of NaOH, the GL conversion and LA yield were significantly higher than those in the presence of KOH. For example, the GL conversion and LA yield were 97.3% and 62.3% with NaOH, while those with KOH were 68.5 and 40.0%, respectively. Further, the yield of FA increased from 5.2% (with KOH) to 9.7% (with NaOH), while that of 1,2-PDO decreased from 4.2%

TH-3456_166107017

(with KOH) to 2.3% (with NaOH). The EG (0.8%) and GLA yields were nearly identical in both cases (Fig. 5.1a). The glycerol conversion rates, and lactic acid yields are higher in the presence of NaOH as compared to KOH; the possible reasons are that KOH and NaOH have different ionic strengths due to the size and charge density of their respective ions (K^+ and Na^+)[1]. The smaller size and higher charge density of K^+ ions compared to Na^+ ions can be led to differences in their interactions with other ions and molecules in solution, affecting their reactivity and, consequently, their conversion rates in chemical processes. In addition to this, the equilibrium constants for dissociation and solubility product constants may vary slightly due to different chemical environments created by potassium and sodium ions in the solution. These variations can influence the availability of hydroxide ions and thus impact the overall reaction conversion rates. Bruno et al.[1] also reported a similar performance with NaOH compared to KOH.

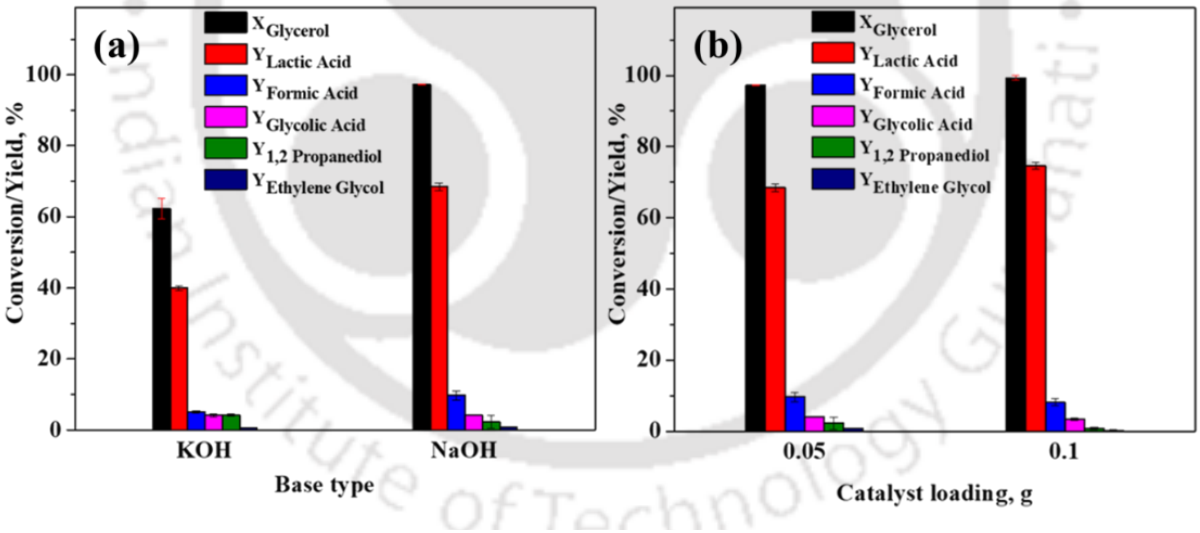

Figure 5.1: Effect of base type (a) catalyst loading (b) on glycerol to lactic acid conversion over Ru-V/AC bimetallic catalysts. The other reaction conditions: 200 °C temperature, 5 bar air pressure, 3 h reaction time, 0.05 g catalyst (glycerol/metal molar ratio: 8800), and 1:1 base (KOH or NaOH) to glycerol molar ratio.

TH-3456_166107017

The effect of catalyst loading on the selective conversion of GL to LA was evaluated using the catalyst loadings in the range of 0.05 and 0.1 g (8800 and 4400 glycerol/metal mol/mol) in the presence of NaOH. A moderate increase in the yield of LA (68.5 to 74.6%) and a marginal increase in glycerol conversion (97.3 to 99.4%) with catalyst loading were observed (Fig. 5.1b). Meanwhile, the yields of byproducts, such as FA, GLA, 1,2-PDO, and EG, decreased with catalyst loading. In subsequent trials, NaOH was used as base material, and the catalyst loading was fixed at 0.1 g (4400 glycerol/metal mol/mol).

5.2.1.2 Effect of temperature and pressure

The effect of reaction conditions, such as temperature (160-200°C) and air pressure (5-15 bar), on the aerobic oxidation of GL to LA was investigated over 1.5Ru-0.5V/AC bimetallic catalysts. The GL conversion and LA yield significantly increased from 76.2 to 98.7% and 47.7 to 75.5%, respectively, as the reaction temperature increased from 160 to 200 °C (Fig. 5.2a). The yields of byproducts, FA, 1,2-PDO, GLA, and EG, decreased slightly from 10.5, 6.0, 5.6, and 0.9% to 9.2, 1.1, 3.9, and 0.5%, respectively. Due to equipment limitations, we have not conducted the experiments beyond 200 ℃ reaction temperature due to safety limitations (limited lifespan due to corrosion under high alkaline conditions and the need to withstand high pressure). The results suggest that the yield of lactic acid was a function of relative reaction rates of two parallel reactions of glyceraldehyde or dihydroxyacetone to lactic acid and glyceric acid (Scheme 5.1) and that the high temperature favors the lactic acid pathway[2–4].

TH-3456_166107017

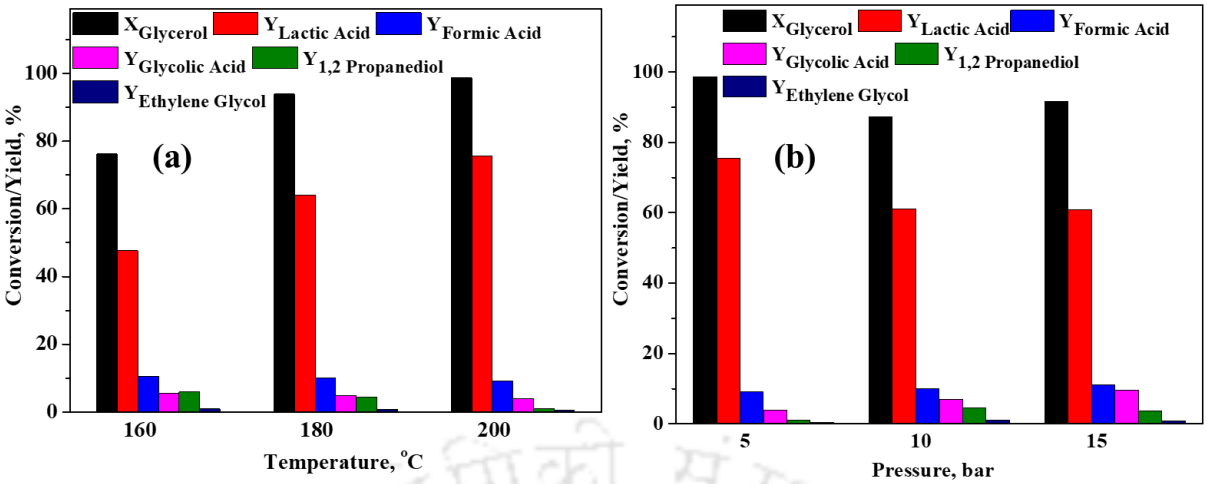

Figure 5.2: Glycerol to lactic acid conversion over Ru-V/AC bimetallic catalysts: Effect of (a) temperature, (b) pressure. The other reaction conditions were: 200 °C temperature, 5 bar air pressure, 3 h reaction time, 0.1 g catalyst (glycerol/metal molar ratio: 4400), and 1:1 base (NaOH) to glycerol molar ratio.

Lactic acid (LA) yield decreased from 75.5 to 60.9% as the air pressure increased from 5 to 15 bar (Fig. 5.2b). The decrease was more, from 75.53% to 61.11%, in the lower pressure range (5 to 10 bar). Additionally, the yields of byproducts such as formic acid (9.2% to 11.2%) and glycolic acid (3.9% to 9.6%) moderately increased with the pressure increase from 5 to 15 bar. However, the yield of 1,2-propanediol (1,2-PDO) and ethylene glycol (EG) first increased with air pressure from 5 to 10 bar and then decreased with a further increase in air pressure from 10 to 15 bar. According to the proposed reaction scheme, the rate of the undesired pathway from glyceraldehyde to glycolic acid through glyceric acid is expected to increase at higher air pressures, resulting in higher selectivities to glycolic acid and therefore, the yield of lactic acid was reduced at higher air pressures. It was demonstrated through experimental investigations, as illustrated in Fig. 5.2b. The formation of lactic acid is determined by the relative rates of the base-catalyzed reaction pathway to lactic acid and the oxidation pathway

TH-3456_166107017

to glycolic acid via glyceric acid (Scheme 5.1). The subsequent trials were conducted at a fixed reaction temperature of 200 °C and an air pressure of 5 bar.

5.2.1.3 Effect of reaction time and oxidant type

The effect of reaction time (Fig. 5.3a) and oxidant type (Fig. 5.3b) on GL conversion and LA yield over 1.5Ru-0.5V/AC were studied. To investigate the further conversion of intermediates and optimize lactic acid yield, the experiments were extended to 6 h. Surprisingly, extending the reaction time to 6 h did not lead to increased lactic acid yield. The yield of LA marginally decreased from 75.5 to 72.4%, with an increase in the reaction time from 3 to 6 h (Fig. 5.3.3a). The yield of other byproducts, FA and GLA, decreased from 9.2 and 3.9 % to 7.9 and 1.8 %, respectively, with reaction time. The byproducts 1,2-PDO and EG were not observed at higher reaction times (6 h). This could be attributed to the fact that at higher reaction times, the 1,2-PDO further converts to lactic acid or pyruvaldehyde[5,6]. The longer reaction times promote further oxidation of LA, FA, and GLA to gaseous products (Scheme 5.1).

A marginal decrease in LA yield (from 75.5 to 72.7%) was observed in the presence of molecular oxygen compared to that in the air (Fig. 5.3b). The glycerol conversion was 100% in both cases. The yields of byproducts FA, GLA, and EG were reduced, and no formation of 1,2-PDO was observed in the presence of molecular oxygen. The results indicate that the over-oxidation is more severe in the presence of molecular oxygen, which further oxidizes the products LA, FA, GLA, 1,2-PDO, and EG into gaseous products (Scheme 5.1).

TH-3456_166107017

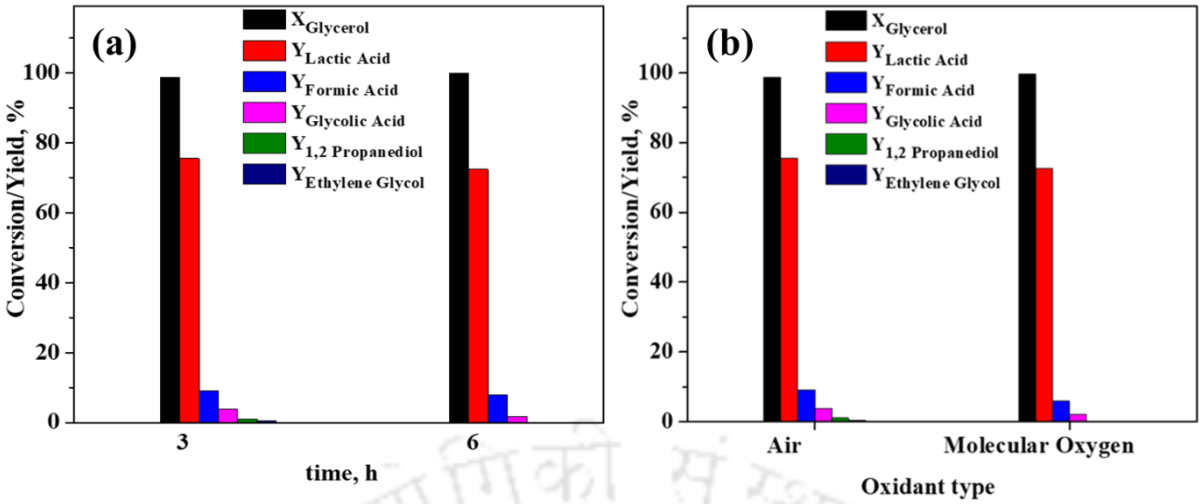

Figure 5.3: Effect of reaction time (a) oxidant type (b) on glycerol to lactic acid conversion over Ru-V/AC bimetallic catalysts. Reaction conditions: 200 °C temperature, 5 bar air pressure, 0.1 g catalyst (glycerol/metal molar ratio: 4400), 3 h reaction time, and 1:1 (NaOH) to glycerol molar ratio.

5.2.1.4 Effect of metal weight ratio in the bimetallic catalyst on its activity

The effect of the metal weight ratio (Ru: V w/w; wt% of vanadium in the form of V_2O_5) Ru-V/AC bimetallic catalysts on the conversion of GL to LA was examined (Fig. 5.4a). Additionally, the performance of bimetallic catalysts was compared to that of monometallic catalysts Ru/AC and V/AC. The conversion of glycerol and yield of LA was the lowest with the V/AC monometallic catalyst. Both conversion and yield were increased with increased Ru concentration in the bimetallic catalyst and passed through a maximum. The yield of LA was the highest with a 1.5Ru-0.5V/AC bimetallic catalyst. At the same time, the conversion of GL was the highest with the 1R-1V/AC bimetallic catalyst. Therefore, the selectivity to LA (yield/conversion) was the highest with 1.5Ru-0.5V/AC bimetallic catalyst, demonstrating synergism between Ru and V, which results in the highest selectivity. The 1.5Ru:0.5V/AC catalysts yielded 75.5 % LA at 98.7% GL conversion. In addition, the 1.5Ru-0.5V bimetallic catalyst supported over TiO_2 was also investigated. The yield of LA was higher (77.9 Vs. 75.5 %), and the GL conversion was lower (97.8 Vs. 98.7%) over 1.5Ru-0.5V/TiO_2 compared to

TH-3456_166107017

those over 1.5Ru-0.5V/AC (Fig. 5.4b). However, the yield of byproducts, FA (12.5%), GLA (4.0%), 1,2-PDO (6.5%), and EG (1.3%), were also higher over 1.5Ru-0.5V/TiO_2 as compared to those with 1.5Ru-0.5V/AC catalyst.

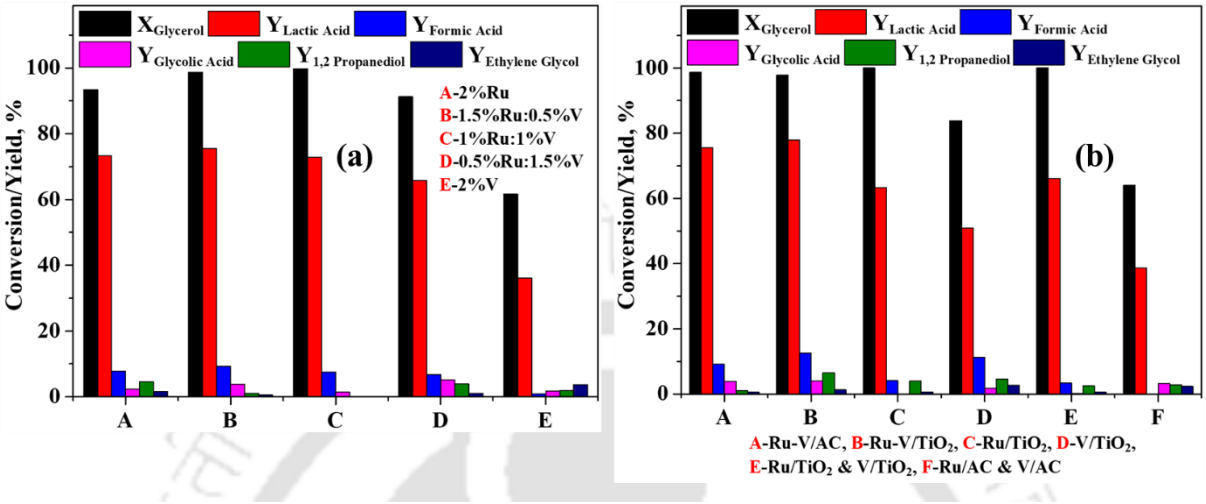

Figure 5.4: Glycerol to lactic acid conversion over Ru-V/AC bimetallic catalysts: Effect of (a) Ru: V metal ratio in the bimetallic catalyst Ru-V/AC and (b) catalyst and support type. The other reaction conditions were: 200 °C temperature, 5 bar air pressure, 3 h reaction time, 0. 1 g catalyst (glycerol/metal molar ratio: 4400), and 1:1 base (NaOH) to glycerol molar ratio.

The synergistic effect between Ru and V for the bimetallic catalyst performance was investigated based on the experiments with a physical mixture of Ru/AC and V/AC and Ru/TiO_2 and V/TiO_2 catalysts. The results showed that the physical mixture of Ru/AC and V/AC gives 64% glycerol conversion, yielding 38.7% LA, 2.4% EG, 3.2% GLA, 2.9% 1,2-PDO, and negligible amounts of FA (Fig. 5.4b). While in the case of Ru/TiO_2 and V/TiO_2 physical mixture, the results showed 100% glycerol conversion with 66.2% of lactic acid yield and 0.55% EG, 0.12% GLA, 2.5% of 1,2-PDO, and 3.4% FA. In addition, experiments with monometallic Ru/TiO_2 and V/TiO_2 were performed. The results showed 100% and 83.9% glycerol conversion and 63.3% and 50.9% lactic acid yields, respectively (Fig. 5.4b). More byproducts were formed over V/TiO_2 (2.7% EG, 1.7% GLA, 4.5% of 1,2-PDO, and 11.2% FA) compared to Ru/TiO_2 (0.65% EG, 0.1% GLA, 3.9% of 1,2-PDO, and 4.1%FA). Based on

TH-3456_166107017

these results, the bimetallic Ru-V/TiO_2 performed better than their monometallic Ru/TiO_2 and V/TiO_2 catalyst counterparts and their physical mixture.

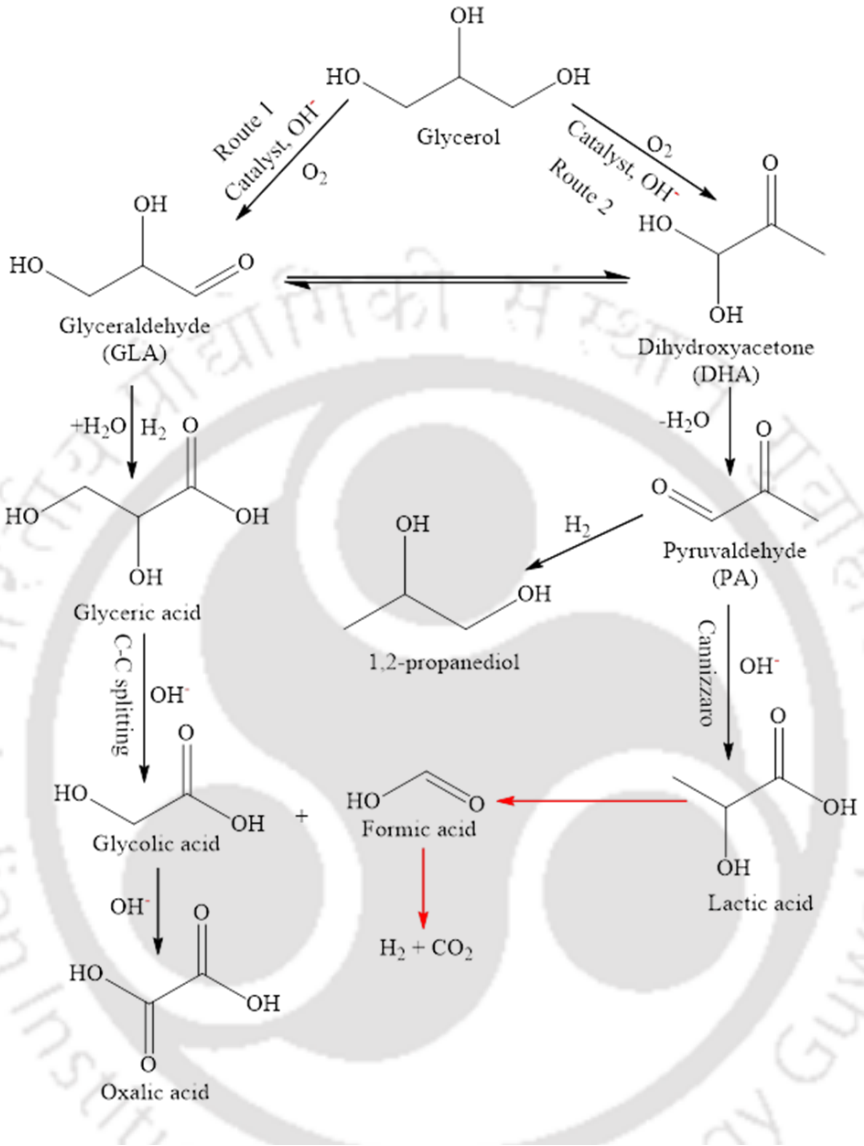

Scheme 5.2: Possible reaction routes for GL oxidation to LA over Ru-V/AC bimetallic

TH-3456_166107017

5.2.1.5 Catalyst Stability Study

The 1.5Ru-0.5V/AC bimetallic catalyst was highly stable for four cycles under the reaction conditions used (Fig. 5.5a), with only a slight decrease in LA yield (76.5 to 71.8%) and no change in GL conversion. The marginal increase in FA yield during the fourth cycle could be attributed to the decomposition of LA to FA (Scheme 5.1). The FETEM analysis of the used catalyst shows an average size of the bimetallic particles of 0.95 nm (Fig. 5.5b). The particle size distribution ranged from 0.39 to 3.8 nm (inset of Fig. 5.5b, and sizes of approximately 163 particles were counted). The average particle size was changed marginally from 1.05 nm (fresh catalyst) to 0.95 nm (used catalyst), indicating a stable bimetallic particle size during the recycle tests. Moreover, the N_2-sorption measurements showed that the BET surface area of the spent catalyst was also significantly less, possibly due to coke deposition onto the surface of meso and micropores (Table 4.1, Entry 7 from Chapter 4). The total mass transfer (external and internal) in the conversion of glycerol to lactic acid depends on stirring speed (external mass transfer) and catalyst particle size (internal mass transfer). External mass transfer can be assessed by varying the stirring speed, while internal mass transfer can be evaluated using catalysts of different particle sizes. I conducted experiments at a high stirring speed of 600 rpm with a powder catalyst, and therefore, the mass transfer limitations are likely negligible.

TH-3456_166107017

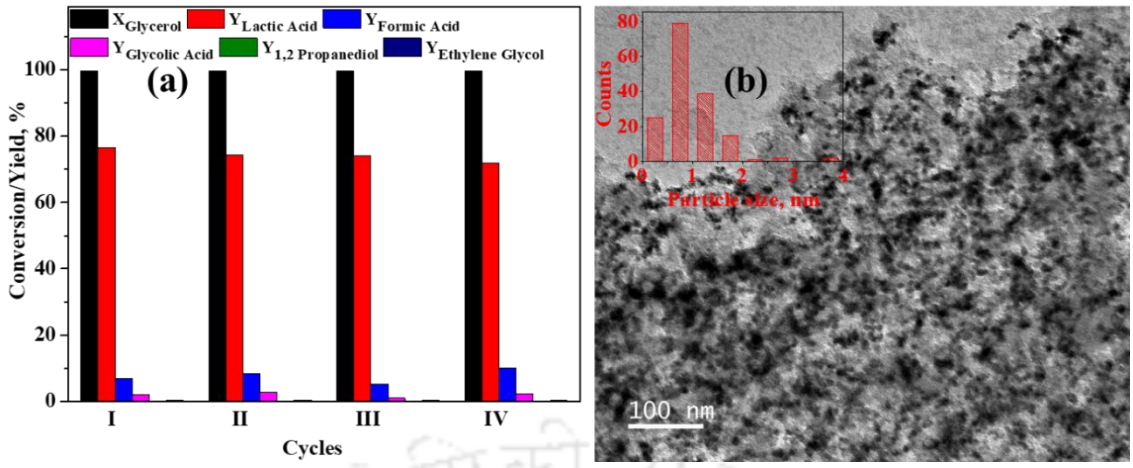

Figure 5.5: (a) Recycle experiments for glycerol to lactic acid conversion over Ru-V/AC bimetallic catalysts. The other reaction conditions: 200 ºC temperature, 5 bar air pressure, 3 h reaction time, 1:1 base (NaOH) to glycerol molar ratio, and 0.1 g of catalyst (glycerol/metal molar ratio: 4400); (b) The FETEM image of the used catalyst (inset: Metal particle size distribution).

5.3 Summary

The Ru-V/AC bimetallic catalysts were successfully synthesized using wet impregnation and a chemical reduction method. Due to synergism between Ru and V_2O_5, the Ru-V_2O_5/AC bimetallic catalysts outperformed their Ru/AC and V_2O_5/AC monometallic counterparts in selective glycerol oxidation to lactic acid under mild reaction conditions. Compared to those with their monometallic counterparts, a higher yield (up to 75.5%) of lactic acid was observed with the bimetallic catalysts. The Ru-V_2O_5/AC bimetallic catalyst was highly stable.

TH-3456_166107017

References

(1) Bruno, A. M.; Simões, T. D. R.; Simões, S.; Souza, M. M. V. M.; Manfro, R. L. Cu Catalysts Supported on CaO/MgO for Glycerol Conversion to Lactic Acid in Alkaline Medium Employing a Continuous Flow Reaction System. 2020. https://doi.org/10.1039/d0ra06547a.

(2) Kishida, H.; Jin, F.; Zhou, Z.; Moriya, T.; Enomoto, H. Conversion of Glycerin into Lactic Acid by Alkaline Hydrothermal Reaction. Chem Lett 2005, 34 (11), 1560–1561. https://doi.org/10.1246/cl.2005.1560.

(3) Purushothaman, R. K. P.; van Haveren, J.; van Es, D. S.; Melián-Cabrera, I.; Meeldijk, J. D.; Heeres, H. J. An Efficient One Pot Conversion of Glycerol to Lactic Acid Using Bimetallic Gold-Platinum Catalysts on a Nanocrystalline CeO2 Support. Appl Catal B 2014, 147, 92–100. https://doi.org/10.1016/j.apcatb.2013.07.068.

(4) Yang, G. Y.; Ke, Y. H.; Ren, H. F.; Liu, C. L.; Yang, R. Z.; Dong, W. S. The Conversion of Glycerol to Lactic Acid Catalyzed by ZrO2-Supported CuO Catalysts. Chemical Engineering Journal. 2016, pp 759–767. https://doi.org/10.1016/j.cej.2015.08.027.

(5) Dimitratos, N.; Antonio Lopez-Sanchez, J.; Meenakshisundaram, S.; Anthonykutty, J. M.; Brett, G.; Carley, A. F.; Taylor, S. H.; Knight, D. W.; Hutchings, G. J. Selective Formation of Lactate by Oxidation of 1,2-Propanediol Using Gold Palladium Alloy Supported Nanocrystals. 2009. https://doi.org/10.1039/b823285g.

(6) Tian, J.; Liu, H.; Li, P.; Huang, Z.; Chen, J. Selective Oxidation of 1,2-Propanediol to Lactic Acid over Cu-Modified Au/Hydrotalcite Catalysts †. New J. Chem 2020, 44, 16311. https://doi.org/10.1039/d0nj02526g.

TH-3456_166107017

Chapter 6

Glycerol selective oxidation to lactic acid over platinum-vanadium bimetallic catalysts supported on activated carbon

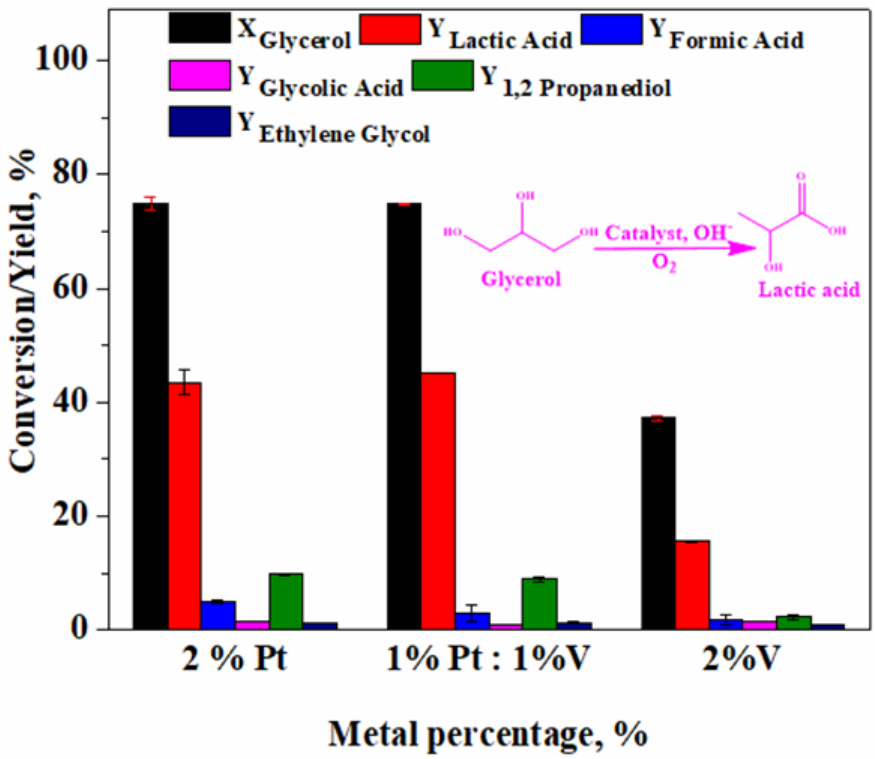

TH-3456_166107017

6.1 Objectives

The present work reports a novel bimetallic (Pt-V) catalyst system supported on activated carbon to convert glycerol to lactic acid for the first time. The catalysts were thoroughly characterized using advanced characterization techniques, such as powder X-ray diffraction (p-XRD) analysis, N_2-sorption studies using BET surface area analyzer, Field emission transmission electron microscopy (FETEM), High-resolution transmission electron microscopy (HRTEM), Energy-dispersive X-ray (EDX) analysis, X-ray photoelectron spectroscopy (XPS). The experiments were carried out at a higher concentration of glycerol (40-60 wt%) at moderate conditions (temperature range 160-200 °C and pressure range 5-15 bar O_2/air) with high glycerol to metal molar ratios (4400-17600 mol/mol). The influence of various reaction parameters, such as temperature, pressure, substrate-to-metal molar ratio, base-to-substrate molar ratio, metal composition (Pt_x: V_{2-x}/AC) in the bimetallic catalyst, and type of base and oxidant on the catalyst activity and product distribution was studied in detail. The performance of bimetallic catalysts was compared with that of monometallic Pt and V catalysts. The activity and selectivity of the catalysts were correlated to their physicochemical properties. Based on experimental studies, a comprehensive reaction pathway for glycerol oxidation was proposed and discussed in detail with the supporting literature data.

TH-3456_166107017

6.2 Results and Discussion

6.2.1 Characterization of the catalysts

The FETEM, XRD, BET, and XPS techniques were used to characterize the physicochemical properties of the prepared Pt-V/AC, Pt/AC, and V/AC catalysts. The field emission transmission electron microscope (FETEM) images of Pt-V bimetallic catalysts show that the metallic (Pt and V) particles were uniformly dispersed on the surface of activated carbon (Fig. 6.1a). The ImageJ software was used to analyze the particle size distribution (inset of Fig. 6.1a). The average particle size (using equation 2.1 from Chapter 2) and the particle size distribution were 2 nm and 0.82-8.66 nm, respectively (counted approximately 800 particles). The high-resolution transmission electron microscopy (HRTEM) imaging (Fig. 6.1b) and selected area electron diffraction (SAED) patterns (Fig. 6.1c) were used to obtain the crystal phases of Pt-V bimetallic catalysts. A crystalline structure with well-defined fringes was observed in the HRTEM image of the 1Pt-1V/AC bimetallic catalyst. The distance (lattice spacing) between two adjacent planes was 0.25 nm (averaged for 10 fringes), as illustrated in Fig. 6.1b, corresponding to the plane of fcc Pt (111).[1] The SAED pattern of 1Pt-1V/AC revealed that most platinum nanoparticles were crystalline and could be attributed to the cubic phase structure of Pt. The clear ring pattern in SAED indicates the polycrystalline nature of the bimetallic catalyst. The elemental mapping in energy-dispersive X-ray spectroscopy (EDX) was used to confirm the proper dispersion of Pt and V species on AC support. The Pt and V elements were mapped in green and red, respectively. Both Pt and V elements were uniformly dispersed in the catalyst (Figs. 6.1d and 6.1e). The EDX analysis estimates the Pt/V ratio to be 2.8 for the 1.5Pt-0.5V/AC bimetallic catalyst, approximately equal to the nominal pt/V ratio of 3.0. The EDX spectrum is given in Fig. 6.2. The EDX elemental mapping confirms that Pt

TH-3456_166107017

nanoparticles are decorated with V species, suggesting that the nanoparticles are composed of Pt-V alloy, as reported by other researchers.[2]

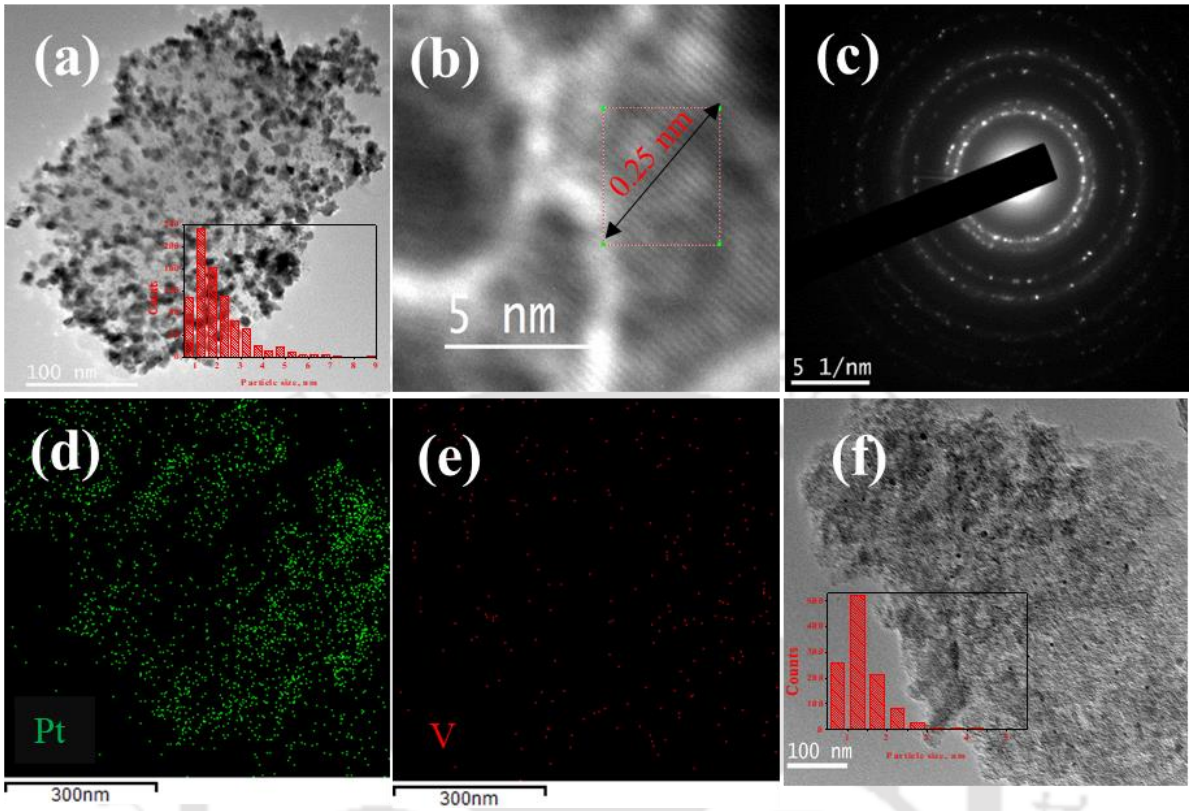

Figure 6.1: (a) Field-Emission transmission Electron Microscopy (FETEM) image (inset: Metal particle size distribution of the fresh catalyst) of 1Pt-1V/AC (b) High-Resolution transmission Electron Microscopy (HRTEM) image and averaged lattice spacing for ten fringes (0.25 nm) (c) Selected area electron diffraction (SAED) pattern indicating the polycrystalline nature (d) Energy-dispersive X-ray spectroscopy (XEDS) image of Pt element (e) Energy-dispersive X-ray spectroscopy (XEDS) image of V element (f) FETEM image (inset: Metal particle size distribution of the fresh catalyst) of 2Pt/AC.

The XRD patterns of Pt and V catalysts supported on activated carbon are shown in Fig. 6.3a. The diffraction planes ((002) at 27° and (100) at 43°) corresponding to the carbon with graphitic nature (JCPDS card No. 00-056-0159) were observed in all the catalysts. Except for 2 wt.% Pt/AC catalyst, the diffraction planes corresponding to Pt and V species were not observed in the XRD patterns, which could be attributed to the low concentration of Pt and V

TH-3456_166107017

species and high dispersion. For 2 wt.% Pt/AC catalyst, the diffraction plane of Pt (111) was observed at 39.7° (JCPDS card NO. 65-6828).

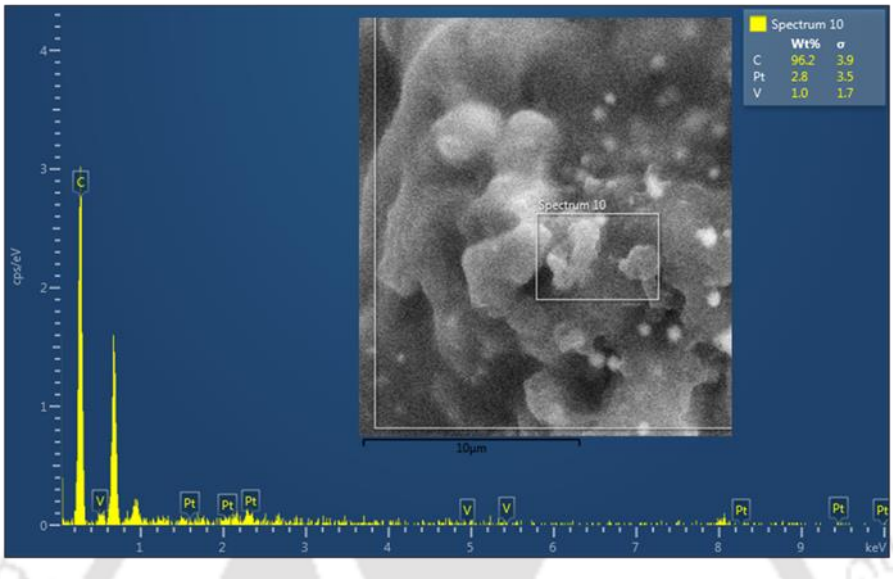

Figure 6.2: EDX spectrum of the 1Pt-1V/AC bimetallic catalyst.

The N_2 sorption isotherms of all the catalysts possess combined Type I and Type IV isotherms (according to the IUPAC classification), illustrating the micro and mesoporous characteristics with the absence of the plateau at high pressures as shown in Fig. 6.3b. The catalysts exhibit an H_4 hysteresis loop, indicating the presence of slit pores in the mesoporous region. The morphology of the pores of AC support remained nearly the same before and after the metal incorporation, except for a marginal decrease in the microporous area. The decrease in the microporous area could be attributed to the occupation of the micropores by the metal particles. The BET surface areas of Pt-V bimetallic and monometallic Pt and V catalysts supported on activated carbon are listed in Table 6.1. The bare AC support possesses a BET-specific surface area (BET-SA) of 775 $m^2\ g^{-1}$, a pore volume of 0.51 $cm^3\ g^{-1}$, and an average pore diameter of 2.63 nm. The BET-SA of monometallic and bimetallic Pt and V catalysts impregnated AC and decreased marginally due to the presence of Pt and V species on the surface of the support. The BET-SA of the 1Pt-1V/AC bimetallic catalyst was 730 m^2/g, which was higher than that of monometallic Pt and V catalysts, as shown in Table 6.1. The surface area of the metal-

TH-3456_166107017

impregnated catalysts (mono and bimetallic) was lower than that of only support (activated carbon). The decrease in surface area for monometallic and bimetallic catalysts is attributed to pore blockage caused by metal particle deposition. The decrease in surface area was higher in the case of monometallic catalysts than in bimetallic catalysts. An increase in particle size was observed, likely due to the formation of larger Pt-V alloy particles without significant pore blockage. Further, comparing the TEM images of 1Pt-1V/AC and 2Pt/AC shows that the particle size slightly increased after adding vanadium to platinum-based catalysts. For the 2Pt/AC catalyst, the average particle size and the particle size distribution were 1.388 nm and 0.88-5.16 nm (inset of Fig. 6.1f), respectively (counted approximately 1100 particles).

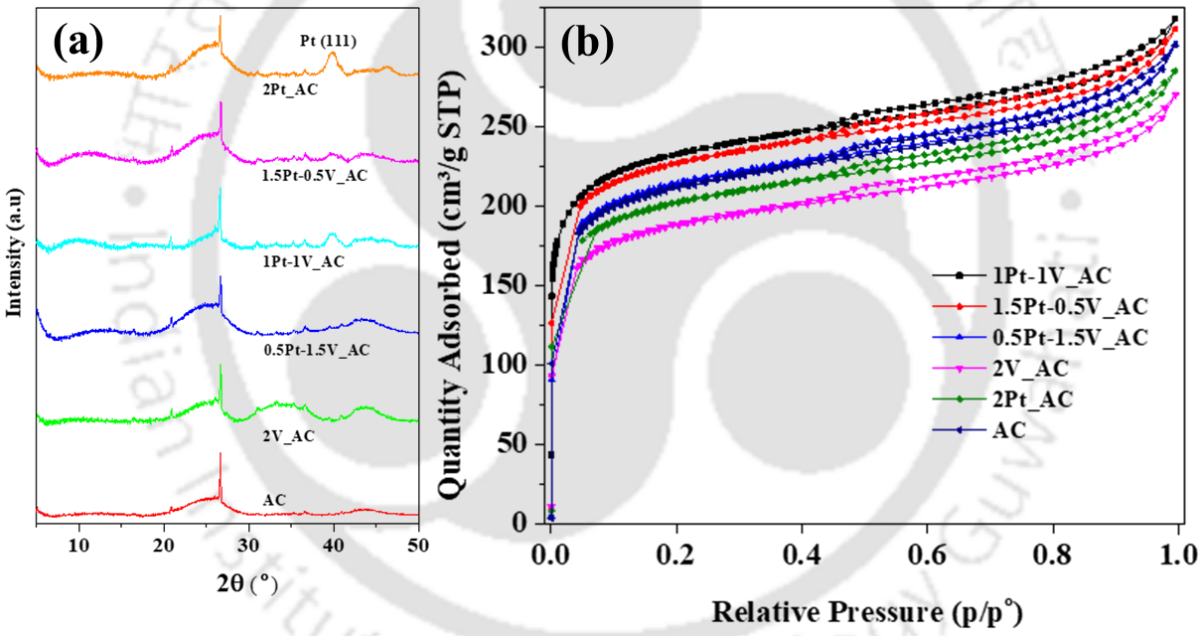

Figure 6.3: (a) XRD patterns (b) N_2 sorption isotherms of various activated carbon supported Pt-V bimetallic catalysts, synthesized in this study. The data for bare activated carbon support also included for the comparison.

TH-3456_166107017

Table 6.1: Specific surface area, pore volume, and average pore size of various Pt-V bimetallic catalysts supported on activated carbon.

Catalyst code	Nominal catalyst composition		S_{BET} (m^2/g)	Pore volume (cm^3/g)	Pore size (nm)	Micropore area (m^2/g)	Micropore volume (cm^3/g)	Meso pore area (m^2/g)	Meso pore volume (cm^3/g)
	Pt%	V%							
1Pt-1V/AC	1	1	730	0.49	2.66	489	0.25	171	0.17
1.5Pt-0.5V/AC	1.5	0.5	712	0.48	2.68	472	0.24	168	0.16
0.5Pt-1.5V/AC	0.5	1.5	672	0.39	2.75	433	0.22	167	0.16
2V/AC	0	2	592	0.34	2.78	373	0.19	154	0.15
2Pt/AC	2	0	631	0.37	2.77	396	0.21	161	0.16
AC	0	0	775	0.51	2.63	543	0.27	83	0.14
1Pt-1V/AC*	1	1	11.5	0.04	13.55	n/d	n/d	12	0.04

AC: Activated carbon, *Spent catalyst after four cycles; n/d: not determined

TH-3456_166107017

The XPS spectra of Pt/AC, V/AC, and 1Pt-1V/AC samples are displayed in Fig. 6.4. The presence of peaks from Pt 4f, V 2p, O 1s, and C 1s in the survey spectrum (Fig. 6.4a) of the 1Pt-1V/AC catalyst indicates that the bimetallic catalyst was successfully synthesized. Fig. 6.4b shows the Pt 4f high-resolution spectra of Pt/AC and Pt-V/AC catalysts. As depicted in the spectrum of the Pt/AC catalyst (Fig. 6.4b), two distinct Pt species are present, as evidenced by the broadening and small valley between the spin-orbit components on the catalyst surface.[3,4] The deconvolution reveals that the 71.9 and 74.8 eV binding energies peaks correspond to the $4f_{7/2}$ and $4f_{5/2}$ of the Pt metallic phase. Those at 71.3 and 75.2 eV relate to $4f_{7/2}$ and $4f_{5/2}$ of Pt oxide phases such as PtO.[3] For the Pt-V/AC catalyst (Fig. 6.4b), similar XPS signals of metallic Pt (72.1 eV for Pt $4f_{7/2}$, 75.0 eV for Pt $4f_{5/2}$) and Pt (II) species (71.4 eV for Pt $4f_{7/2}$, 75.3 eV for Pt $4f_{5/2}$) were also observed. Two deconvoluted peaks in the Pt-V/AC V2p high-resolution XPS spectra (Fig. 6.4c) were noticed. These peaks translate into two distinct valence states of the V element: the metallic V peaks at 510.8 eV and 519.6 eV, and V(IV) species at 516.4 eV and 522.3 eV.[4–6] Furthermore, the binding energy of metallic V in 1Pt-1V/AC shows a negative shift when compared to the corresponding value published in the literature.[6] The V2p spectrum of monometallic 2V/AC catalyst showed pentavalent oxidation states of vanadium (V(V)) at 517.5 eV and 524.0 eV.[4–6] The peak position of metallic Pt in the 1Pt-1V/AC was shifted positively (0.3 eV) compared to that in 2Pt/AC. The electron cloud shifts from V to Pt in the 1Pt-1V/AC due to the higher electronegativity of Pt (2.28) as compared to that of V (1.63). The strong electronic interaction between Pt and V changes the electronic structure of Pt. The shift in the binding energies of Pt $4f_{5/2}$ and Pt $4f_{7/2}$ suggests the formation of alloy nanoparticles between Pt and V species.[4,7,8] The XPS analyses suggest that the Pt-V bimetallic catalyst performed better due to the electronic interactions between Pt and V metals. The significant interactions between the Pt and V metals are explained based on the

TH-3456_166107017

change in binding energies of Pt metal in the 1Pt-1V/AC bimetallic catalyst as compared with that of the monometallic 2Pt/AC catalyst. As a result, the catalyst activity may be enhanced.

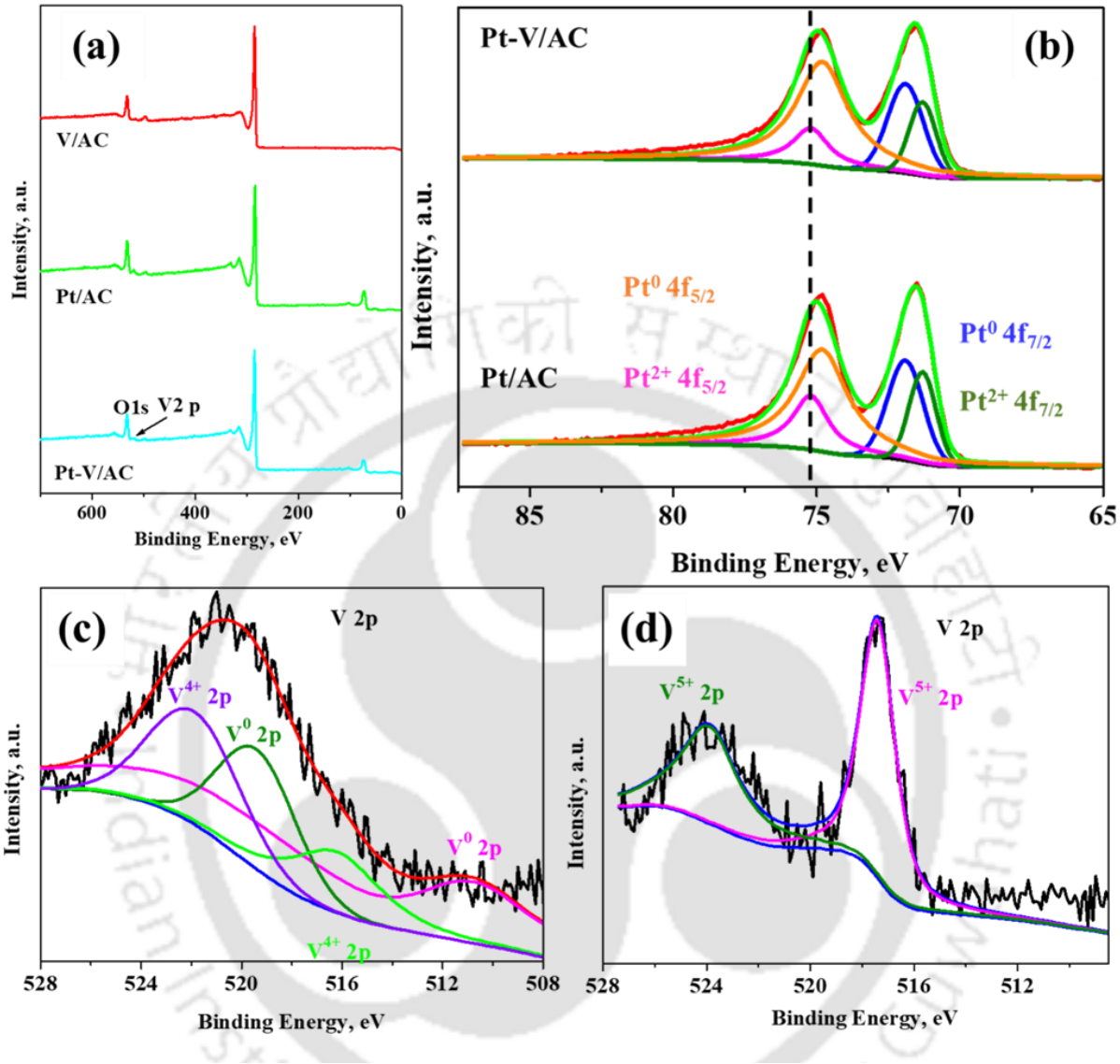

Figure 6.4: The X-ray photoelectron spectroscopy (XPS) spectra (a) Comparison of survey plots of 2Pt/AC, 2V/AC, and 1Pt-1V/AC catalysts (b) high-resolution spectra of Pt 4f of 1Pt-1V/AC and 2Pt/AC catalysts, high-resolution spectra of V 2p of 1Pt-1V/AC catalyst (c), 2V/AC catalyst (d).

TH-3456_166107017

6.3 Catalyst Activity Tests

6.3.1 Effect of reaction conditions

The effect of reaction parameters, such as temperature (Fig. 6.5a), pressure (Fig. 6.5b), reaction time (Fig. 6.5c), base (KOH) to glycerol molar ratio (Fig. 6.5d), type of base (Fig. 6.6), and type of oxidant (Fig. 6.7), on the GL oxidation to LA was studied. The reaction parameters were optimized over 1Pt-1V/AC bimetallic catalyst at a loading of 0.1 g. The GL conversion and LA yield were remarkably affected by the temperature. They increased from 55.2 to 89.1% and from 24.4 to 57.1%, respectively, with a rise in temperature from 160 to 200°C (Fig. 6.5a). The 1,2-PDO yield marginally decreased from 7.4 to 6.4%. The other products, such as formic acid (FA), ethylene glycol (EG), and glycolic acid (GLA), were observed in minor quantities. Nevertheless, the yield of these products increased with the increase in temperature, indicating that the side reactions are also favored at high temperatures.[9–11] The effect of air pressure (in the 5-15 bar range) was negligible on GL conversion and LA yield (Fig. 6.5b). However, the increase in air pressure resulted in a marginal increase in FA and GLA yields. Hence, the subsequent trials fixed the reaction temperature and air pressure at 200°C and 5 bar air pressure.

Next, the effect of reaction time on the conversion of GL and the yield of LA in the presence of KOH (Fig. 6.5c) or NaOH (Fig. 6.8) was studied, keeping all other parameters constant. The conversion of GL was 78.8 and 84.6%, and the yields of products LA, GLA, FA, 1,2-PDO, and EG were 40.5, 0.9, 0.5, 8.0 and 1.1% and 52.3, 0.9, 0.0, 8.6 and 1.3%, respectively, in the presence of KOH and NaOH, at 3 h reaction time. The yield of LA was increased with the reaction time from 40.5 and 52.3% at 3 h to 57.1 and 79.6% at 12 h in the presence of KOH and NaOH, respectively. In contrast, GLA, FA, and EG yields decreased with reaction time with NaOH and KOH presence. The decrease in 1,2-PDO yield was significant in NaOH compared to the presence of KOH. This could be attributed to the conversion of 1,2-PDO to

TH-3456_166107017

LA or pyruvaldehyde[12,13] in the presence of NaOH. The longer reaction times may also promote further oxidation of GLA and FA to gaseous products.

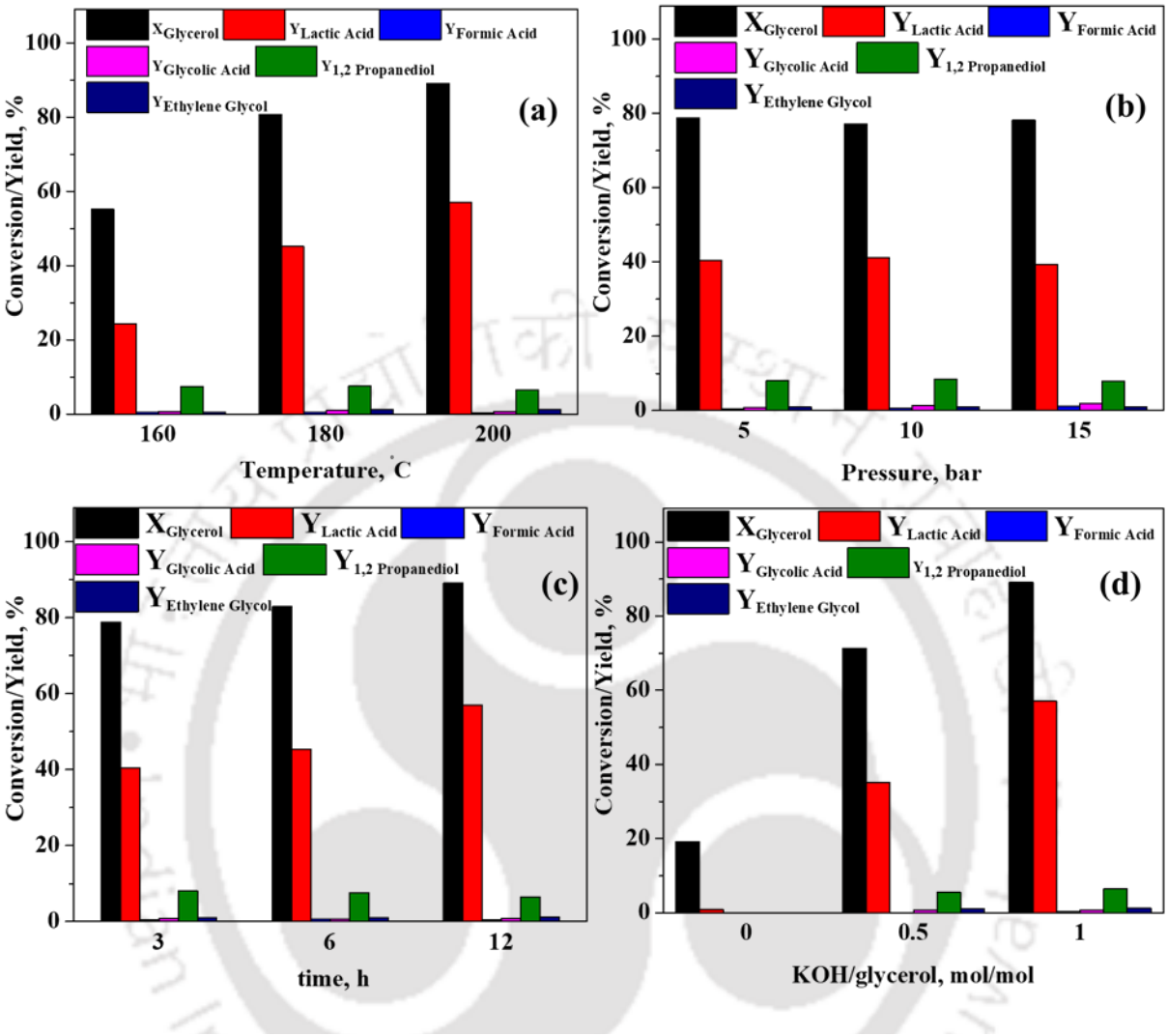

Figure 6.5: Glycerol to lactic acid conversion over 1Pt-1V/AC bimetallic catalyst: Effect of (a) temperature, (b) pressure, 3 h, (c) time, and (d) molar ratio of base (KOH)/glycerol. The other reaction conditions were: 200 °C temperature, 5 bar air pressure, 12 h reaction time, 1:1 KOH to glycerol molar ratio, and 0.1 g catalyst.

The effect of base/glycerol molar ratio on the activity and LA yield is presented in Fig. 6.5d. Without a base, the GL conversion was 19.1%, and the LA yield was 0.8%, with no additional byproducts. This result indicates that the GL decomposes to gaseous products without a base. The addition of a small amount of base (0.5 base/glycerol molar ratio) resulted in a significant increase in the GL conversion (from 19.1 to 71.3%) as well as LA yield (from

TH-3456_166107017

0.8 to 35.1%). The increase of the base/glycerol molar ratio from 0.5 to 1.0 mol/mol resulted in a further rise in glycerol conversion (71.3 to 89.1%) and LA yield (35.1 to 57.1%). No effect of the base/glycerol molar ratio on yields of byproducts, such as FA, 1,2-PDO, GLA, and EG, was observed.

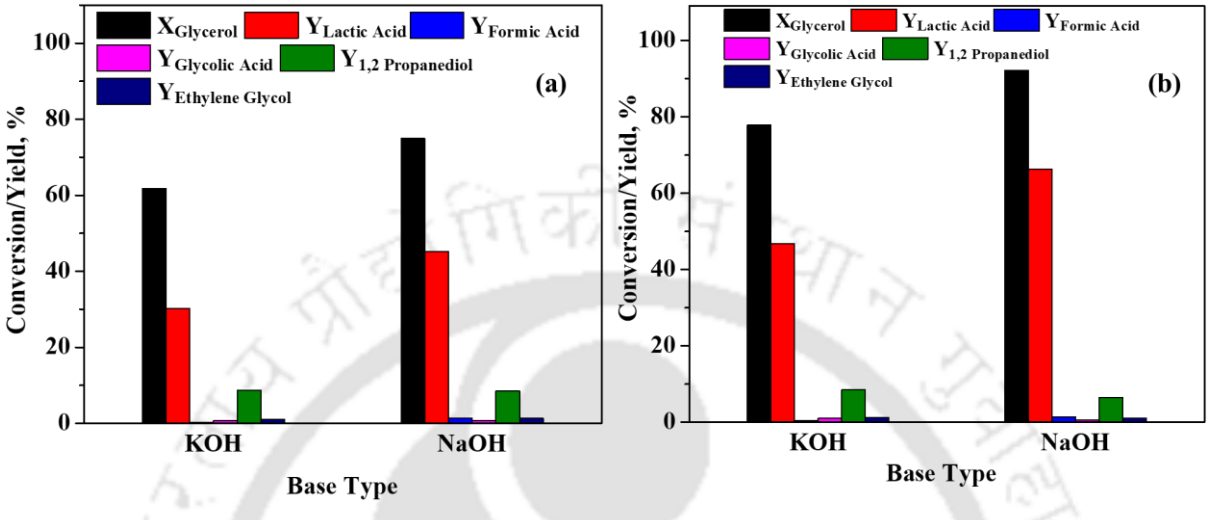

Figure 6.6: Effect of base type on glycerol to lactic acid conversion over 1Pt-1V/AC bimetallic catalyst: (a) 3 h and (b) 12 h. The other reaction conditions: 200 °C temperature, 5 bar air pressure, 1:1 base (KOH or NaOH) to glycerol molar ratio, and 0.05 g catalyst (8800 glycerol to metal molar ratio).

Fig. 6.7 depicts the effect of oxidants (molecular oxygen and air) for the oxidation of GL to LA under the same reaction conditions. The GL conversion and LA yield were lower in molecular oxygen (78.0 and 46.5%, respectively) than those in the presence of air (89.1% and 57.1%, respectively). Furthermore, the FA and GLA yields were marginally higher in molecular oxygen, while the yield of 1,2-PDO remained nearly the same in both cases. The dehydrogenation and oxidation steps occur more effectively in the presence of air than in molecular oxygen over Pt-V/AC catalysts. In the presence of molecular oxygen, the reaction proceeds via Route 1 to form glycolic acid. Furthermore, the lactic acid may over-oxidize to form formic acid, as shown in reaction scheme 6.1.

TH-3456_166107017

The effect of GL concentration on the conversion of GL to LA over the 1Pt-1V/AC bimetallic catalyst was also studied. With the increase of glycerol/metal molar ratio from 4400 to 6580 mol/mol, the GL conversion was nearly the same, and the yield of LA marginally decreased from 46.5 to 44.5%. the other by-products, such as FA, 1,2-PDO, GLA, and EG, were decreased from 1.2%, 6.2%, 2.5% and 0.89% to 1.1%, 5.9 %, 2.4%, and 0.85%, respectively. The results were compared in entries 3 and 8 in Table 6.2.

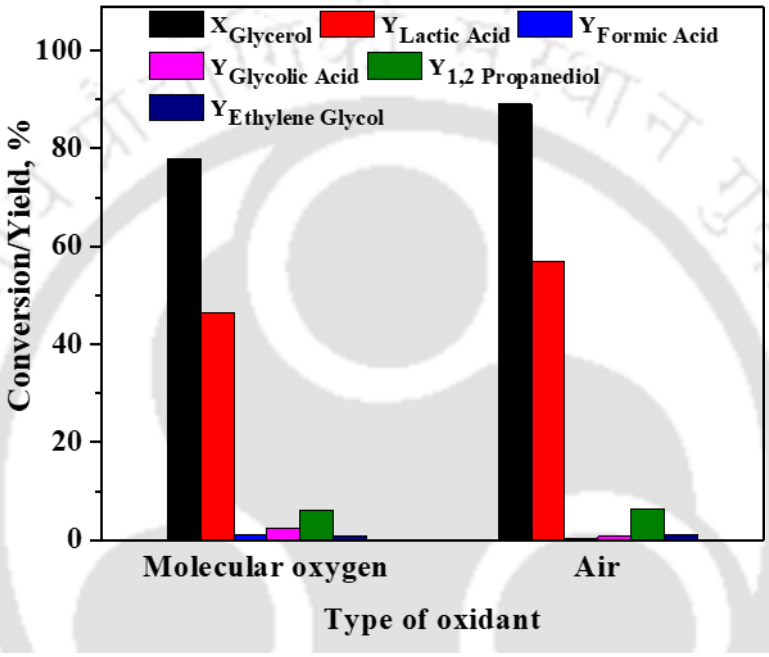

Figure 6.7: Effect of oxidant type on glycerol to lactic acid conversion over 1Pt-1V/AC bimetallic catalyst. (Reaction conditions: 200 °C temperature, 5 bar air pressure, 12 h reaction time, 1:1 base (KOH) to glycerol molar ratio, and 0.1 g catalyst).

6.3.2 Effect of catalyst loading and composition

The effect of catalyst loading on the oxidation of GL to LA was also studied in the presence of NaOH at 3 and 12 h reaction time (Fig. 6.9a). A substantial increase in GL conversion (from 64.5 to 84.6%) and LA yield (37.9 to 52.3%) was observed with the increase in catalyst amount from 17600 mol/mol to 4400 mol/mol of glycerol to metal molar ratio. The metal here refers to Pt + V present in the bimetallic catalyst. The yield of FA was relatively higher at lower catalyst loading (17600 mol/mol), decreased with catalyst loading, and finally diminished to

TH-3456_166107017

0% at a catalyst loading of 4400 mol/mol, indicating that the reaction proceeds via the dihydroxyacetone route or the formic acid converts into gaseous products.[14] No change in the yield of 1,2-PDO with an increase in catalyst loading was observed at lower reaction times, i.e., 3 h (Fig. 6.9a). At higher reaction time (12 h), the GL conversion (92.1 to 100%) and LA yield (66.3 to 79.6%) were significantly enhanced with the catalyst loading (Fig. 6.9a). The 1,2-PDO yield was reduced from 6.5 to 2.2% at higher catalyst loading (4400 mol/mol) and higher reaction time (12 h), indicating that 1,2-PDO is converted to LA or pyruvaldehyde[12,13]. Similar observations were made with KOH as a base. With the increase of catalyst loading from 0 to 0.05 (8800 mol/mol glycerol to metal molar ratio) and 0.1 g (4400 mol/mol), the GL conversion and the LA yield were significantly enhanced from 27 to 62.5 and 79.2% and from 5.5 to 31.0 and 41.0%, respectively (Fig. 6.10a). Further, with an increase in the reaction time of 3 to 12 h, the GL conversion and LA yields were increased from 78.7 to 90.0% and 47.7 to 57.7%, respectively (Fig. 6.10b). However, there is no formation of byproducts with a bare (0.0 g) catalyst, which means the process is a hydrothermal conversion. A considerable amount (8.23%) of 1,2-PDO was formed with an increasing catalyst amount to 0.05 and further increasing to 0.1 g; there is no change in 1,2-PDO yield. However, an increase in reaction time from 3 to 12 h showed a slight decrease in 1,2-PDO yield. The typical carbon balance for the experiments carried out in this study is given in Table 6.3. The average carbon balance is found to be above 75%. The lower carbon balance can be attributed to the formation of unknown/undetermined intermediates, gases (such as carbon dioxide), and coke.

TH-3456_166107017

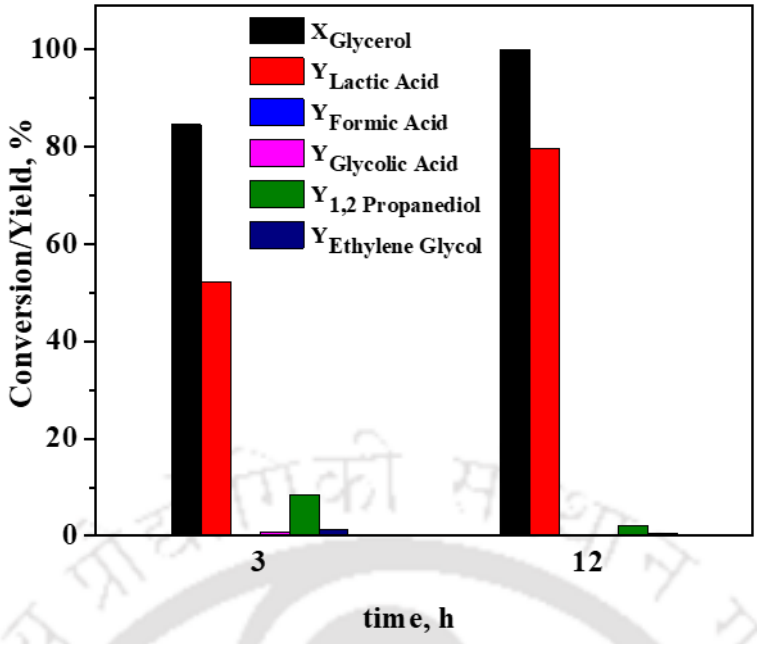

Figure 6.8: Glycerol to lactic acid conversion over 1Pt-1V/AC bimetallic catalyst: Effect of (a) reaction time (with NaOH as a base). The other reaction conditions: 200 °C temperature, 5 bar air pressure, 1:1 base (NaOH) to glycerol molar ratio, and 0.1 g catalyst.

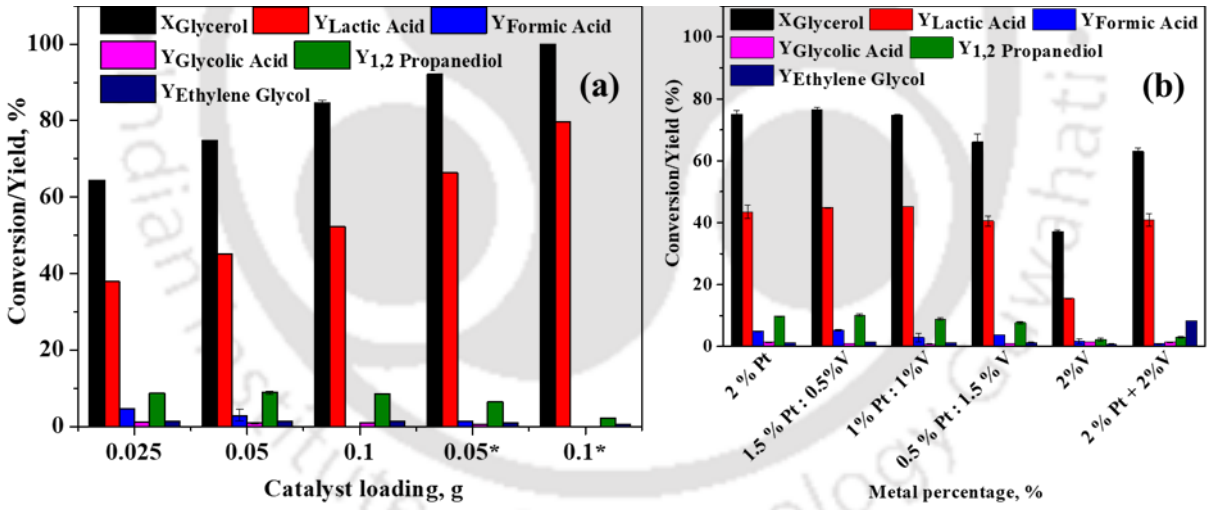

Figure 6.9: Glycerol to lactic acid conversion over 1Pt-1V/AC bimetallic catalyst: Effect of (a) catalyst loading (with NaOH as a base) and (b) metal wt percentage (0.05 g catalyst). The other reaction conditions: 200 °C temperature, 5 bar air pressure, 3 h reaction time, and 1:1

The effect of the metal weight ratio (Pt: V w/w) in Pt-V/AC bimetallic catalysts on the conversion of GL to LA was investigated (Fig. 6.9b). The performance of bimetallic Pt-V catalysts with different Pt/V ratios was compared with that of Pt and V monometallic

TH-3456_166107017

counterparts. This study was to understand the role of vanadium addition on the activity and LA yield. In addition, we investigated the performance of the physical mixture of 2Pt/AC and 2V/AC monometallic catalysts. We compared it with bimetallic 1Pt-1V/AC catalysts, with the same weights of Pt and V in both experiments. For example, the weight of 1Pt-1V/AC was 0.05 g, and that of the physical mixture 2Pt/AC + 2V/AC was also 0.05 g with 0.025 g of 2Pt/AC and 0.025 g of 2V/AC. The physical mixture of monometallic Pt/AC and V/AC catalysts for converting glycerol to lactic acid showed 63% glycerol conversion with a 40.86 % lactic acid yield. In addition, 0.92, 8.44, and 3.09 % of formic acid, ethylene glycol, and 1,2-Propanediol, respectively, were formed. Compared to monometallic 2% Pt/AC, the conversion of glycerol to lactic acid was lower with the physical mixture of 2% Pt/AC and 2% V/AC catalysts. The bimetallic catalysts with Pt content of more than 1 wt.% performed better than physical mixtures and monometallic 2Pt/AC catalysts (Fig. 6.9b). When vanadium content exceeded 1 wt.%, or the platinum content dropped below 1 wt.%, the bimetallic catalyst generated more gaseous by-products such as CO and CO_2.[14] Therefore, the optimal bimetallic concentration was determined to be 1 wt.% Pt and 1 wt.% V.

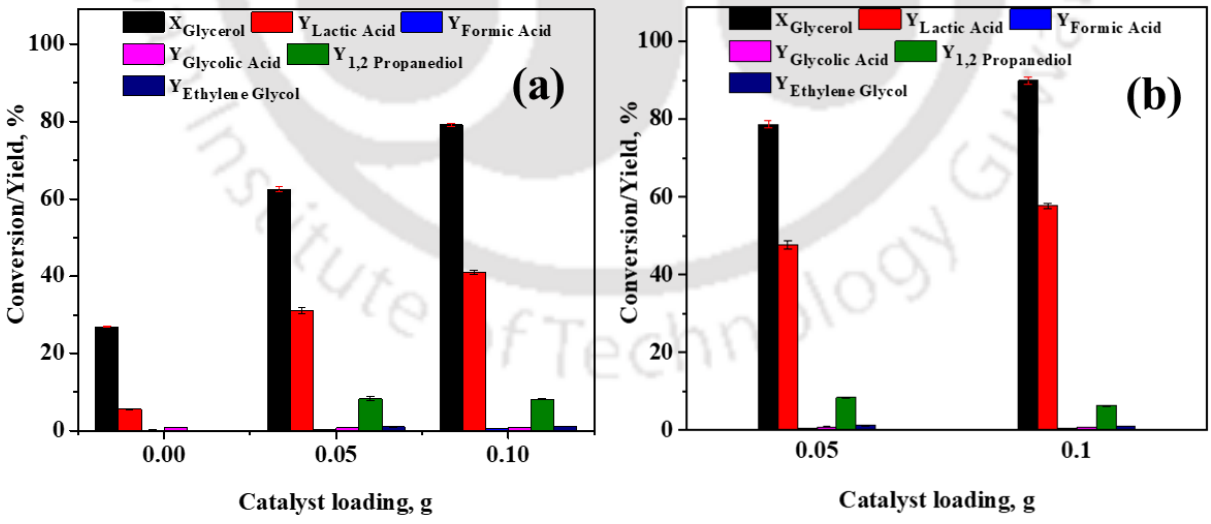

Figure 6.10: Effect of catalyst loading on glycerol to lactic acid conversion over 1Pt-1V/AC bimetallic catalyst (a) 3 h (b) 12 h. The other reaction conditions: 200 °C temperature, 5 bar air pressure, and 1:1 base (KOH) to glycerol molar ratio.

TH-3456_166107017

Arcanjo et al.[15] investigated the HNO_3-treated Pt/AC catalyst with different metal loadings (1, 5, and 10% Pt) for converting glycerol to lactic acid. They showed that the yield of lactic acid increases with increasing Pt loading from 1 to 5 wt% Pt (54% to 72%) and then decreases (to 60%) at higher Pt loading (10 wt%). Mitran et al.[16] investigated the role of vanadium content in VAIPO catalysts for converting glycerol to methanol and dihydroxyacetone. The vanadium presence in the catalysts leads to the formation of dihydroxyacetone or glyceraldehyde, intermediates for converting glycerol to lactic acid. Pemmana et al.[17] recently reported glycerol oxidation to lactic acid using Ru-V bimetallic catalysts. The findings indicated lactic acid yields of 75.5% and 77.9% at glycerol conversion rates of 98.7% and 97.8% when utilizing activated carbon and TiO_2 as supports, respectively, under mild operating conditions (1 NaOH/glycerol molar ratio, 4400 glycerol/metal molar ratio, 473 K temperature, 5 Bar air pressure and 3 h reaction time). Further, vanadium-based catalysts have been used for vapor phase oxidation of glycerol to acrylic acid.[18] The vanadium-based catalysts have oxidized 5-hydroxymethylfurfural to 5-Diformylfuran[19] and diesel.[20]

The GL conversion to LA experiment was conducted at a 10 times higher scale in a 500 mL high-pressure autoclave. The experiment was carried out under the previously optimized reaction conditions (200 ^oC temperature, 5 bar air pressure, 3 h reaction time, molar ratio of base (NaOH)/glycerol l:1, catalyst loading 4400 mol/mol of glycerol to metal molar ratio). The maximum GL conversion obtained was 66.9%, with 32.5% of LA yield (Table 6.2, Entry 9). The FA, 1,2-PDO, GLA, and EG yields were 4.0, 1.6, 8.6, and 0.8%, respectively. The conversion of GL and yield of LA were lower in the more significant volume reaction mixture (250 mL) than in the 25 mL reaction volume. This could be attributed to poor mixing at a large scale. The comparison suggests that the reaction conditions for the large-scale operation should be further optimized.

TH-3456_166107017

6.3.3 Catalyst Stability Performance

The stability of the bimetallic catalyst was tested by reusing the same catalyst sample for four cycles. The bimetallic catalyst was reasonably stable for four cycles. A noticeable decrease in activity in terms of GL conversion (92.5 to 81.1%) and yield of LA (65.7 to 60%) was observed from the first cycle to the second cycle. From the second cycle onwards, the catalyst was stable with no appreciable changes in activity, as shown in Fig. 6.11a. The FETEM analysis was carried out on the used catalyst to understand the activity loss. The average size of the bimetallic particle was marginally decreased (1.18 vs. 2 nm), and the particle size distribution was in the range of 0.8-3.6 nm (inset of Fig. 6.11b), considering approximately 74 particles. The activity of the catalyst is slightly decreased due to coke deposition on the surface of micro and meso pores.

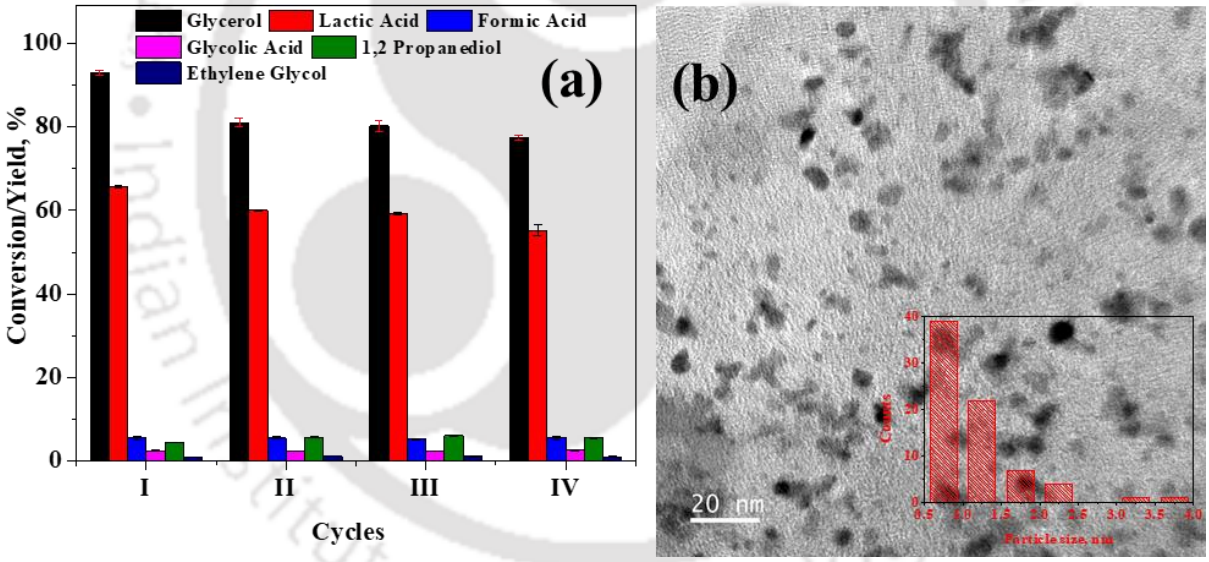

Figure 6.11: (a) Recycle experiments for glycerol to lactic acid conversion over 1Pt-1V/AC bimetallic catalyst. Reaction conditions: 200 ^{o}C temperature, 5 bar air pressure, 3 h reaction time, base (NaOH)/glycerol molar ratio: 1, and 0.107 g of catalyst (glycerol/metal molar ratio: 4110) (b) FETEM image of the used catalyst (inset: Metal particle size distribution).

TH-3456_166107017

6.3.4 Reaction Pathways

The catalytic conversion of GL to LA in a basic solution under an air atmosphere was explored using activated carbon-supported Pt-V bimetallic catalysts. The significant products formed were LA and 1,2-PDO, while the other products, such as formic acid, glycolic acid, and ethylene glycol, were observed in trace amounts. Various experiments were conducted to understand the reaction intermediates and pathways. When the GL is treated in alkaline media and without any metal catalyst, the yield of LA is lower under milder reaction conditions. For example, in this study, the conversion of GL was 26.9%, and the yields of LA and GLA were 5.7% and 0.9%, respectively, in the absence of metal catalysts. These were very low compared to those obtained when both a catalyst and a base were present. The reaction was also carried out without a base, and 19.1% of GL conversion and 0.8% of LA yield were observed, with no other byproducts (Entry 7). Recently, researchers (Lopez et al.[21], Kishida et al.[9], and Shen et al.[22]) found that glycerol could be converted to lactic acid by a hydrothermal process under alkaline conditions. The reaction of glycerol with NaOH or KOH is thought to produce sodium or potassium glyceroxide. By releasing hydride ions, it transforms into glyceraldehyde. Further, the glyceraldehyde isomerizes to dihydroxyacetone under alkali conditions. It is proposed that glyceraldehyde and dihydroxyacetone are the intermediates in the reaction. Previously, Tian et al.[12] and Dimitratos et al.[13] demonstrated that 1,2-PDO could selectively be oxidized to LA in the presence of a base and a catalyst at moderate reaction conditions with high selectivities (89.9% and 96%).

Based on our experimental investigations and associated literature data[9–13,21–24], a plausible reaction pathway for the 1Pt-1V/AC catalyzed oxidation of glycerol to lactic acid in alkaline (KOH or NaOH) solution was established, as summarized in Scheme 6.1. The first step of the reaction involves the selective oxidation of glycerol to glyceraldehyde and dihydroxyacetone. One possible route is the conversion of dihydroxyacetone to pyruvaldehyde

TH-3456_166107017

via dehydration. Subsequently, the pyruvaldehyde is converted to lactic acid via the Cannizzaro reaction[9,21,22]. The second possible route, particularly at higher reaction times and catalyst loadings, is converting intermediate product 1,2-PDO to LA and pyruvaldehyde, which enhances lactic acid production [12,13]. However, the higher reaction times also favor the further oxidation of glycolic acid and formic acid to gaseous products. The hydration followed by dehydrogenation, for converting glyceraldehyde to glyceric acid, occurs in tandem with the dehydration followed by hydrogenation of dihydroxyacetone (DHA) to 1,2-propanediol occurs in tandem[25]. Further, the C-C cleavage reaction produces glycolic acid, oxalic acid, and formic acid from glyceric acid.[9,22,26]

TH-3456_166107017

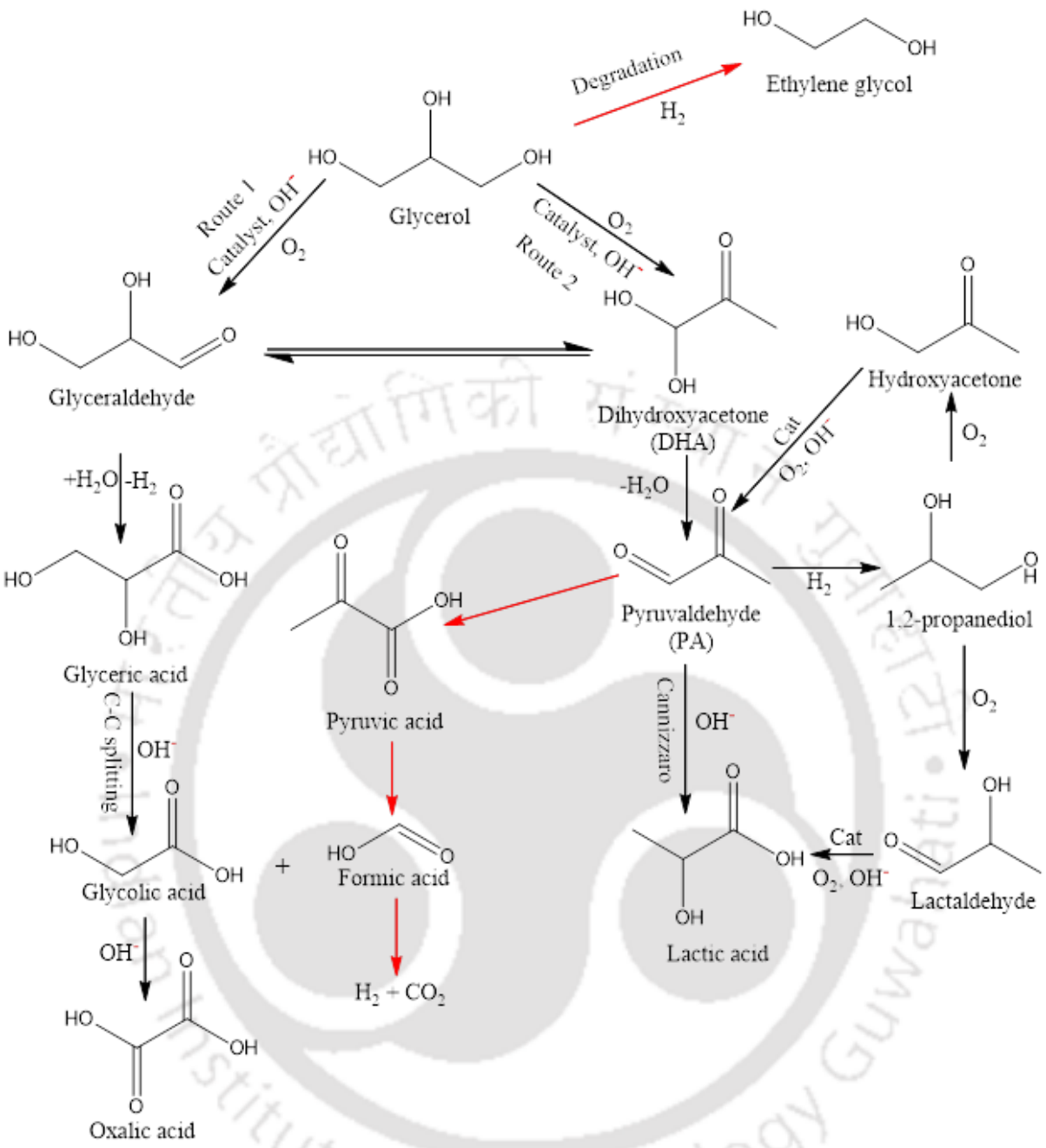

Scheme 6.1: Possible reaction routes for GL oxidation to LA over Pt-V/AC bimetallic catalyst.

TH-3456_166107017

Table 6.2: Synthesis of lactic acid from glycerol over Pt-V/AC bimetallic catalysts.

Entry No.	Oxidant	time (h)	base	Glycerol/metal (mol/mol)	Glycerol conversion (%)	Lactic acid yield (%)
1	Air	12	NaOH	4400	100	79.62
2	Air	12	KOH	4400	89.10	57.05
3	O_2	12	KOH	4400	78.0	46.5
4	Air	3	NaOH	8800	74.95	45.16
5	Air	12	NaOH	8800	92.10	66.30
6	Air	3	KOH	blank	26.9	5.52
7[a]	Air	12	BF	4400	19.12	0.78
8	O_2	12	KOH	6580	78.93	44.53
9[$]	Air	3	NaOH	4400	66.9	32.5

[a] base-free, [$]scaleup study. Reaction conditions: base/glycerol molar ratio = 1, 5 bar oxidant pressure, 200 ^{o}C.

TH-3456_166107017

Table 6.3: Carbon balance at various process conditions.

Entry No.	Process Conditions (Temperature, pressure, base/glycerol molar ratio, glycerol/metal molar ratio)	Carbon Balance (%)
1	160, 5b air, 12h, KOH/Gly = 1 (mol/mol), Gly/Metal = 4400 (mol/mol)	77.36
2	180, 5b air, 12h, KOH/Gly = 1 (mol/mol), Gly/Metal = 4400 (mol/mol)	75.05
3	200, 5b air, 12h, KOH/Gly = 1 (mol/mol), Gly/Metal = 4400 (mol/mol)	78.4
4	200, 5b air, 3h, KOH/Gly = 1 (mol/mol), Gly/Metal = 4400 (mol/mol)	72.4
5	200, 10b air, 3h, KOH/Gly = 1 (mol/mol), Gly/Metal = 4400 (mol/mol)	75.53
6	200, 15b air, 12h, KOH/Gly = 1 (mol/mol), Gly/Metal = 4400 (mol/mol)	72.62
7	200, 5b air, 6h, KOH/Gly = 1 (mol/mol), Gly/Metal = 4400 (mol/mol)	72.82
8	200, 5b air, 12h, Base free, Gly/Metal = 4400 (mol/mol)	81.7
9	200, 5b air, 12h, KOH/Gly = 0.5 (mol/mol), Gly/Metal = 4400 (mol/mol)	71.13

TH-3456_166107017

6.4 Summary

The Pt-V/AC bimetallic catalysts were prepared successfully through a wet-impregnation technique and were highly active for selective glycerol oxidation to lactic acid. Due to the synergism, the Pt-V/AC bimetallic catalysts performed better than the Pt/AC and V/AC monometallic catalysts. Very high selectivities (80%) to lactic acid were achieved with complete conversion of glycerol under moderate reaction conditions (NaOH/glycerol: 1:1 mol/mol, 4400 glycerol/metal molar ratio, 473 K, 5 bar air, 12 h). This could be attributed to the fact that the reactions (dehydrogenation and hydrogenation) that produce lactic acid and its byproducts, glyceric acid and glycolic acid, occur in tandem. The Pt-V/AC bimetallic catalyst was reusable and stable for 4 reuse cycles. The selective oxidation pathway developed in this study is a new green lactic acid synthesis method as an alternative to the current fermentation technology.

TH-3456_166107017

References

(1) Darabdhara, G.; Boruah, P. K.; Borthakur, P.; Hussain, N.; Das, M. R.; Ahamad, T.; Alshehri, S. M.; Malgras, V.; C-W Wu, K.; Yamauchi, Y. Reduced Graphene Oxide Nanosheets Decorated with Au-Pd Bimetallic Alloy Nanoparticles towards Efficient Photocatalytic Degradation of Phenolic Compounds in Water †. Nanoscale 2016, 8, 8276. https://doi.org/10.1039/c6nr00231e.

(2) TakatoMitsudome; KazuyaMiyagawa; ZenMaeno; TomooMizugaki; KoichiroJitsukawa; JunYamasaki; YasutakaKitagawa; KiyotomiKaneda. Mild Hydrogenation of Amides to Amines over a Platinum-Vanadium Bimetallic Catalyst. Angew. Chem., Int. Ed. 2017, 56, 9381–9385.

(3) Prasad, L.; Pala, R.; Rao Peela, N. Green Hydrogen Production in an Optofluidic Planar Microreactor via Photocatalytic Water Splitting under Visible/Simulated Sunlight Irradiation. 2021. https://doi.org/10.1021/acs.energyfuels.1c02686.

(4) Zhang, J. M.; He, J. J.; Wang, X. Q.; Fan, Y. J.; Zhang, X. J.; Zhong, J. P.; Chen, W.; Sun, S. G. One-Step Synthesis in Deep Eutectic Solvents of PtV Alloy Nanonetworks on Carbon Nanotubes with Enhanced Methanol Electrooxidation Performance. Int J Hydrogen Energy 2019, 44 (54), 28709–28719. https://doi.org/10.1016/J.IJHYDENE.2019.09.104.

(5) Niu, C.; Huang, M.; Wang, P.; Meng, J.; Liu, X.; Wang, X.; Zhao, K.; Yu, Y.; Wu, Y.; Lin, C.; Mai, L.; Berlin, S.-V. Carbon-Supported and Nanosheet-Assembled Vanadium Oxide Microspheres for Stable Lithium-Ion Battery Anodes. https://doi.org/10.1007/s12274-015-0896-6.

TH-3456_166107017

(6) Romanyuk, A.; Oelhafen, P. Oxidation of Vanadium with Reactive Oxygen Plasma: A Photoelectron Spectroscopy Study of the Initial Stages of the Oxide Growth Process. Thin Solid Films 2007, 515 (16), 6544–6547. https://doi.org/10.1016/J.TSF.2006.11.055.

(7) Shen, L.; Zhou, X.; Wang, A.; Yin, H.; Yin, H.; Cui, W. Hydrothermal Conversion of High-Concentrated Glycerol to Lactic Acid Catalyzed by Bimetallic CuAu: X (x = 0.01-0.04) Nanoparticles and Their Reaction Kinetics. RSC Advances. 2017, pp 30725–30739. https://doi.org/10.1039/c7ra04415a.

(8) Zhang, G.; Jin, X.; Guan, Y.; Yin, B.; Chen, X.; Liu, Y.; Feng, X.; Shan, H.; Yang, C. Toward Selective Dehydrogenation of Glycerol to Lactic Acid over Bimetallic Pt-Co/CeOx Catalysts. Ind Eng Chem Res 2019, 58 (31), 14548–14558. https://doi.org/10.1021/ACS.IECR.9B01918.

(9) Kishida, H.; Jin, F.; Zhou, Z.; Moriya, T.; Enomoto, H. Conversion of Glycerin into Lactic Acid by Alkaline Hydrothermal Reaction. Chem Lett 2005, 34 (11), 1560–1561. https://doi.org/10.1246/cl.2005.1560.

(10) Purushothaman, R. K. P.; van Haveren, J.; van Es, D. S.; Melián-Cabrera, I.; Meeldijk, J. D.; Heeres, H. J. An Efficient One Pot Conversion of Glycerol to Lactic Acid Using Bimetallic Gold-Platinum Catalysts on a Nanocrystalline CeO2 Support. Appl Catal B 2014, 147, 92–100. https://doi.org/10.1016/j.apcatb.2013.07.068.

(11) Yang, G. Y.; Ke, Y. H.; Ren, H. F.; Liu, C. L.; Yang, R. Z.; Dong, W. S. The Conversion of Glycerol to Lactic Acid Catalyzed by ZrO2-Supported CuO Catalysts. Chemical Engineering Journal. 2016, pp 759–767. https://doi.org/10.1016/j.cej.2015.08.027.

(12) Tian, J.; Liu, H.; Li, P.; Huang, Z.; Chen, J. Selective Oxidation of 1,2-Propanediol to Lactic Acid over Cu-Modified Au/Hydrotalcite Catalysts †. New J. Chem 2020, 44, 16311. https://doi.org/10.1039/d0nj02526g.

TH-3456_166107017

(13) Dimitratos, N.; Antonio Lopez-Sanchez, J.; Meenakshisundaram, S.; Anthonykutty, J. M.; Brett, G.; Carley, A. F.; Taylor, S. H.; Knight, D. W.; Hutchings, G. J. Selective Formation of Lactate by Oxidation of 1,2-Propanediol Using Gold Palladium Alloy Supported Nanocrystals. 2009. https://doi.org/10.1039/b823285g.

(14) Shen, L.; Yin, H.; Wang, A.; Lu, X.; Zhang, C. Gas Phase Oxidehydration of Glycerol to Acrylic Acid over Mo/V and W/V Oxide Catalysts. Chemical Engineering Journal 2014, 244, 168–177. https://doi.org/10.1016/J.CEJ.2014.01.051.

(15) Arcanjo, M. R. A.; Paniagua, M.; Morales, G.; Iglesias, J.; Melero, J.; da Silva, I.; Rodríguez-Castellón, E.; Vieira, R. S. Temperature Effect on Pretreatment of the Activated Carbon Support (Pt/AC and Pd/AC) for Glycerin into Lactic Acid. Ind Eng Chem Res 2020, 59 (33). https://doi.org/10.1021/acs.iecr.0c01588.

(16) Mitran, G.; Neațu, F.; Neațu, Ștefan; Trandafir, M. M.; Florea, M. VAlPOs as Efficient Catalysts for Glycerol Conversion to Methanol. Catalysts 2020, 10 (7), 728. https://doi.org/10.3390/catal10070728.

(17) Pemmana, H. R.; Barnwal, P. K.; Uppaluri, R. V.; Peela, N. R. Selective Aerobic-Oxidation of Glycerol to Lactic Acid over Ruthenium-Vanadium Bimetallic Catalysts. Journal of Industrial and Engineering Chemistry 2023, 124, 224–231. https://doi.org/10.1016/J.JIEC.2023.04.010.

(18) Bezerra, F.; Altino, H.; Soares, R. Oxidative Dehydration of Glycerol over Molybdenum- and Vanadium-Based Catalysts. J Braz Chem Soc 2018, 30, 1025–1033. https://doi.org/10.21577/0103-5053.20180251.

(19) Lai, J.; Zhou, S.; Cheng, F.; Guo, D.; Liu, X.; Xu, Q.; Yin, D. Efficient and Selective Oxidation of 5-Hydroxymethylfurfural into 2, 5-Diformylfuran Catalyzed by Magnetic

TH-3456_166107017

Vanadium-Based Catalysts with Air as Oxidant. Catal Letters 2020, 3, 1301–1308. https://doi.org/10.1007/s10562-019-03041-w.

(20) Huang, H.; Jiang, B.; Gu, L.; Qi, Z.; Lu, H. Promoting Effect of Vanadium on Catalytic Activity of Pt/Ce–Zr–O Diesel Oxidation Catalysts. Journal of Environmental Sciences 2015, 33, 135–142. https://doi.org/10.1016/J.JES.2014.10.026.

(21) Ramírez-López, C. A.; Ochoa-Gómez, J. R.; Fernández-Santos, M.; Gómez-Jiménez-Aberasturi, O.; Alonso-Vicario, A.; Torrecilla-Soria, J. Synthesis of Lactic Acid by Alkaline Hydrothermal Conversion of Glycerol at High Glycerol Concentration. Industrial and Engineering Chemistry Research. 2010, pp 6270–6278. https://doi.org/10.1021/ie1001586.

(22) Shen, Z.; Jin, F.; Zhang, Y.; Wu, B.; Kishita, A.; Tohji, K.; Kishida, H. Effect of Alkaline Catalysts on Hydrothermal Conversion of Glycerin into Lactic Acid. Industrial and Engineering Chemistry Research. 2009, pp 8920–8925. https://doi.org/10.1021/ie900937d.

(23) Haixu Yin; Changhua Zhang; Hengbo Yin⇑; Dezhi Gao; Lingqin Shen; Aili Wang. Hydrothermal Conversion of Glycerol to Lactic Acid Catalyzed by Cu_hydroxyapatite, Cu_MgO, and Cu_ZrO2 and Reaction Kinetics. Chemical Engineering Journal 2016, No. 288, 333–342.

(24) Shen, Y.; Zhang, S.; Li, H.; Ren, Y.; Liu, H. Efficient Synthesis of Lactic Acid by Aerobic Oxidation of Glycerol on Au-Pt/TiO2 Catalysts. Chemistry - A European Journal. 2010, pp 7368–7371. https://doi.org/10.1002/chem.201000740.

(25) J. Gilkey, M.; Xu, B. Heterogeneous Catalytic Transfer Hydrogenation as an Effective Pathway in Biomass Upgrading. ACS Catal 2016, 6 (3), 1420–1436. https://doi.org/10.1021/acscatal.5b02171.

TH-3456_166107017

(26) Carrettin, S.; McMorn, P.; Johnston, P.; Griffin, K.; Hutchings, G. J. Selective Oxidation of Glycerol to Glyceric Acid Using a Gold Catalyst in Aqueous Sodium Hydroxide. Chemical Communications 2002, 7, 696–697. https://doi.org/10.1039/b201112n.

TH-3456_166107017

TH-3456_166107017

Chapter 7

Conclusions and Future Work

TH-3456_166107017

7.1 Conclusions

Drawing upon the findings presented in Chapters 3, 4, 5, and 6, the following conclusions can be inferred:

I. Successful design and fabrication of a helically coiled microreactor (HCMR) for high-yield chemical production from renewable sources in an organic solvent.

II. Sulfuric acid (SA) and maleic acid (MA) demonstrated higher activity and selectivity in catalyzing fructose dehydration to 5-hydroxymethylfurfural (HMF) in HCMR. The highest HMF yield of 95% was achieved at 100 °C, 0.1 mL min^{-1} flow rate, and 3.5 wt% fructose concentration using 0.5 wt% SA catalyst.

III. The maximum HMF productivity reached 380 gHMF/gCat/h at 180 °C, 0.2 wt% SA concentration, 5 mL min^{-1} flow rate, and 50 wt% fructose concentration.

IV. Maleic acid (3 wt%) showcased notable efficacy, achieving an 80% HMF yield while effectively preventing degradation and inhibiting humin formation. Intriguingly, maleic acid demonstrated commendable selectivity (83%) toward HMF, surpassing that of sulfuric acid (80%).

V. Bimetallic and monometallic catalysts were effectively synthesized using wet impregnation and chemical reduction methods. They demonstrated the excellent activity of bimetallic catalysts for the base-free oxidation of HMF to FDCA compared to their monometallic counterparts. The highest FDCA yields of 74.4% and 65.3% were achieved with the Ru- V_2O_5/AC and Ru-Ni/AC bimetallic catalysts, showcasing their effectiveness in the oxidation process.

VI. The Ru-V_2O_5/AC bimetallic catalyst exhibited stability after washing with acetone, indicating its robust performance and durability in the oxidation reaction.

TH-3456_166107017

VII. The Ru-V/AC bimetallic catalysts were effectively synthesized using wet impregnation and a chemical reduction method. The synergism between Ru and V_2O_5 in the Ru-V_2O_5/AC bimetallic catalysts resulted in superior performance compared to their Ru/AC and V_2O_5/AC monometallic counterparts.

VIII. The Ru-V_2O_5/AC bimetallic catalysts exhibited higher selectivity and yield in glycerol oxidation to lactic acid under mild reaction conditions, outperforming their monometallic counterparts. The bimetallic catalysts achieved a higher yield of lactic acid, reaching up to 75.5%, compared to their monometallic counterparts. The Ru-V_2O_5/AC bimetallic catalyst demonstrated high stability, indicating its robust performance throughout the oxidation reaction.

IX. The Pt-V/AC bimetallic catalysts were successfully prepared through a wet-impregnation technique and exhibited high activity for selective glycerol oxidation to lactic acid. Due to synergism, these bimetallic catalysts outperformed their Pt/AC and V/AC monometallic counterparts, achieving very high selectivities (80%) to lactic acid with complete glycerol conversion under moderate reaction conditions (NaOH/glycerol: 1:1 mol/mol, 4400 glycerol/metal molar ratio, 473 K, 5 bar air, 12 h). This superior performance is attributed to tandem reactions (dehydrogenation and hydrogenation) producing lactic acid and byproducts glyceric acid and glycolic acid. The Pt-V/AC bimetallic catalyst also demonstrated reusability and stability for four cycles, presenting a green synthesis method as an alternative to current fermentation technology.

TH-3456_166107017

7.2 Future Work

I. To evaluate the scalability of HMF production, the homogenous catalysts are positioned for testing in scale-up reactions. A crucial aspect of achieving scalability involves concurrently developing an efficient purification process customized for HMF production.

II. Advancing a one-step process for the synthesis of 5-hydroxymethylfurfural derivatives, such as 2,5-bis(hydroxymethyl)furan (BHMF) and 2,5-diformylfuran, from fructose utilizing microreactor technology.

III. The synthesized catalysts can be evaluated for the scale-up of FDCA production from purified and crude HMF, employing fixed bed reactors.

IV. Various supports may synthesize bimetallic catalysts, including CeO_2, ZrO_2, TiO_2, and MgO. The resulting catalysts may then be tested for the oxidation of high concentrations of HMF to FDCA using both high-pressure autoclaves and fixed-bed reactors. The synthesized catalysts may be tested for converting glycerol to formic acid and hydrogen production, employing oxidation and dehydrogenation processes.

TH-3456_166107017

Research Output

Patents

1. Peela, N. R., **Hanumanth Reddy Pemmana,** Ramagopal V. S. Uppaluri, and Ramu Reddi. "Conversion of glycerol to lactic acid" Indian patent granted on 06/11/2023 (Patent number: 466319 and Application number: 202131057709).
2. Peela, N. R., **Hanumanth Reddy Pemmana,** Prince Kumar Barnwal, Ramagopal V. S. Uppaluri. "Bimetallic Catalysts and Catalytic Process for the Conversion Of 5-Hydroxymethylfurfural to 2,5-Furandicarboxylic Acid" Indian patent filed on 31-08-2023 (Reference number: 202331058615).
3. Peela, N. R., **Hanumanth Reddy Pemmana,** Prince Kumar Barnwal, Ramagopal V. S. Uppaluri. "Continuous Synthesis of 5-Hydroxymethylfurfural from High Concentration Fructose Feedstock in a Micro-Helical Coiled Reactor using Sulfuric Acid and Maleic Acid as Catalysts" Indian patent filed on 04.11.2023 (Reference number: 202331075425).

Journal papers

1. **Pemmana, H. R.,** Barnwal, P. K., Uppaluri, R. V., & Peela, N. R. (2023). Selective aerobic-oxidation of glycerol to lactic acid over ruthenium-vanadium bimetallic catalysts. *Journal of Industrial and Engineering Chemistry*, *124*, 224-231.
2. **Pemmana, H. R.,** Reddi, R., Uppaluri, R. V., & Peela, N. R. (2023). Glycerol selective oxidation to lactic acid over platinum–vanadium bimetallic catalysts supported on activated carbon. *Reaction Chemistry & Engineering*.
3. **Pemmana, H. R.,** Barnwal, P. K., Uppaluri, R. V., & Peela, N. R. Continuous Synthesis of 5-Hydroxymethylfurfural from High Concentration Fructose Feedstock in a Micro-Helical Coiled Reactor using Homogeneous Catalysts (To be Submitted).

TH-3456_166107017

4. **Pemmana, H. R.,** Barnwal, P. K., Uppaluri, R. V., & Peela, N. R. Catalytic conversion of 5-hdroxymethylfurfural to 2,5-furandicarboxylic acid over carbon-supported ruthenium-vanadium bimetallic catalysts under base-free mild reaction conditions (To be submitted).

TH-3456_166107017